University of Bergen

Faculty of Mathematics and Natural Science

Department of Chemistry

uniCIPR

December 2015

An investigation of the correlation between interfacial properties and phase composition in the crude oil/water system

Author:

Tina Trydal Rønsberg

Supervisor:

Kristine Spildo

Abstract

Enhanced oil recovery can be obtained by flooding the reservoir with chemical fluids. However, complex interactions between the crude oil components, floodwater composition and reservoir rock minerology have to be comprehended in order to exploit the potential efficiency of these techniques.

This thesis will focus on the effect of varying the water composition on the crude oil/water interfacial tension. The pendant-drop method was utilized for dynamic interfacial tension measurements, where the equilibrium interfacial tension was estimated by two different calculation-methods. The aim of this investigation has been to inspect whether differences in interfacial activity can be related to differences in the composition for two medium density crude oils, both retrieved from the North Sea. Organic analysis techniques imply that one of the crude oils is highly acidic and biodegraded, while the other oil is high in asphaltene content. Multivariate analysis methods have been utilized in order to develop an experimental plan and to identify the most significant variables at different conditions.

At simulated reservoir conditions, i.e. pH close to neutral, both crude oils' interfacial activity showed relatively low variance with respect to changes in ionic strength and concentration of divalent ions. At caustic conditions, it was discovered that the emulsion stability increased drastically for the acidic oil dispensed in water at low ionic strength and in the absence of divalent ions. Addition of Ca^{2+} completely eliminated the high interfacial activity. Furthermore, it was found that the crude oil with the higher asphaltene concentration reacted completely different at these conditions, and did not form stable emulsions. To the contrary, high water phase ionic strength promoted drastic changes in the crude oil's consistency.

Overall, pH appeared to be the most efficient promoter for reductions in the interfacial tension. The variance in crude oil acidity and asphaltene concentration was hypothesized to be the main sources of observed differences in interfacial activity.

Acknowledgements

First of all, I would like to thank Kristine Spildo for excellent supervision during this thesis. The many productive discussions and constructive feedback that she provided throughout both experimental work and data interpretation was greatly appreciated. Also, I would like to thank Professor Tanja Barth and staff engineer Terje Lygre for always being available to answer my questions, and for the many good suggestions and guidance during crude oil characterization techniques. Also, thank you to Egil Nodland for answering my questions concerning the efficient use of the Sirius software.

I would also like to thank Gine and Yvonne for a great cooperation in pursuing our common interest within this thesis research. I wish you both the best of luck with completing your thesis work.

I would also like to thank my extraordinary class mates that have made my time as a student truly eventful and memorable. A special thanks to Hilde and Louise for keeping up the good spirit at the office during this last semester. Furthermore, I would like to thank my parents and my sister for all the support they have provided.

Finally, I want to thank Ole for his endless support, encouragement and patience throughout this thesis work.

Thank you,

Tina Trydal Rønsberg

List of abbreviations and symbols

Abbreviations

EOR	Enhanced Oil Recovery
IFT	Interfacial Tension
CO/W	Crude Oil/Water
LSW	Low Salinity Water
HSW	High Salinity Water
ppt	Parts Per Thousand
ppm	Parts Per Million
SARA	Saturates, Asphaltenes, Resins and Aromatics
NSO	Nitrogen, Sulphur and Oxygen or Norwegian Standard Oil
TAN	Total Acid Number
BAN	Total Base Number
EDL	Electrical Double-Layer
PRS	Pattern Recognition System
CCD	Central Composite Design
FCD	Face Centered Design
PCA	Principal Component Analysis
PC	Principal Component
PLS	Partial Least-Squares
RSD	Residual Standard Deviation
WOGC	Whole Oil Gas Chromatography
FID	Flame Ionization Detector
UCM	Unresolved Complex Mixture
FT-IR	Fourier Transformation Infrared Spectroscopy
CO-Wet	Crude Oil Wettability
OCA	Optical Contact Angle
API	American Petroleum Institute
SG	Specific Gravity
ATR	Attenuated Total Reflection

rpm	rounds per minute
Exp	Experiment
Ax	Axial point
CP	Centerpoint
DA	Drop Age

Symbols

N_c	Capillary number [-]
μ	Viscosity [cP]
ν	Velocity [m·s^{-1}]
θ	Contact Angle [^{o}]
γ	Interfacial Tension [mN·m^{-1}]
ΔP	Capillary Pressure [kg·m^{-1}·s^{-2}]
r	Radius [m]
M_w	Molecular Weight [g·mol^{-1}]
pK_a	Acid dissociation constant [-]
pK_b	Base dissociation constant [-]
$[HA]_o$	Total concentration of acids in oil phase [mol·L^{-1}]
$[HA]_w$	Total concentration of acids in oil phase [mol·L^{-1}]
P	Partition coefficient [-]
γ_{eq}	Equilibrium interfacial tension [mN·m^{-1}]
γ_o	Initial interfacial tension [mN·m^{-1}]
T	Time [s], absolute temperature [K or ℃] or period of oscillation [s]
τ	Interfacial reorganization time [s]
ψ_o	Surface potential [mV]
ψ_δ	Stern potential [mV]
ζ	Zeta-potential [mV]
κ^{-1}	Debye length [nm]
ε	Dielectric constant [F·m^{-1}]
ε_0	Permittivity of free space [F·m^{-1}]
R	Gas constant [J·mol^{-1}·K^{-1}]

e	Elementary charge [C]
N_{AV}	Avogadro's number [mol^{-1}]
I	Ionic Strength [$mol \cdot kg^{-1}$]
z	Valency [-]
C	Concentration [$mol \cdot L^{-1}$ or $mol \cdot kg^{-1}$]
$\hat{y}$	Predicted response
β_n	Regression coefficient for n'tn variable [-]
x_n	n'th variable
θ_{AB}	Angle between vectors A and B [^{o}]
z_{ij}	Entity in matrix position (i, j) [-]
$\mathbf{X_c}$	Column-centered data matrix $\mathbf{X}$
$\mathbf{X}$	Raw data matrix
$\bar{\mathbf{x}}^T$	Transpose of mean data matrix
R^2	Coefficient of determination [-]
ρ	Density [$g \cdot cm^{-3}$]
m	Mass [g or kg] or molality [$mol \cdot kg^{-1}$]
V	Volume [μL, mL or L]
f	Oscillation frequency [s^{-1}]
B	Shape parameter [-] or air pressure [mmHg]
F	Relative humidity [%]
wt%	Weight per cent [g/100g]
M	Molar concentration [$mol \cdot L^{-1}$]
X_{Ca2+}	Molar fraction of calcium [-]
pH_i	Initial pH [-]
pH_f	Final pH [-]
d	Diameter of the pendant-drop needle [mm]
g	Acceleration of gravity [$m \cdot s^{-2}$]

Table of content

1. Background

1.1. Introduction

Approximately 60% of the oil is left behind in the reservoir after termination of conventional production methods [1-3]. In order to increase the recovery efficiency, a variety of techniques collectively denoted enhanced oil recovery (EOR) have been developed and extensively researched. This thesis will be concerned with the EOR-technique referred to as chemical injection. The recovery efficiency of this method relies on the specific chemical composition of the flood water that is injected into the reservoir [3].

Enhanced recovery by utilizing chemical injection has been reported by various researchers [2, 4-6]. However, EOR demand a long-term commitment to high-cost techniques without the guarantee of immediate success. The problematic aspect emerges in the attempt to correlate the observed recovery benefits to the recovery technique's physical-chemical conditions. These conditions are governed by complex crude oil/water/reservoir rock interactions [1-5, 7]. Thus, identification of the mechanisms and optimum conditions for chemical injection has been the main aim of this field of research, and will be the objective of this thesis.

1.2. Enhanced oil recovery

Conventional production methods include the exploiting of natural reservoir energy and subsequent augmentation of the reservoir pressure by utilizing an external source, e.g. injection of gas or water. The two techniques substitute the primary and secondary recovery stages [3, 8]. Tertiary recovery techniques are initiated once primary and secondary recovery no longer proves efficient [2, 3, 8]. The three main techniques implemented at the tertiary stage are thermal injection, gas injection and chemical injection. [5, 8-11].

The efficiency of tertiary methods depends on the ratio of viscous forces to interfacial tension forces. This relationship can be summarized by the capillary number (**Equation 1-1**) [2, 3].

$$N_c = \frac{\mu v}{\gamma cos\theta}$$

Equation 1-1

Where N_c is the capillary number, μ is the dynamic viscosity of the liquid, ν is the velocity, θ is the contact angle and γ is the interfacial tension (IFT). The capillary number has to be maximized to increase the mobilization and displacement of residual reservoir oil. This can be obtained either by increasing the floodwater viscosity or by decreasing the IFT [3].

1.2.1. Chemical injection

Chemical injection utilizes different compositions of floodwater to aim at altering the equilibrium conditions in the reservoir. Two criteria must be met in order for this to be obtained. The first is related to the sweep efficiency of the injected fluid, i.e., its ability to reach the reservoir's capillary-like pores and come into contact with the trapped oil. The second criterion is the injected fluid's ability to displace the trapped oil once in contact [3]. The latter is analogous to the fluid's ability to reduce the IFT between trapped crude oil and injected water, and ultimately increasing the capillary number (**Equation 1-1**). The IFT is defined more precisely in Chapter 1.6, but can be considered as a measure of the immiscibility of two fluids [3, 12].

In a reservoir pore-space containing two immiscible phases, e.g., crude oil and water, water tends to wet the pore-walls at equilibrium conditions (**Figure 1-1**). Wetting is defined as a fluid's tendency to spread on a solid surface [3, 12]. This property is quantified by the contact angle between the fluid and the solid, which can take on values from 180° (complete wetting) to 0° (completely non-wetting). In real crude oil/water/reservoir rock systems, the contact angle is an intermediary value.
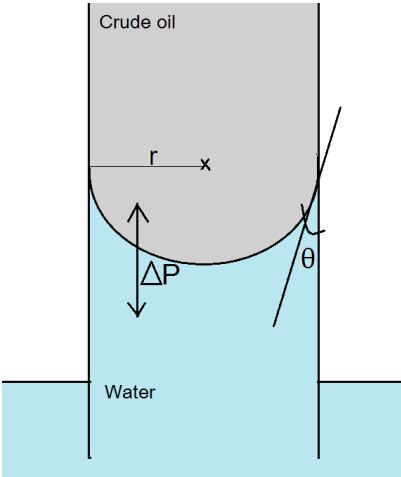
Figure 1-1: An illustration of crude oil trapped in a capillary pore-space in a permeable reservoir rock.

A distinct interfacial film will form spontaneously between the liquid phases. Due to water having a higher density than crude oil, the buoyancy force will position the oil at the inner part of the capillary pore-space, where it is inaccessible for oil production. The crude oil pressure immediately above the interface will be higher than the water pressure directly below the interface. This pressure-difference is denoted capillary pressure [3]. At capillary equilibrium, the capillary pressure is directly proportional to the interfacial tension existing between the two fluids, defined by **Equation 1-2** [3, 12].

$$\Delta P = P_{NWP} - P_{WP} = \frac{2\gamma\cos\theta}{r} \qquad \textbf{Equation 1-2}$$

Where ΔP is the capillary pressure and subscripts NWP and WP refers to pressures of the non-wetting phase and wetting-phase, respectively. γ is the interfacial tension, θ is the contact angle between the wetting-phase and the solid pore-wall and r is the radius of the pore throat, as displayed in **Figure 1-1**. In a permeable reservoir rock, the capillary pressure is the force required to displace the crude oil droplets through the pore throat [3]. By reducing the interfacial tension between the two phases, this force is correspondingly reduced, thus allowing the trapped oil to be displaced more readily.

1.3. Mechanisms in chemical injection

As early as 1925, P. G. Nutting concluded that sand grain's affinity for hydrocarbons were completely destroyed by the use of salts for a strong base [9]. Cooke et al. [5] later suggested the following mechanism for displacement of crude oils with alkaline water: (1) drastic reduction in the crude oil/water IFT, (2) wetting of the matrix grains by oil, (3) formation of water drops inside the oil phase, and (4) drainage of oil from the volume between alkaline water drops to produce an emulsion containing very little oil. This mechanism has been supported by subsequent reports, and the general process is described by Speight [8, p126] as IFT reduction followed by spontaneous emulsification or wettability alteration.

Stable crude oil/water (CO/W) emulsions can be obtained by adding surfactants or by activating the natural surfactants in the crude oil [13, 14]. The latter is facilitated by adding basic species that promote saponification of amphiphilic molecules to make their compounds more hydrophilic. However, mixed injection fluids are often necessary for emulsification

alone to provide adequate sweep efficiency. This can involve alkaline or low salinity injection water with added polymer or surfactant (**Figure 1-2**) [8].
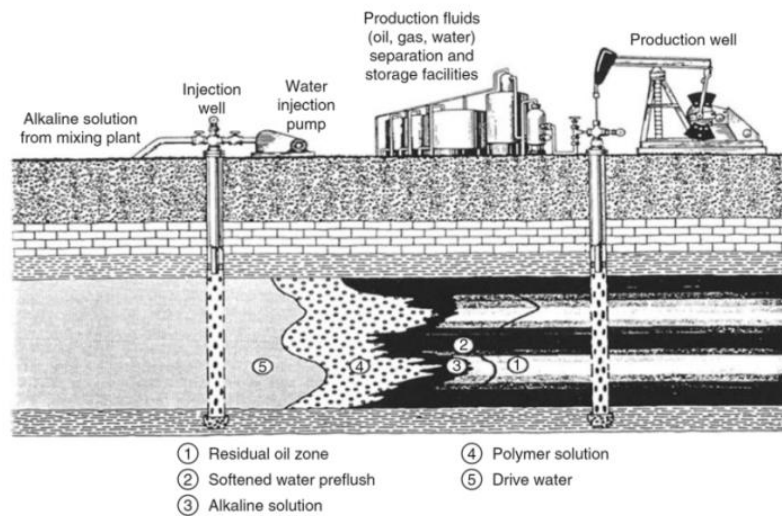
Figure 1-2: Oil recovery by chemical flooding [15].

1.3.1. Effect of floodwater salinity

Saline water is defined as water that contains a significant amount of dissolved salts. Low-salinity water (LSW) is usually characterized as water with a salt concentration of 1 to 3 parts per thousand (ppt), whereas high salinity water (HSW) has a salt concentration of 10 to 35 ppt [16]. The cations commonly used to alter water salinity are those of alkali and earth-alkali elements, particularly sodium, calcium and magnesium. The recovery efficiency associated with water phase salinity is commonly discussed as an electrostatic phenomenon of CO/W emulsion stability [1, 4, 17]. In this case, the ionic strength of the water-phase (defined in Chapter 1.7) is the conventional property of interest.

The EOR-effect of LSW injection has been most successful in combination with surfactant or polymer flooding, where LSW is injected during secondary recovery [6]. EOR-effects at tertiary recovery stages suggest that electrical double-layer expansion is a dominant mechanism [1, 4, 6, 18]. However, the large diversity of salts naturally present in the formation water pose some challenges with respect to controlling the optimum salinity conditions once they are identified [4, 7]. Rock minerology has also been found to play a central role in obtaining wetting-alteration by LSW injection [1, 4].

1.3.2. Effect of floodwater alkalinity

Alkaline water contains negatively charged ion species that are associated with the alkali and earth-alkali group elements. Typical species found in alkali water are carbonates, oxides and hydroxides. These species have basic properties and therefore elevate the pH of water [16]. Caustic Soda (NaOH) is frequently used in the alkaline waterflooding, in which "caustic" is used to denote the water phase [10, 19, 20].

The effectiveness of alkaline flooding relies on the degree of in situ formation of surfactants during the neutralization of petroleum acids in the crude oil by the alkaline chemicals in the displacing fluids [8]. Several studies have concluded on the positive EOR-effects of alkaline waterflooding [5, 10, 13, 19-23], and it has been utilized in fields containing crude oils of high acid numbers [8]. However, it has been found that the responsible mechanism for IFT-lowering highly depend on the type of metal cations present in the formation water [5, 10, 18-20, 23, 24].

1.4. Crude oil

Petroleum is defined as naturally occurring mixture of hydrocarbons, which may also include compounds of sulfur, nitrogen, oxygen (heteroatoms), metals and other elements [25]. The composition of crude oil varies with geographical location, depth and age of the field, but can be categorized in terms of main group compounds or fractions. **Figure 1-3** [26] provides an overview of the most occurring components found in crude oils. Other common groupings are based on fractions of saturates, aromatics, resins and asphaltenes (SARA-fractions) [8].
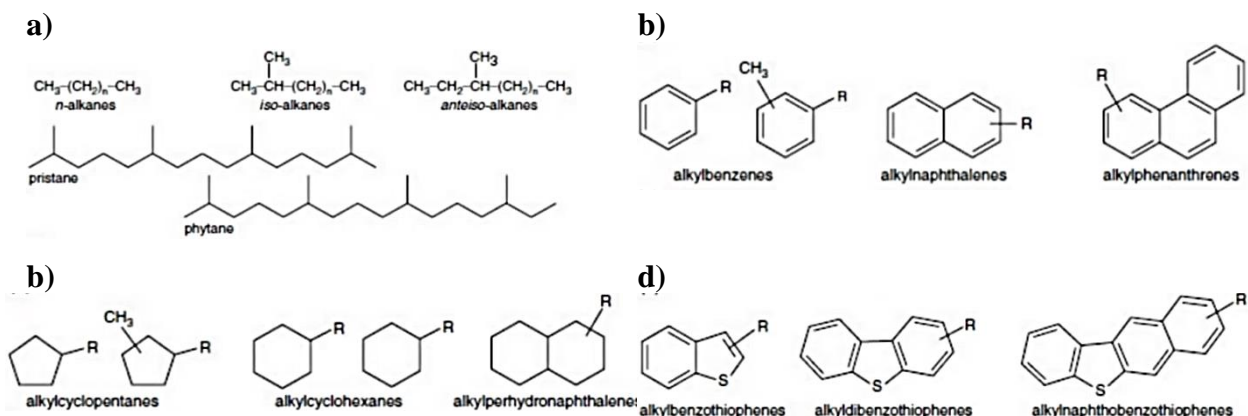
Figure 1-3: An overview of the most abundant species found in crude oils [26]. a) Paraffins, b) naphthenes, c) aromatic hydrocarbons and d) sulphur-containing aromatics.

1.4.1. Interfacially active components in crude oil

The crude oil components of main interest to this thesis are those which are interfacially active. In physical terms, these are the species that gain a free energy profit by migrating from the crude oil bulk to the interfacial area. In chemical terms, these are the components that possess an amphiphilic structure. An amphiphilic compound is composed of a polar, hydrophilic part and a nonpolar, hydrophobic part [12]. The hydrophilic part can be alcohols, amides, ethers, electronegative heteroatoms (NSO) or basic or acidic functional groups. The hydrophobic part is nonpolar hydrocarbons that can be structured in a large variety of simple chains or cyclic arrays with alkyl-groups [8, 14, 27]. These molecules are commonly referred to as "surface active agents" or "surfactants", due to their spontaneous adsorption at the interfacial region [12].

The most common interfacially active molecules in crude oil are asphaltenes, resins and naphthenic acids [5, 8, 14, 27-29]. The latter is used as a collective reference to carboxylic acids present in crude oil [29-31]. Naphthenic acids thus have the general formula RCOOH, where R is a cycloaliphatic structure [31]. These are quantified by the crude oil total acid number (TAN), while the basicity of the crude oil is quantified by its total base number (BAN) [13, 28].

Asphaltenes and resins are heavy, naturally occurring molecules in crude oil with M_w 700 – 2000 $g \cdot mol^{-1}$ [13, 32]. Asphaltenes molecules are polyatomic sheets of cyclic alkanes surrounded by aliphatic branches containing some heteroatoms, polar groups (esters, ethers, carbonyls) and/or functional groups such as acids and bases [8, 13, 14, 32-35]. Van der Waals attraction and hydrogen bonding between these sheets may form aggregates in the order of M_w $10^4 – 10^5$ $g \cdot mol^{-1}$ [33, 34].

1.4.2. Biodegradation

Crude oil biodegradation is the process of aerobe or anaerobe microbial degradation of light hydrocarbons in the oil. The consequence is an increase in crude oil density, emulsion stability and increased concentrations of polar NSO compounds and acids. [36]. Higher concentrations of acids may also result from products of the degradation process, as microbial growth is found to be promoted by organic acids as well as short-chained saturates. Thus, biodegradation entails an increase in interfacially active components, which are commonly denoted "biosurfactants" [37].

1.5. Acid/base equilibria in CO/W systems

Several equilibria are involved in CO/W systems that contain naphthenic acids, as illustrated by **Figure 1-4**. The most important of these is considered to be the partitioning of non-dissociated naphthenic acids at low pH, the dissociation of the carboxylic acid at pH above the acid's pK_a, and the continuous adsorption and desorption at the interface. At high pH, the formations of micelles in the water-phase and reverse micelles in the oil phase are also thought to affect the equilibrium [29, 31]. Dissociated acids may also form metal soaps with divalent salts, which tend to solubilize in the aqueous phase [24].
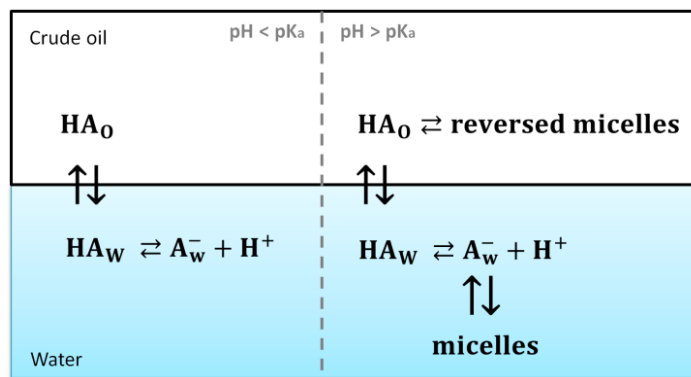
Figure 1-4: Schematic illustration of the mass transfer of basic and acidic species across the CO/W interface. Adapted from [31].

The ratio between the total acid concentration partitioned in the oil phase ($[HA]_o$) to that partitioned in the water phase ($[HA]_w$) is quantified as the partitioning coefficient (**Equation 1-3**), which is a measure of an acidic surfactant's relative solubility in the system.

$$P = \frac{[HA]_o}{[HA]_w}$$

Equation 1-3

It has been found that equal partitioning corresponds to the minima in the IFT [13, 24, 31]. Thus, optimum conditions for interfacial activity have often been estimated based on these parameters, with IFT-measurements at varying water phase pH and salinity as empirical evidence for the model. The effect of the water phase salinity on the solubility of amphiphilic organic molecules is denoted the salting-out effect. This effect is due to the disturbance in the solubilizing water-structure surrounding petroleum species, caused by the interference of dissolved inorganic salts. The following decrease in the solubility of petroleum species cause them to rather arrange at the interface, which allows for amphiphilic structures [24, 38, 39].

1.6. Interfacial tension

The intermolecular forces existing in a system of two immiscible liquids will differ between bulk and the interface. Bulk molecules will experience an equal pull of forces in all directions, while interfacial molecules experience a net pull towards the interior, which consequently create an environment of higher energy for the molecules. This resistance to mix is manifested in the interfacial tension that forms in the interfacial layer separating the two liquids. This value is proportional to the energy required to bring a molecule from the bulk phase to the interface. More precisely, the interfacial tension is the mechanical energy required to create a new unit interfacial area between two immiscible liquids [12, p26].

The IFT (γ, mN·m^{-1}) is proportional to the capillary pressure (ΔP) and inverse proportional to the degree of drop-curvature (defined by radii R_1 and R_2), as is displayed in the Young-Laplace equation (**Equation 1-4**, [40]). This equation can be derived directly from the capillary pressure equation modelling the reservoir pore-space, as displayed by **Figure 1-1** and **Equation 1-2**.

$$\Delta P = \gamma \left(\frac{1}{R_1} + \frac{1}{R_2} \right)$$ **Equation 1-4**

IFT is a time-dependent property [10, 18, 22, 23, 27, 29]. By monitoring the IFT as a function of interfacial age, information about the extent of various dynamic processes can be extracted and compared to variations in the CO/W combinations. The decay of the IFT as a function of time-dependent reorganization at the interface has been proposed to follow the monoexponential decay-function in **Equation 1-5** [13, 23, 29, 32, 41].

$$\gamma(T) = \gamma_{eq} + (\gamma_o - \gamma_{eq})e^{-T/\tau}$$ **Equation 1-5**

where T is the drop age and τ is the characteristic time constant for interface reorganization and subscripts eq and o refer to the equilibrium (T>τ) and initial (T=0) IFT, respectively. The most widely accepted dynamic mechanism for interfacial equilibration is that the rate-determining step is diffusion-controlled, i.e., the rate of diffusion to- and across the interface is slower than the rate of interfacial reactions [18, 19, 29, 32]. It has also been reported that the dynamic IFT may possess a characteristic minimum value, followed by a gradual increase towards a plateau [10, 18-20]. This behavior has been attributed to the onset of convective diffusion across the interface, especially in the case of caustic CO/W systems containing Ca^{2+} or surfactants, which may promote the hydrophilic character of crude oil species.

1.7. The electrical double-layer

The electrical double-layer (EDL) is the structure that is formed in the vicinity of the interface. It is described in terms of the electrical surface potential (ψ_o) relative to the potential in the bulk solution. The surface potential is modeled as a concentration profile, $\psi(x)$, where x is the distance from the interfacial film (**Equation 1-6**). The inner layer (at distance x=δ) is modeled as a monolayer of counter-ions that is almost equal to the amount of ions required to neutralize the surface charge (**Figure 1-5**). This is denoted the Stern-plane, and has a potential ψ_δ. This is often taken to be more or less equal to the zeta potential (ζ), which is the conventional measure of electrostatic emulsion stability [12].

At distance x $>\delta$, the Gouy-Chapman model for the diffuse layer explains the potential profile, in which the remaining surface charge is neutralized by bulk-ions moving freely back and forth across the EDL. The thickness of the EDL is governed by the Debye length (κ^{-1}, **Equation 1-7**). The Debye length decrease as the ionic strength (**Equation 1-8**) of the bulk phase increase [12]. Thus, it provides an important theoretical background for inspecting the colloidal stability of emulsions.

$$\psi(x) = \psi_o e^{-\kappa x}$$

$$\Updownarrow \qquad \text{\textbf{Equation 1-6}}$$

$$\psi(x) = \frac{\psi_o}{e^{x/\kappa^{-1}}}$$
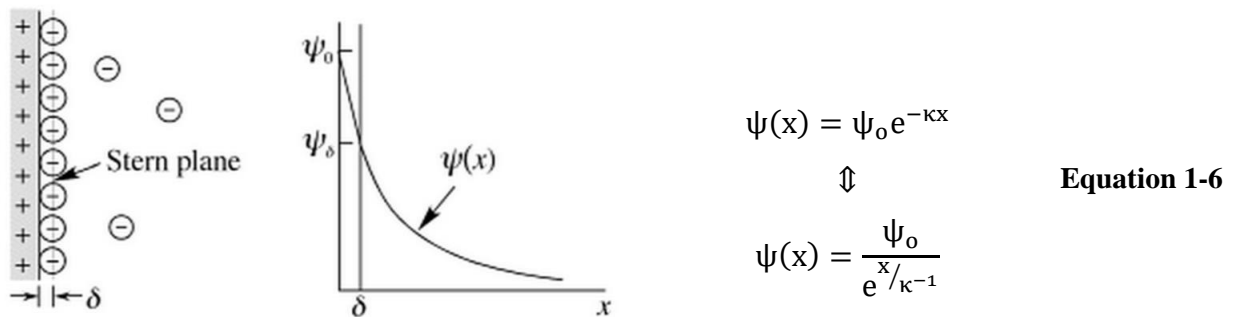
Figure 1-5: The Stern-model for the electrical double-layer [12, p480].

$$\kappa^{-1} = \sqrt{\frac{\varepsilon \varepsilon_0 RT}{2000 e^2 N_{AV}^2 I}} \qquad \text{\textbf{Equation 1-7}}$$

$$I = \frac{1}{2}\sum_{i=1}^{n} z_i^2 m_i \qquad \text{\textbf{Equation 1-8}}$$

Where ε is the dielectric constant for the solvent, ε_0 is the permittivity of free space, R is the gas constant, T is the absolute temperature, e is the elementary charge and N_{AV} is Avogadro's

number. I is the ionic strength, where z_i and m_i are the valency and molality of ionic component i, respectively.

1.8. Thesis objective

The objective of this thesis is to correlate the crude oil composition to the IFT in a CO/W system. Two crude oils will be characterized by selected organic analysis techniques, and the pendant-drop technique will be used for IFT-measurements. The experimental domain of main interest to this thesis is that of reservoir conditions, where the pH is close to neutral, and caustic conditions, where NaOH is introduced to increase the pH. Both conditions will be investigated at varying ionic strength and Ca^{2+} concentrations.

The ionic strength will be modeled as displayed in **Equation 1-8**, while the presence of divalent cations will be evaluated as the unit-less molar fraction of Ca^{2+}, as displayed in **Equation 1-9**.

$$X_{Ca2+} = \frac{n_{Ca^{2+}}}{n_{Ca^{2+}} + n_{Na^+} + n_{Cl^-}}$$ **Equation 1-9**

Where X_{Ca2+} is the molar fraction of Ca^{2+} and n_x is the amount of ion specie X present (Ca^{2+}, Na^+ and Cl^-) in units of mole.

The experimental plan will be developed and interpreted in a multivariate framework. The rationale for utilizing multivariate design methods in this thesis is to obtain as much information as possible from the experiments performed. Additionally, multivariate designs offer a good assortment of graphical representations of the underlying structure in the data. Univariate interpretations of data will also be utilized in cases where this is best suited for the information of interest.

Also, data from a more comprehensive study of this thesis' inquiry, performed by Buckley et al. [23, 41-44], will be interpreted in a multivariate framework. This database is sufficiently large for exploiting the full potential of multivariate methods. The crude oils utilized in this thesis will also be integrated in this dataset.

2. Crude oil characterization

2.1. Whole Oil Gas Chromatography

Gas chromatography (GC) separates mixtures into individual components by vaporization, which allows for the identification of each component present, as well as their concentration. The separation of mixtures in GC is time-dependent, i.e., the vaporize mixture-components pass through the column at different rates. This is due to the different component's individual affinity for the stationary and mobile phase [45]. The mobile phase used in this thesis is Helium gas, while the stationary phase is a fused silica column. Thus, polar components will be slowed down by electrostatic association with the silica coating on the column walls, while non-polar components will associate with the inert Helium gas and flow through the column more quickly. **Figure 2-1** shows the components involved in the GC-apparatus.

In this thesis the sample material is non-diluted crude oil, which is referred to as Whole Oil GC (WOGC). For high sample concentrations (the analyte constitute >0.1 % of the sample), like that of WOGC, it is necessary to use high split-ratios (70:1 – 100:1) and/or low injection volumes ($\leq 1\mu L$) to obtain good quality chromatograms [46]. The split-ratio correspond to the portion of the sample that does not reach the column, i.e. a 100:1 split-ratio means that one part reaches the column while 100 parts does not (1 %).
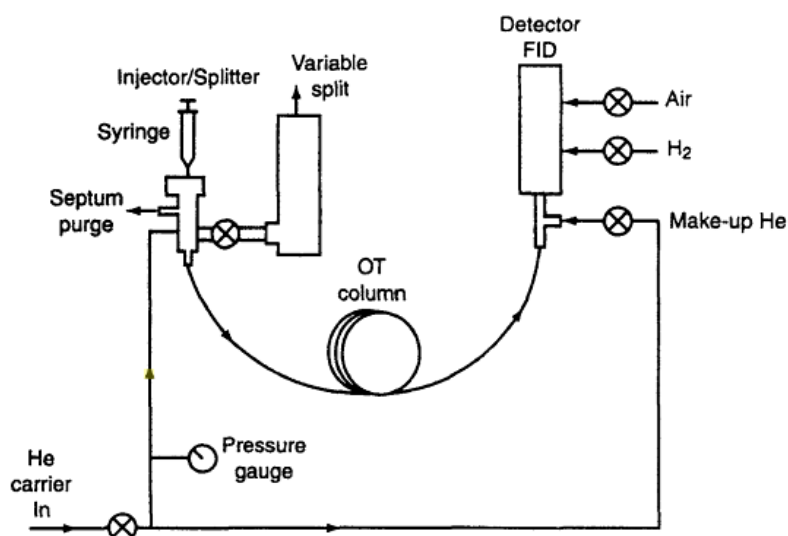
Figure 2-1: Schematic of gas chromatography instrument [46, p148]

The end terminal of the column is equipped with a Flame Ionization Detector (FID) that has high sensitivity towards organic components. The FID is a small H_2-Air flame that is warm enough to produce CHO^+-ions from the CH-radicals following with the Helium gas [46]:

$$CH + O \rightarrow CHO^+ + e^-$$ **Equation 2-1**

The flow of the produced ions constitutes a small current which is amplified and sent to the data acquisition system. The resulting chromatogram consists of peaks in which their placement in time corresponds to a characteristic mixture-component and the peak size (height or area) corresponds to the component's concentration [45].

WOGC is also an efficient analysis technique for recognizing biodegradation in crude oils. This is visible in the form of broad inclinations in the baseline of the chromatogram, which are denoted unresolved complex mixtures (UCMs) [47].

2.2. FT Infrared Spectroscopy

Infrared spectroscopy is an analytical technique in organic and inorganic chemistry that takes advantage of the fact that molecules adsorb infrared light at frequencies that are characteristic of their structure. A molecule consisting of N molecules will exert $3N - 6$ vibrational modes, where each vibrational mode is characterized by a discrete value. This value is equal to the energy difference between two adjacent energy levels, i.e. the discrete quantity of energy sufficient to cause the atomic bond to vibrate, bend, stretch or rotate [48].

When the molecule is subjected to infrared radiation at this exact intensity, the molecule will adsorb the energy, thus reviling the atomic bonds it possesses. However, only bonds with a significant dipole moment will adsorb enough energy to be visible in the IR-spectra. Adsorption bands are measured in frequency-units denoted wavenumbers (in units of cm^{-1}). Infrared light expands the region from $400 - 4000$ cm^{-1} [49].

The IR-spectrometer utilized in this thesis applies a Fourier transformation (FT) to the sample scan, which allows for a computerized summation of scans to increase the signal-to-noise ratio. The Fourier transformation coverts the digitalized signals to a signal that is a function of frequency, which is proportional to the wavenumber reported in the spectra [48].

2.3. Density measurements

The density of a material (ρ) is defined as the material's mass (m) divided by its volume (V).

$$\rho = \frac{m}{V}$$

<div align="right">**Equation 2-2**</div>

The density of crude oil is usually given in units of API gravity (American petroleum Institute gravity), which is related to the fluid density through the following equation:

$$API^o = \frac{141.5}{SG^o} - 131.5, \qquad \text{where } SG^o = \rho_{oil}/\rho_{water}$$

<div align="right">**Equation 2-3**</div>

Where API^o is the API gravity, SG^o is the specific gravity and ρ_{oil} and ρ_{water} are the fluid density of oil and water, respectively. This specific gravity thus gives the density of a petroleum liquid relative to that of water. API gravity is used to classify crude oils in three different categories, as shown in **Table 2-1**.

Table 2-1: Categorizing of petroleum liquids with respect to API gravity [50].

Category	API gravity	Fluid density, ρ [g·cm^{-3}]
Light	$> 31.1^o$	< 0.870
Medium	$22.3^o - 31.1^o$	$0.870 - 0.920$
Heavy	$< 22.3^o$	$0.920 - 0.100$

The method utilized for density measurements in this thesis is denoted "the oscillating U-tube method" [51]. The tube is electronically excited to oscillate at its characteristic frequency (**Equation 2-4**). This frequency changes in response to the density of the sample.

$$f = \frac{1}{2\pi}\sqrt{\frac{k}{m + \rho \cdot V}}, \qquad \text{where } f = \frac{1}{T}$$

<div align="right">**Equation 2-4**</div>

Where f is the oscillation frequency, k is a power constant, ρ is the density of the fluid, and m and V are the mass and volume of the oscillator, respectively. T is the period of the oscillation. By squaring and rearranging the equation and setting the mass of the oscillator equal to zero, we get the following:

$$\rho = \frac{k}{4\pi^2 V}T^2 = A \cdot T^2$$

<div align="right">**Equation 2-5**</div>

$$\rho_i - \rho_{air} = A(T_i^2 - T_{air}^2)$$

<div align="right">**Equation 2-6**</div>

A is the instrumental constant, and is determined by rearranging **Equation 2-6** and using a reference system consisting of fluids with known densities, e.g., for a water/air system (i = water). The density of water at 298,15 K is 0.997 g·cm^{-3} [52]. The density of air is dependent on atmospheric pressure (B), temperature (T) and relative humidity (F), which can be expressed as the following:

$$\rho_{air} = 0.46464 \left(\frac{B - 0.08987F}{T} \right) \times 10^{-3}$$

Equation 2-7

The density of i = crude oil is calculated from **Equation 2-6** once the instrumental constant is determined.

2.4. Asphaltene quantification

Asphaltenes are defined as the crude oil fraction that is insoluble in alkanes, but soluble in aromatic solvents [14]. Alkanes that have the ability to precipitate asphaltenes are referred to as flocculants when utilized for this task. In this experimental work, the asphaltene-content is quantified by precipitation with n-heptane, i.e., the content of nC$_7$-asphaltene.

The quantitative results from asphaltene-precipitation depend both on the type of flocculant and the volume-ratio between crude oil and flocculant [53]. For a volume-ratio of 20:1 for n-heptane and crude oil, the volume of n-heptane ($V_{n\text{-hep}}$) for precipitation of a crude oil mass (m_{CO}) with known density (ρ_{CO}) can be calculated by **Equation 2-8**.

$$V_{n-hept} = \frac{1}{20} \times \frac{m_{CO}}{\rho_{CO}}$$

Equation 2-8

3. Previous research on CO/W interfacial properties

3.1. Crude oil composition

Many attempts [2, 18, 23, 31, 41, 43, 54, 55] have been made to correlate the crude oil composition to the IFT and emulsion stability of the CO/W system. Varadaraj and Brons [54, 55] investigated both the effect of asphaltenes and naphthenic acid's structure on interfacial activity. It was hypothesized that basic nitrogen-containing asphaltenes and crude oil naphthenic acids interact to form acid-base complexes that aggregate at the interface to reduce the IFT [55].

To the contrary, Buckley et al. [23] reported that the wt% of asphaltenes was a crude oil property that showed positive correlation with the IFT, independently of variations in water-phase pH and salinity. No explanation for this observation was presented, despite the conclusion that asphaltenes did not act as surfactants in the CO/W system.

Poteau and Argillier [13] reported opposite results from IFT-measurements between different concentrations of asphaltenes dissolved in toluene, where it was found that the IFT decreased with increasing asphaltene-concentration. These results also showed indications of synergistic effects between asphaltenes and acids; a mixed composition of 5% maltene (the deasphaltened fraction) and 1% asphaltenes had an overall lower IFT than oil-fractions of either 1% asphaltenes or 5% maltene. Thus, the combined interfacial activity of asphaltenes and naphthenic acids present in the maltene-fraction was higher than the two fractions acting alone. Emulsion stability tests also indicated a stabilizing interaction between asphaltenes and naphthenic acids. This effect was different from the well-known interactions found between asphaltenes and larger resin-molecules, which are assumed to deprive asphaltene's interfacial activity by solubilizing them in the oil-phase [14, 27]. The conclusion was, similarly as reported by Varadaraj and Brons [54, 55], that asphaltenes and dissociated naphthenic acids co-adsorb at the interface at high pH, to reduce the IFT [13].

Several studies have also been devoted to studying the correlation between crude oil acids and CO/W IFT. Many of these have focused on the correlation between crude oil TAN and IFT [10, 20, 41], while others suggest that the acid structure is more important with respect to

interfacial activity [31, 54, 56]. It should also be noted that crude oil TAN has been found to increase with crude oil BAN [41, 57]. Thus, many of the same mechanisms have been reported for crude oils with high BAN.

Buckley et al. [23, 41] found that BAN and viscosity were most important for predicting the IFT at acidic conditions (pH ~3). At strongly basic conditions (pH >10), TAN was the most determining variable in predicting IFT, and the IFT was too low to be measured by the pendant drop. This conclusion was based on crude oils with TAN >0.1 mg KOH/g oil. Crude oils with low acid numbers (TAN <0.1 mg KOH/g oil) and varying base numbers (0.1≤ BAN ≤2.5 mg KOH/g oil) were measurable at all pH-values inspected, but had an abrupt decrease in IFT upon increasing the aqueous pH to 9-10. Thus, crude oil properties other than TAN are necessarily affecting interfacial activity at high pH [43].

Jennings [20] reported a similar conclusion upon investigating 164 crude oils gathered from 78 different fields. At caustic conditions, the surface activity was found to correlate to TAN, API gravity and viscosity of the crude oil. An IFT of <0.01 mN·m^{-1} was measured for all crude oils with API gravity of <20° in caustic solution, and 90% of these oils reached a maximum measurable surface activity at a caustic concentration of ~0.1 wt%.

It is however important to note that both of these studies [20, 41] also reported considerable scatter between crude oil properties and the measured IFT. Correlations that were included in the conclusion may not necessarily be finite, but gives an indication as to what crude oil properties that promote IFT lowering, versus what properties that oppose it.

Trujillo [10] concluded that TAN only provides a qualitative indication of crude oil reactivity in caustic solution. This was concluded upon fitting activity coefficients of the crude oil to increasing aqueous pH, and observing that the no correlation could be made between TAN and the activity of the crude oil. Thus, the interfacial activity at increasing pH was considered to be a combined effect of many different interfacially active species. For especially high TAN oils (~2.0 mg KOH/g oil), however, there was a significant decrease in IFT at caustic conditions compared to oils with TAN <1.0 mg KOH/g oil.

At neutral conditions, i.e., in non-caustic solution, crude oil acids may affect the IFT as well. This is reported in studies where the IFT is correlated to the partition coefficient for CO/W systems [18, 24, 31, 56]. Thus, the difference in crude oils' relative ability to solubilize their hydrophilic components, which are often modeled as acidic species, may influence the IFT of the system. Havre et al. [31] reported correlations between the partitioning of crude oil

naphthenic acid structures in acidic model oil/water systems and interfacial activity. A typical pK_a of 4.9 was reported for the extracted naphthenic acids with two to three rings. This value has also been used by other researchers to model the diffusion and mass transfer in acid-containing CO/W systems [28, 29], and is the same as the pK_a for water-soluble aliphatic acids like cyclohexane carboxylic acid [52]. Additionally, Havre et al. [31] reported the naphthenic acids with three-ring structures were most hydrophilic, and that in general, the logarithm of the partition coefficient varied linearly with the number of carbons in the naphthenic acid molecule. The proposed model showed a misfit at pH>8. This was suggested to be due to the naphthenic acid's ability to form micelles and reversed micelles in the bulk phases once a sufficient concentration of the acids have been dissociated. The model was coupled to IFT-measurements, which revealed minimum values to be present at pH-values almost twice the size of the pK_a [31].

Hoeiland et al. [56] studied three different model oils with various naphthenic acids extracted from crude oil. It was found that the most interfacially active oil was dominated by complicated ring structures of high molecular weight, while the least interfacially active oil was mainly composed of cyclohexane/cyclopentane acids. Also, the IFT as a function of aqueous pH was not lowered much upon diluting the oils. Thus, it was concluded that interfacial activity possibly is more dependent on acids structure than acid concentration [56].

Interfacial activity in asphaltene-systems have been studied by Jeribi et al. [32], Langevin et al. [14] and Poteau and Argillier [13]. All reported formations of rigid "skins" of bulk aggregates of asphaltenes that form irreversibly at the CO/W interface. Langevin et al. [14] proposed that in stable emulsions with dense, elastic and viscous skin-like surface layers, the surface rheology is more important than the interfacial tension. Poteau and Argillier [13] measured the elasticity of the CO/W interface (measured as the compression elastic modulus) as a function of pH, and found that it increased along with a decreasing IFT. Thus, it was concluded that, especially for high asphaltene concentrations, interfaces are more rigid at high and low pH, compared to neutral pH. Jeribi et al. [32] proposed that the size, growth and stability of these aggregates depended on the crude oil's ability to solubilize the asphaltenes. Poor solubility led to larger aggregates due to their preferred interaction with each other rather than with the oil-phase. It was also found that interfacial reorganization was more rapid at high asphaltene-concentrations [32].

3.2. Water composition

3.2.1. pH

The IFT's pH-dependency in CO/W systems has been confirmed in various literature [5, 10, 18, 19, 21-23, 28, 58]. The IFT is generally reported to be highest near neutral pH, whereas it decreases at low or high pH, due to the increased concentration of interfacially active ionized species [13, 24].

Farooq et al. [18] reported pendant-drop measurement between pH-regulated water and three different oil phases: one where acidic species were extracted, one where basic species were extracted and one non-threated crude oil. The non-acidic fraction had consistently higher IFT at basic pH conditions, which was attributed to the lack of acid dissociation. However, the acid-containing crude oil also had a lower IFT at neutral pH, indicating that also non-dissociated acidic components are interfacially active. The non-basic fraction's IFT was slightly higher at low pH, which was attributed to the lack of base protonation [18].

It has been reported that more than one optimum occurs in the modeling of IFT as a function of pH. One optimum may be recognized at the onset of acid or base dissociation. This pH is related to the pK_a or pK_b, respectively. For naphthenic acids, the pK_a has often been estimated to a typical value of 5 [28, 29, 31].

Kelesoglu et al. [29] found large differences in the dynamic IFT for pH<5 compared to pH>5 when utilizing model oils containing naphthenic acids with this pK_a. Complementary zeta-potential measurements revealed that the negative charge increased abruptly as the pH increased from 4 to 5. A further increase in pH caused a slow decrease in zeta-potential, before another abrupt decrease was observed as the pH increased from 10 to 11 [29]. Hoeiland et al. [56] found similar patterns upon inspecting various aqueous pH for models oil containing different concentrations of naphthenic acid. For the crude oil with the highest TAN (2.84 mg KOH/g oil), a smooth leveling of the IFT was found as the pH was increased to 5, followed by a sharp reduction at pH>8.

A possible explanation of this trend in pH-dependence has been provided by Havre et al. [31]. It was suggested that the trend can be attributed to the difference between bulk-pH and interfacial pH in saline CO/W systems. A quantitative measure of this phenomena was adapted from the mathematical model derived by Cratin [59]. This model approximated the interfacial pH as a function of bulk pH and EDL effects, where the EDL was modeled as a

Boltzmann distribution of counterions. The consequence of this relation was that the interfacial pH was lower than the bulk-pH for negatively charged interfaces, which is the case at high pH. This means that the concentration of dissociate acids is higher in the bulk phase than at the interface. Calculations of the partition coefficient (**Equation 1-3**) showed that P = 10^{-5} at the pK_a of the acid. Thus, at pH $\approx pK_a$, dissociated acids will be present and adsorb at the interface, but in very low concentrations. Consequently, the total concentration of dissociated and non-dissociated acids was found to be equal once the pH reached 5 units above the pK_a, according to Cratin's model. This approximation was validated by IFT-measurements that showed an abrupt decrease occurred after the pH was raised to 9 – 11, despite pK_a-values being closer to 5 [31]. This would also explain the consecutive optimum at pH 10 – 11 in Kelesoglu et al.'s zeta-potential measurements, as they also utilized naphthenic acids with pK_a 5 [29]. It would also explain the IFT's pH-dependence in Hoeiland et al.'s study, which also assumed average pK_a values of 4 – 5 for naphthenic structures of monovalent alkyls, cyclic and aromatic [56].

3.2.2. Ionic strength

Standal et al. [24] investigated the connection between the partition coefficient and IFT for polar organic species in contact with various aqueous compositions. In general, lower IFT-values were observed when monovalent ions were present. This was attributed to the salting-out effect which evidently caused an increase in the partition coefficient to promote lower portions of interfacially active components to solubilize in the aqueous bulk phase. The salting-out effect was significantly higher for 0.5 M NaCl compared to pure water, but not as pronounced when increasing the salinity from 0.5 to 1.0 M NaCl. This was attributed to EDL-effects, i.e., an optimum screening of the interfacial charge may exist between an ionic strength of zero and 1.0 M NaCl [24].

Lashkarbolooki et al. [38] reported a decrease in the IFT between crude oil and saline water once the concentration of monovalent salts was increased past 1000 ppm. A subsequent increase was observed once the concentration was raised to 15 000 ppm. Alotaibi et al. [2, 4] have also reported the existence of optimums in the IFT as function of aqueous ionic strength. This is thought to be caused by an EDL-effect related to the optimum screening length (κ^{-1}, **Equation 1-7**) allowing the maximum concentration of charged species to be accumulated at the interface. At this optimum, repulsion between charged interfacially active species is minimized, while simultaneously lowering their solubility in the bulk-phases to further

promote interfacial accumulation. Thus, further compression of the EDL-thickness past this optimum length may be related to some saturation of the interface in terms of available adsorption-area or charge neutralization. This mechanism is however highly debated, and is also considered to rely on the rock minerology of the reservoir system [1, 2, 7].
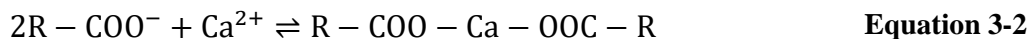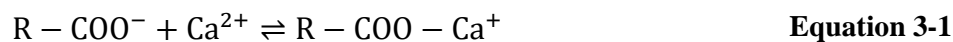
Farooq et al. [18] found that IFT reduction at caustic conditions was promoted by the presence of electrolyte, while pure water did not show any significant pH-dependence in the IFT. The explanation that was suggest was similar as that by Havre et al. [31], i.e. Cartin's model [59] for the interfacial pH. In pure water, only H^+ ions are available for screening of the negative interfacial charge. Thus, they accumulate at the interface and lower the interfacial pH compared to the bulk pH. Consequently, the dissociation of acids at the interface will be suppressed, and the IFT is not lowered as drastically. However, by increasing the ionic strength of the aqueous bulk phase, the H^+ ions can be partitioned more uniformly instead of being accumulated at the interface. This will decrease the difference between the interfacial – and bulk pH, thus allowing more acids to undergo saponification at the interface, and lower the IFT [18].

3.2.3. Presence of divalent cations

Trujillo [10] reported that the concentration of Ca^{2+} ions was the determining factor in obtaining ultralow IFT ($<10^{-3}$ mN·m^{-1}) between crude oil with caustic solution. Also highly acidic crude oils were insufficient if $[Ca^{2+}] \geq 200$ ppm. Jennings [20] reported that $[Ca^{2+}] = 25$ ppm was sufficient to increase the IFT considerably, whereas $[Ca^{2+}] = 250$ ppm disabled the IFT-reduction completely for all caustic concentrations $\leq 1\%$ [20]. Sharma et al. [19] and Jennings [20] found that the IFT-reduction in caustic solution was observed at lower NaOH-concentration if large concentrations of NaCl were present. The IFT was too high to be measured (by the spinning drop method) when Ca^{2+} was added, even at trace concentrations of <100 ppm [19]. Jennings [20] found that 131 of the 164 crude oils studied showed a marked surface activity against caustic solution. 90% of these crude oil samples reached a maximum measurable surface activity at caustic concentrations of ~0.1 wt%. However, these effects were lost once divalent ions were introduced to the system.

Farooq et al. [18] suggested that Na^+ cations and Ca^{2+} cations have two separate effects on the interfacial activity between crude oil and aqueous solution at elevated pH, i.e., in the presence of charged species. High Na^+-concentrations were considered to compress the diffuse layer

surrounding the interface and result in more efficient screening of the repulsion between neighboring negative charges. On the other hand, Ca^{2+} will accumulate effectively at the interface and form strong complexes with dissociated acids. The complexes formed are either positively charged (**Equation 3-1**) or neutral complexes (**Equation 3-2**) [7, 18].

$$R - COO^- + Ca^{2+} \rightleftharpoons R - COO - Ca^+ \qquad \text{Equation 3-1}$$
$$2R - COO^- + Ca^{2+} \rightleftharpoons R - COO - Ca - OOC - R \qquad \text{Equation 3-2}$$

Some researchers [18, 24, 30] have also found that $Ca(OH)_2$ precipitation destroys the possibility of obtaining IFT results at sufficient concentrations of NaOH, due to the specie's emulsifying effect. $Ca(OH)_2$ particles are basic and can stabilize CO/W emulsions by interaction with acidic groups in asphaltenes, resins and/or naphthenic acids adsorbed at the interface [14].

$$Ca^{2+}(aq) + 2OH^-(aq) \rightleftharpoons Ca(OH)_2(s) \qquad \text{Equation 3-3}$$
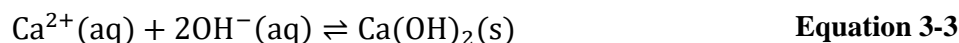
Whereas several studies have found a highly significant IFT-effect of Ca^{2+} ions at alkaline conditions, mixed reports have been presented on the effect at neutral pH-conditions [18, 24, 38]. This may be attributed to the varying degree of dissociation constants that exist in the crude oil mixture. Ca^{2+}-complexes may form as long as dissociated acidic species are present. However, if the pK_a value is >7 it is necessary to increase the aqueous pH. Farooq et al. [18] did not observe Ca^{2+}-complexation at high pH for crude oil where the acid-fraction had been removed prior to measurement, i.e. the presence of dissociated acids appeared to be necessary. Others [4, 38] have reported that Ca^{2+} also have efficient ionic screening abilities that served to enhance the effect of EDL-compression and interfacial accumulation of charged surfactants.

4. Method

4.1. Multivariate data analysis

Multivariate data analysis may be executed by utilizing pattern recognition systems (PRS). PRS is the scientific discipline of machine learning that aims at classifying data into a number of categories or classes [60, p169]. This involves the conversion of the original multivariate data into latent variables, i.e. fundamental factors that reflect the most important patterns from the original dataset, while reducing noise. Latent variables are, in other words, compressed variables and therefore more readily interpreted. This thesis will implement the PRS in the Sirius 9.0 software package. Sirius offers a range of graphical outputs to represent this data compression [61, 62].

4.1.1. Experimental design

Experimental designs offer a way of introducing consistency and aim to your experimental data gathering procedure [63]. The aim is to extract the most relevant information by carrying out as few experiments as possible within the experimental domain.

The variables $(x_1, x_2, \ldots, x_n)$ are set to one is high level $(x_i = +1)$ and one is low level $(x_i = -1)$. This constitutes a factorial design on two levels, in which variables are referred to as factors. The number of experiments needed for a full design with n variables is thus 2^n [64]. The variation in the response at varying factor-levels is summarized in an empirical model:

$$\hat{y} = \beta_0 + \sum_{i=1}^{n} \beta_i x_i + \sum_{i=1}^{n} \sum_{j>i}^{k} \beta_{ij} x_i x_j + \varepsilon \qquad \textbf{Equation 4-1}$$

Where $\hat{y}$ is the predicted response as a function of n independent variables x_1, x_2, …, x_n and β_0, β_1, $\beta_{2, \ldots}$ β_n are the regression coefficients. The third term from the left is the interaction term, which accounts for two-factor effects on the response, and ε is the residual, i.e., $\hat{y} - y$. Regression coefficients can be obtained directly from the experimental design matrix through applying Yate's algorithm[1] [65].

---

[1] for an elaboration on this method, visit http://www.itl.nist.gov/div898/handbook/eda/section3/eda35i.htm

The choice of variable-levels is of crucial importance to the resultant response. If the two levels are too close in magnitude, the variation in response values will not be significant, whereas if they are too far apart, optimum configurations that might exist in between the levels can be missed. Extreme values can also cause the response to move away from the smooth area of the response surface, and onto areas that are beyond control [63, 66]. The response-variable is most likely not a line or plane, but a curved surface. Therefore it will contain a set of variable-settings that define its optimal response which may be surrounded by local maxima and saddle-points. If variable-settings fall into one of these configurations, important information about the system will be lost. This may be avoided by initiating the research plan with a screening design, by adding centerpoints to the design and by utilizing central composite designs (CCD) instead of factorial designs [64, 65].

4.1.1.1. Screening experiments

Screening of variables can be carried out many different ways. The method used in this thesis is a screening of factors in two factorial designs with five independent variables (n=5) at three levels (3^5 experiments). This design is reduced to only model two of the variables per design, thus reducing the number of experiments to 3^{5-3}. 3 – 5 parallels were performed for each experiment in order to determine the standard deviation.

For the first screening (**Table 4-1**), the ionic strength and pH are threated analogously to a full three-level factorial design, whereas other variables of interest were held constant or varied parallel to the ionic strength. The second set of screening experiments (**Table 4-2**) was also performed with a three-level reduced factorial design, but executed for both crude oils. However, some variable combinations were excluded for further reduction of the design.

Table 4-1: The experimental design for the first screening of variables. Ionic strength and pHi are full factorial variables while the molar fraction of Ca^{2+} is varied parallel to the ionic strength.

Exp#	Crude oil	Xca^{2+}	I [mol·kg^{-1}]	pHi
1	A	0.13	**0.40**	3
2	A	0.13	**0.40**	7
3	A	0.13	**0.40**	11
4	A	0.65	**0.23**	3
5	A	0.65	**0.23**	7
6	A	0.65	**0.23**	11
7	A	0.00	**0.09**	3
8	A	0.00	**0.09**	7
9	A	0.00	**0.09**	11
10*	A	0.02	**0.09**	11

*Included to inspect the effect of adding trace-amounts of Ca^{2+} at basic conditions and low ionic strength

Table 4-2: The experimental design for the second screening of variables. The molar fraction of Ca^{2+} and ionic strength are varied between three levels, but not in a complete factorial design.

Exp#	Crude oil	X_{Ca2+}	I [mol·kg^{-1}]	pH
1	A	0.06	0.09	7
2	A	0.24	0.41	7
3	A	0.00	0.36	7
4	A	0.26	0.10	7
5	A	0.00	0.24	7
6	A	0.06	0.24	7
7	B	0.06	0.09	7
8	B	0.24	0.41	7
9	B	0.00	0.36	7
10	B	0.26	0.10	7
11	B	0.00	0.24	7
12	B	0.06	0.24	7

4.1.1.2.   Centerpoints

Centerpoints (CP) are added to the design if one suspects the response surface to be curved. An indication of this is when center points are not distributed evenly around the mean response for the design. For two-level designs, center points are chosen midway between the levels, i.e. $x_{CP} = 0$ for all factors [63]. Centerpoints may also be used as a measure of the uncertainty within measurements.

4.1.1.3.   Central Composite Designs

CCDs are quadratic model design where axial points (Ax) are added to the factorial design to estimate the curvature of the response surface [65]. The CCD used in this thesis is the face centered design (FCD). This estimates the curvature within the main design by inspecting the center of each face for the factorial space (**Figure 4-1**). Hence, the axial points are chosen to be $x_{Ax} = \pm1$. This is analogous to modeling three levels for each factor [64, 65].

The disadvantage of the FCD is its inability to rotate around the center. Rotatability allows for the variance of the predicted response to be determined at any distance **x** from the center point [67]. To maintain rotatability, axial points for n factors are set at $x_{Ax} = [2^n]^{1/4}$ [65].

The main experimental design consisted of two face centered designs for two (I and X_{Ca2+}) and three (I, X_{Ca2+} and pH) independent variables and one dependent variable (equilibrium IFT). The red parts of **Table 4-3** refers to experimental points that were included in both the two- and three-dimensional FCD.
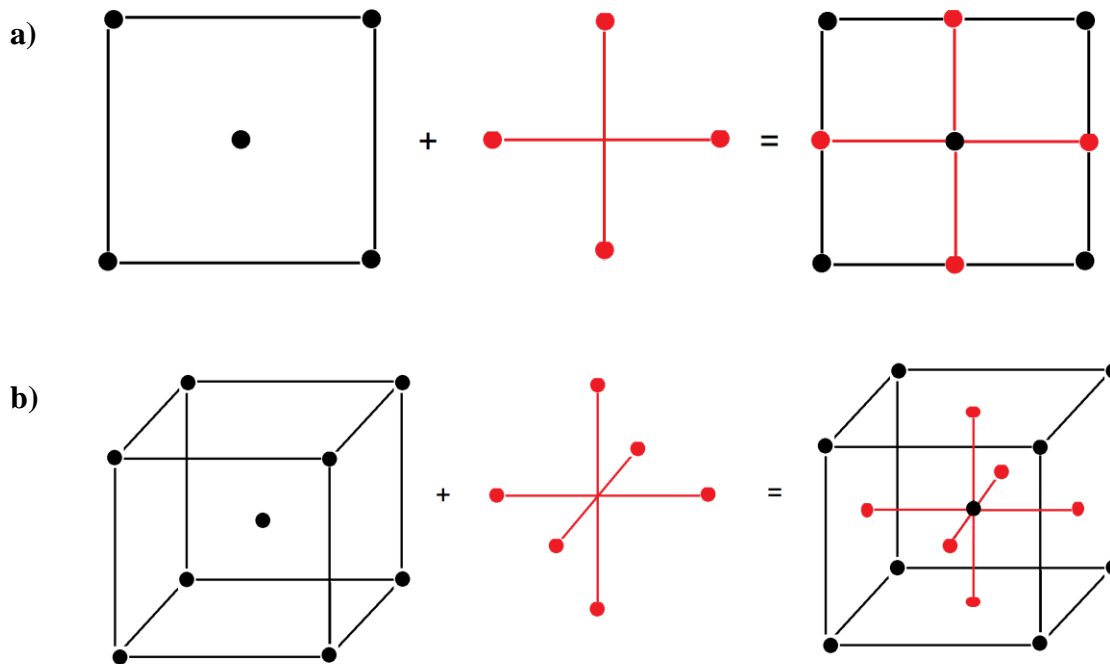
Figure 4-1: Visual representation of face centered design for a) two factors and b) three factors. The black points are the experimental points and center point from the factorial design. The red points are the axial points.

The designs were executed once for each crude oil. Four center points were included, to decide the reproducibility of the experiments, and to inspect the curvature of the response surface. Regression coefficients were calculated by Yate's algorithm [68]. The coefficient's significance on the model was determined based on their distribution in a normal plot.

Table 4-3: The full FCD for three variables on two levels in Yate's order, with four centerpoints (CP) and axial points (Ax).

Exp #	I [mol·kg^{-1}]	X_{Ca2+}	pH
Exp1	0.03	0.00	7
Exp2	0.65	0.00	7
Exp3	0.03	0.09	7
Exp4	0.65	0.09	7
Exp5	0.03	0.00	11
Exp6	0.65	0.00	11
Exp7	0.03	0.09	11
Exp8	0.65	0.09	11
Ax1	0.03	0.05	9
Ax2	0.65	0.05	9
Ax3	0.34	0.00	9
Ax4	0.34	0.09	9
Ax5	0.34	0.05	7
Ax6	0.34	0.05	11
CP1	0.34	0.05	9
CP2	0.34	0.05	9
CP3	0.34	0.05	9
CP4	0.34	0.05	9

4.1.2. Principal Component Analysis

Principal Component Analysis (PCA) describes the dataset in terms of uncorrelated, new variables called principal components (PCs). These are linear combinations of the original variables, decomposed into orthogonal variables. Principal components arrange in the variable –and object space according to the direction of maximum variation, as is displayed in **Figure 4-2**. The biggest advantage in using PCA is the intuitive interpretation of the resultant visual graphics, and the ability to easily inspect covariance between interacting variables [69]. The mathematical background for PCA will not be elaborated on in this thesis, but the reader is referred to the works of Isaksson and Næs [69].

The decomposition of the original data into latent variables can be illustrated as shown below.

$$
\underset{N \times M}{\begin{bmatrix} X \end{bmatrix}} = \underset{N \times A}{\begin{bmatrix} T \end{bmatrix}} \underset{A \times M}{\begin{bmatrix} P^t \end{bmatrix}} + \underset{N \times M}{\begin{bmatrix} E \end{bmatrix}}
$$

X is a N×M matrix composed on N objects and M variables. This is the raw dataset that is being decomposed into two parts; one which carries the information (**TP^t**) and one which carries the noise (**E**). The **T**-matrix consist of the score vectors and the **P**-matrix consist of the loadings vectors. A loading plot represents the projection of the object space onto the decomposed PCs while the score plot represents the projection of the variable space onto the decomposed PCs. These plots can also be combined in a biplot to show the relationship between objects and variables [69].
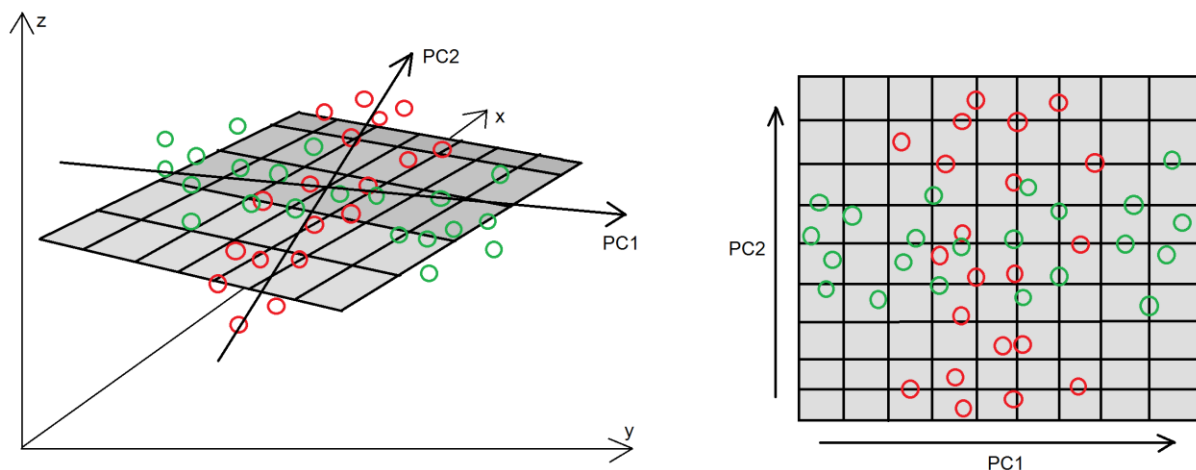
Figure 4-2: A visual representation of a loading plot.

The explanatory powers of the PCs are dictated by the ratio of explained variance in the decomposed dataset as supposed to the original dataset. If the explained variance is low, then the PCs carry little information [69]. A possibility could be to include more PCs until the variance explained has reached a threshold value. However, the aim of PCA is to decompose the dataset to consist of as few variables as possible.

The score plot can be interpreted with respect to the similarity between objects. Two criteria decide this: (1) The closer the objects are spaced, the more similar they are, and (2) the smaller the angle between the object vectors (measured with respect to the origin), the more similar they are [61]. Similarity between objects may also be inspected in a scores dendrogram. This presents the similarity between objects by comparing the euclidian distance between the object's score vectors. Score vectors that are closely spaced are similar, and hence are connected at the bottom of the dendrogram hierarchy [70].

The loading plot can be interpreted with respect to the covariance between variables, in which the following criteria apply: (1) the smaller the angle between the variable vectors (measured from the origin), the more positively correlated they are, and (2) the larger the angle, the more negatively correlated they are [61]. These are the measure of the reproduced correlation (r^2) between the variables. The reproduced correlation between loading vectors A and B is found by the dot product, as displayed in **Equation 4-2**.

$$\cos\theta_{AB} = \frac{\vec{x}_A^t \times \vec{x}_B}{\|\vec{x}_A\| \times \|\vec{x}_B\|}$$ **Equation 4-2**

The distribution of objects and variables in score –and loading plots may also be interpreted in terms of the contribution of an object or variable to the PCA-model. Hence, this gives information about the object or variable's importance with respect to the variation in the dataset. The principle for deciding this is that the larger the score/loading, the more the object/variable contributes. It is however unfortunate if one object contributes too much to the total model. Objects with large scores can be inspected in a RSD vs. leverage plot, where RSD is the residual standard deviation of the object. Objects with large RSD compared with leverage, or vice versa, should be considered removed from the model [61].

4.1.3. Partial Least-Squares Regression

While PCA is effective in extracting information about the variance in **X**, partial least-squares (PLS) is effective in extracting information about the covariance between **X** and **y** [71]. Thus, the PLS-regression model decomposes the raw dataset into latent variables that explain as much as possible of the interdependence between the response-variable and the independent variables. The resultant PLS-model predicts the response ($\hat{\boldsymbol{y}}$) analogously as for the experimental design model in **Equation 4-1**, but without considering interaction-terms.

4.1.4. Pre-processing of data

The raw data matrix is most likely subjected to noise, baseline drift, dominant variables and other interferences due to instrumental drift. These effects can lead to a biased view of the data if not processed prior to analysis [72]. This can be eliminated by standardizing the variables (**Equation 4-3**). However, in the case of chromatographic or spectroscopic data, standardizing will eliminate the information of interest by attributing each peak-value an equal variance.

$$z_{ij} = \frac{x_{ij} - \overline{x}_j}{s_j}$$

Equation 4-3

Where z_{ij} is the standardized object *i* in variable *j*, x_{ij} is the non-standardized object *i* in variable *j*, $\overline{x}_j$ is the mean value of variable *j* and s_j is the standard error of variable *j*.
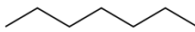
In PCA, the raw data matrix also has to be centered relative to the mean of the decomposed object –and variable space. This allows object-similarities and variable-covariance to be more readily interpreted by their relative placement around the mean value of the dataset. This is executed as displayed in **Equation 4-4**, where $\mathbf{X}_c$ is the centered matrix and $\overline{\mathbf{x}}^T$ is the transpose of the data matrix containing the mean object-values. $\overline{\mathbf{x}}^T$ is multiplied with a N×1 unit matrix and subtracted from the original data matrix, **X** [69]**.**

$$\mathbf{X}_c = \mathbf{X} - \mathbf{1} \times \overline{\mathbf{x}}^T$$

Equation 4-4

4.2. Materials

Table 4-4 provides an overview of chemicals utilized in the experimental method. The two crude oils were supplied by Statoil ASA and originate from the North Sea, but from different fields. The crude oils are denoted crude oil A and crude oil B.

Table 4-4: Overview of chemicals.

Name (IUPAC)	M_w [g·mol^{-1}]	Structure	Supplier	Purity [wt%]
Sodium chloride	58.44	NaCl	Sigma-Aldrich	>99.8
Calcium chloride dihydrate	147.01	$CaCl_2 \cdot 2H_2O$	Merck	>99.5
n-decane	142.29		Sigma-Aldrich	>99.5
n-heptane	100.21		Sigma-Aldrich	>99.5
Hydrogen chloride	36.46	HCl	Sigma-Aldrich	>99
Sodium hydroxide	40.00	NaOH	Sigma-Aldrich	>98

4.3. Whole Oil Gas Chromatography

Both crude oils were measured with a WOGC apparatus form the 5890 Hawlett-Packard series II. The apparatus was equipped with a HP-ULTRA 2 column from Agilent technologies, with dimensions 25m×0.20mm×0.33µm. The output chromatogram was logged by the chameleon integrated software (v. 7.2) [73].

The crude oils were homogenized by heating to 50°C prior to measurement. A Hamilton syringe (10 µL) was utilized for injection of the warm sample. A sample volume of approximately 0.5 ±0.1 µL was injected trough the FID flame, which held an injection temperature of 260°C. Each measurement was done using a split injection with a 75:1 split ratio. The temperature program is displayed in **Table 4-5**. The syringe was washed three times with a 30:70 mix of DCM:MeOH, and then three times with hexane.

Table 4-5: Overview of the temperature program for WOGC.

Temperature / temperature interval [^{o}C]	Hold time [min]	Ramp [℃/min]	Time [min]
30	10	-	10
30 → 60	-	1.5	20
60	0	-	0
60 → 300	-	4.0	60
300	0	-	0
	Total measurement time:		**90**

4.4. Infrared Spectroscopy

All samples were analyzed with a Nicolet Protegè 380 FT-IR instrument equipped with an Attenuated Total Reflection (ATR) diamond crystal. The crude oils were homogenized by heating to 50°C prior to measurement. A background specter was recorded to determine if the crystal was cleaned properly before applying the crude oil samples. The sample spectra were recorded with a 32-bit scan, and the average peak values were reported in the OMNIC integrated software (v. 7.3). The crystal was carefully cleaned with ethanol before, after and in between each measurement. Four parallels were measured for each crude oil, and the mean specter was analyzed in Sirius [61] by means of PLS with discrimination analysis.

4.5. Density measurements

The density was measured using a DMA 60 density meter from Anton Paar which is measures the fluid density based on Anton Paar's law of harmonic oscillations. The density meter was equipped with a DMA 602 hollow, glass U-tube which holds 1 mL of fluid. The tube is placed inside a stainless steel tube that is surrounded by constant-temperature water from a connected water bath. The sample was injected into the hollow U-tube using a plastic syringe (5 ml). The oscillator was washed with the sample due for measurement prior to each measuring cycle. The sample is injected continuously until no air bubbles can be seen in the tube. The temperature can be assumed to be stable once period-readings are not fluctuating more than $\pm 1 \cdot 10^{-6}$.

The first measurement was water/air, to determine the instrumental constant (**Equation 2-6**). The crude oil samples are then measured analogously, by utilizing **Equation 2-6** and **Equation 2-7** for the density of air. A consecutive measurement for air is performed before

and after each measurement to validate the accuracy of the instrument. The oscillator was washed with toluene, ethanol and acetone before, after and in between measurements.

4.6. Asphaltene quantification

This method was adapted from the method reported by Fonnes [74]. The crude oil samples were homogenized by slow-heating minor samples on a water-bath. The samples were shaken vigorously every 15 minute until they reached a temperature of approximately 50°C. Sample masses of approximately 1 g homogenized crude oil was then weighed (±0.0001 g) in tared centrifuge glass-tubes. Four parallels were prepared for each crude oil.

The *n*-heptane volume was measured with a glass pipette (10 ±0.006 mL) equipped with a peleus balloon. The appropriate volume of *n*-heptane (calculated from **Equation 2-8**) was immediately added to the samples. Slow addition of *n*-heptane and continuous stirring will avoid high local concentration of precipitate [53]. The samples were immediately sealed with a Teflon-lined screw cap and placed in a heating cabinet at 40°C overnight. Higher temperatures were avoided due to the existence of short-chain alkanes found to be present by WOGC, which would pose problems with pressure build-up.

After being left to cool down to ambient temperature, the samples were put on a centrifuge at 2000 rpm for 10 minutes. The maltene fraction was then removed by a glass-pipette. The following additions of *n*-heptane serve to wash away residue of the maltene fraction, and is not though to promote any further asphaltene precipitation. The washing-procedure (addition of *n*-heptane, heating to 40°C, centrifuging and removal of maltene-fraction) was repeated until the addition of *n*-heptane no longer obtained a coloring from the asphaltene-residue.

After complete washing, the asphaltene precipitate and a small left-over maltene fraction from the last washing was left in a fume hood for two days, to allow the *n*-heptane solvent to dry off. The samples were then weighed, placed in an exicator for further drying, and then weighed again. Once the exicator had no further effect on the weight, the dry asphaltenes were quantified by means of weight per cent of original crude oil sample.

4.7. Interfacial Tension

4.7.1. Equipment

Measurements were carried out on the video-based optical contact angle measuring instrument (OCA20) from DataPhysics [75]. The OCA20 utilizes the SCA20 integrated data acquisition system. Due to the surrounding phase (water) being denser than the drop-phase (crude oil), an inverted needle is necessary. The inverted needle (**Figure 4-3**a) has an inner/outer diameter of 1.65/1.19 mm and is 19 mm in length. The glass cuvette has an inner volume of 8 cm^3. The OCA 20 is equipped with a high speed CCD camera, a light source and an automatically controlled piston for connecting the syringe (**Figure 4-3**).

a)

b)

c)
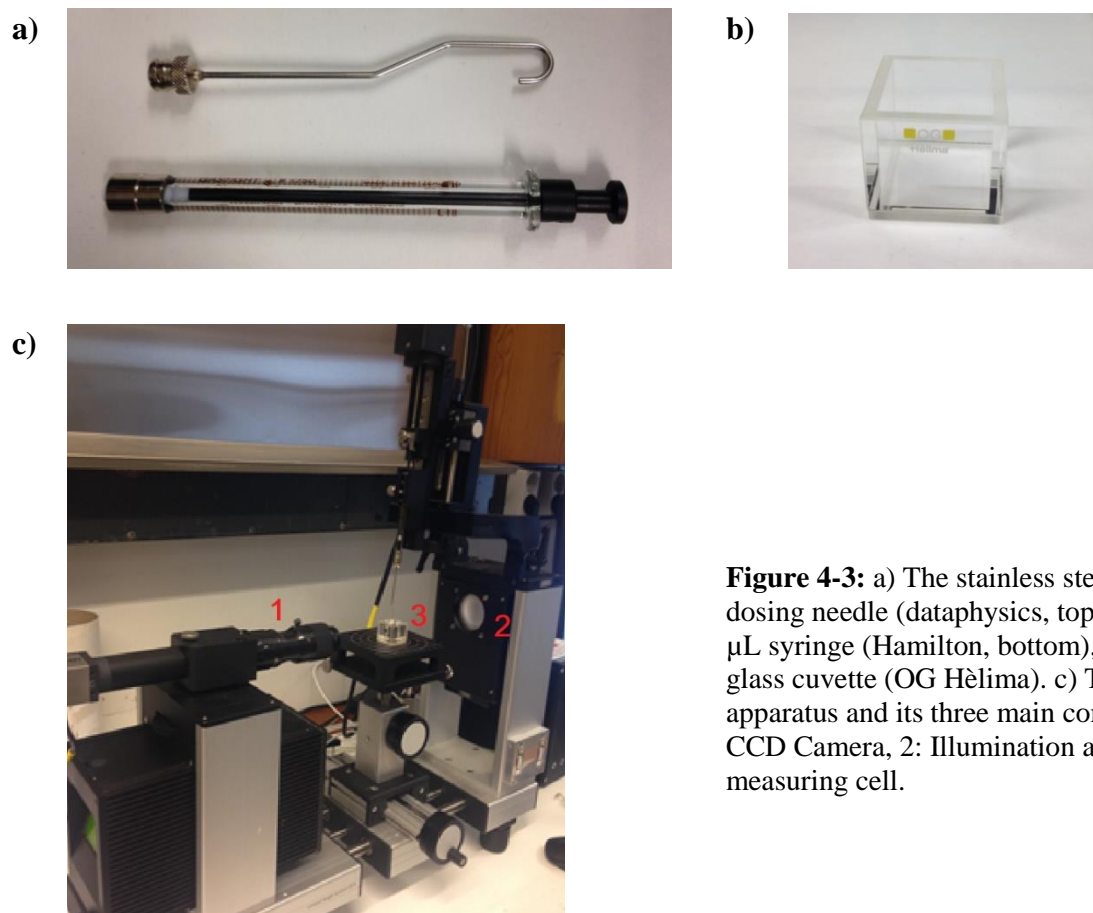
Figure 4-3: a) The stainless steel inverted dosing needle (dataphysics, top) and the 500 µL syringe (Hamilton, bottom), and b) the glass cuvette (OG Hèlima). c) The OCA20 apparatus and its three main components; 1: CCD Camera, 2: Illumination and 3: measuring cell.

4.7.2. Sample preparation

Appendix II contains tabulated values for water compositions for each experimental design. The desired water composition was prepared by weighting (± 0.0001 g) and then left to stir for 2 – 3 hours until all the salt was dissolved. The initial pH (pH_i) of the water phase is regulated using 1 M unbuffered solutions of HCl and NaOH. The concentration of NaOH and Ca^{2+} was kept below the solubility product in order to avoid $Ca(OH)_2$ precipitation.

The crude oil was homogenized by heating it on a water bath. The lid was loosened slightly to avoid pressure build-up upon heating. The glass bottle was carefully shaken from side to side and up-side-down every 15 minutes until it reached a temperature of 50^oC. A CO/W emulsion was prepared in by adding 1 mL of crude oil, followed by 15 mL of water to produce a 7% CO/W emulsion. The water-phase was added to the oil-phase in portions of ~1 mL by a glass-pipette, which allowed the two phases to mix. No additional shaking or stirring was performed. For all emulsions except for certain basic pH compositions, the crude oil started creaming momentarily after adding the water-phase, and an unstable emulsion is obtained within seconds.

The CO/W system is left to equilibrate for 24 hours before the IFT-measurement in cases where the pH was included as a variable. The water phase was then extracted into a beaker by penetrating the oil phase with a glass pipette. A consecutive extraction was necessary to obtain a clear water phase. The final water phase pH (pH_f) was measured with a metrohm pH-meter equipped with a metrohm Cl-Ag calomel electrode. The electrode was calibrated prior to measurements, using metrohm buffer solutions in the range pH 2 – 12. The water phase was then transferred to the measurement cell and the oil phase in drawn into the syringe.

4.7.3. The Pedant-drop Method

The Pendant-drop method determines the profile of the drop of one liquid suspended in another liquid at mechanical equilibrium [12, 43, 75-77]. The pendant-drop is a transient method, i.e. the ratio of mass to interfacial area is set at the beginning of the experiment. Thus, changes in the interfacial area can be modeled as a function of interfacial age [23]. The shape of the pendant drop is influenced by two main forces; (1) the gravitational force and (2) the IFT between the drop phase and the surrounding phase. The relationship between these is quantified by the shape parameter (**Equation 4-5**), derived by Bashford and Adams [78]. For B ~0, IFT dominates the force acting on the drop, and the drop is almost spherical. For

0<<B<1, the gravitational force deforms the drop. The extent to which a spherical form is obtained is proportional to the IFT between the drop and the surrounding phase. This technique is denoted drop-shape analysis [75].

$$B = -\frac{R_0^2 \vec{g} \Delta\rho}{\gamma}$$

Equation 4-5

Where B is the shape parameter, R_0 is the radius of curvature at the apex of the drop, g is the gravitational constant, $\Delta\rho$ is the density-difference between the two phases and γ is the IFT. Additionally, the IFT can be modeled as displayed by the Harkins and Brown [79] equation (**Equation 4-6**).

$$\gamma = \frac{V\Delta\rho\vec{g}}{d\pi F}$$

Equation 4-6

Where V is the drop-volume, d is the diameter of the needle and F is a dimensionless empirical correlation-constant fitted by the drop shape analyzer. The remaining parameters are analogous to **Equation 4-5**.

The procedure for IFT measurements with the pendant drop method was adapted from the OCA20 user manual available at the laboratory [75]. The integrated SCA20-software served as a digital interface for dispensing the drop and logging the dynamic IFT (**Figure 4-4** a and b). The IFT of *n*-decane was used as a standard reference for validating IFT-measurements of the crude oils. The IFT of *n*-decane was measured prior to –and after all crude oil measurements.

Some test runs were performed initially to determine the best suited drop-volume. By checking the box for "continuous dosing", the drop is dispensed until stopped manually. The ultimate drop volume is that in which the drop is stable with respect to the buoyancy force (does not slip the tip of the needle) but as large as possible. After this volume is decided, the drop dispense rate can be set to "Very fast".

The lines depicted in **Figure 4-4**a are set at the far left side of the drop, each side of the needle tip, and the far right side of the needle. Preferences are set to detecting "right drop", to allow for maximum drop coverage of the screen. The "Dynamic Tracking"-setting is enabled at 2 frames pr. minute. This setting allows for an automatic drop-curvature detection and Young-Laplace fitting (**Equation 4-5**) every 30 seconds. The dynamic tracking was enabled

immediately after the drop was dispensed, and continued for 60 minutes[2]. The glass cuvette and needle (and syringe, if the oil phase is to be changed) was washed three times with toluene, ethanol and water before, in between and after each experiment.

a)

b)

c)
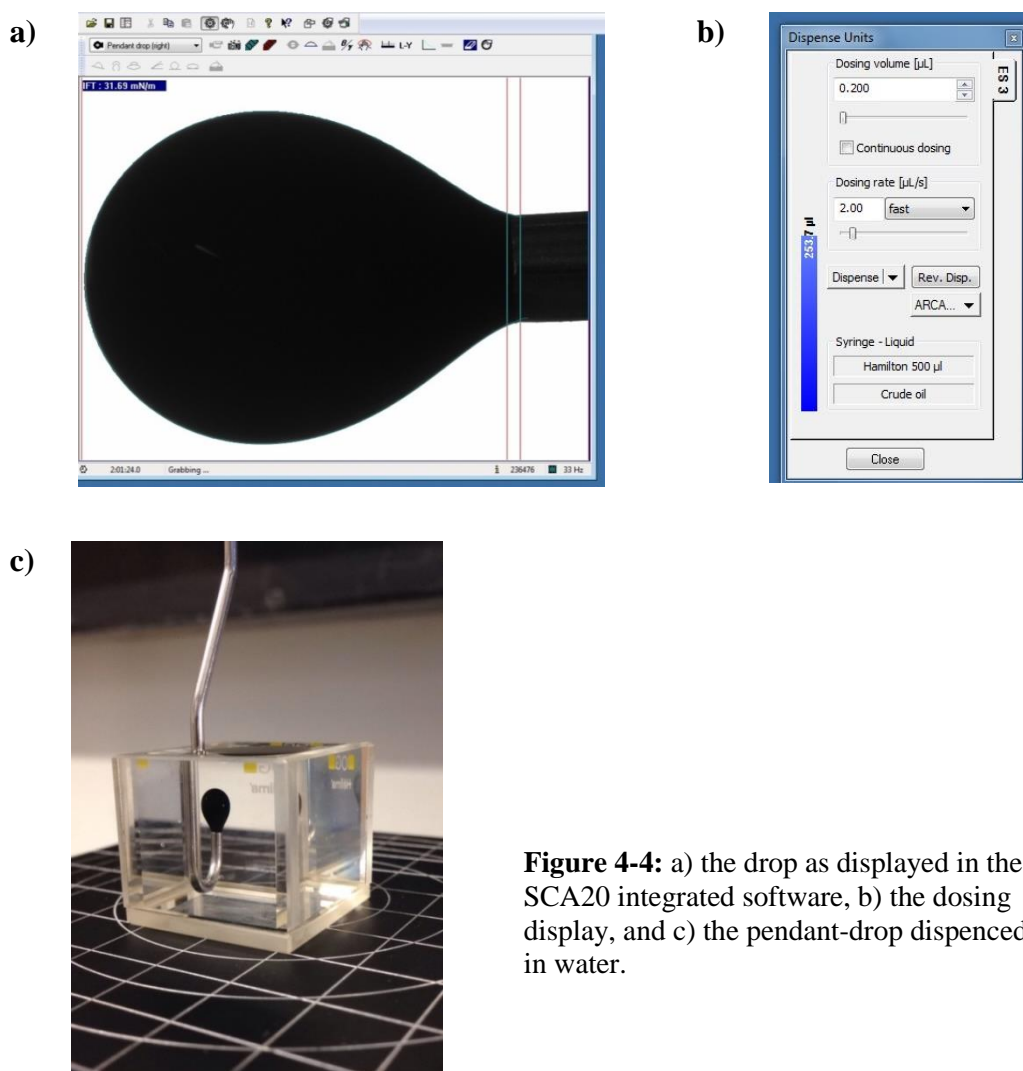
Figure 4-4: a) the drop as displayed in the SCA20 integrated software, b) the dosing display, and c) the pendant-drop dispenced in water.

It is important to note that the IFT of all samples were evaluated exclusively in terms of drop curvature. The density-difference between the crude oil and water phase was kept constant at $\Delta\rho=0.15$ g·cm^{-3} for the IFT-calculation by the Young-Laplace fitting for all samples. The consequence of this is that the calculated IFT will only be affected by the relative changes in the independent variables, recorded exclusively as their effect on drop-curvature. However, this thesis is also concerned with the actual IFT-values between the crude oils and water. This property is of interest in comparative studies, which is carried out in this thesis as the meta-

---

[2] Only applies to main experiments. Screening experiments continued until $|\Delta IFT/\Delta DA|<0.05$ mN·m^{-1} for at least 10 consecutive minutes, which resulted in measurement times varying from 0.5 hours to 3 hours.

analysis of Buckley and Fan's CO-Wet database. Thus, the IFT between crude oil and pure water, and crude oil and 0.1 M NaCl, will be measured with the actual fluid densities measured for the crude oils.

4.7.4. Determining the equilibrated IFT

Failing to apply a systematic method for deciding the equilibrated IFT can introduce biased data, and is hence an important part of the experimental method. The most common method is choosing a sufficiently long equilibration time, and therefore letting the mass transfer across the interface run its course. This time-scale varies between 2000 seconds and 24 hours within the inspected literature, but equilibration of the IFT is considered obtainable within 1000 seconds for most CO/W systems [22, 29, 41]. In this thesis, a method has been proposed for calculating an estimate of the equilibrium IFT after a 1 hour experimental run. A calculated example of the method is given in Appendix I, and a validation of the method is discussed in chapter 5.5.

4.8. The CO-Wet database

Buckley et al. [17, 23, 42, 43, 80, 81] have, in cooperation with the US Department of Energy, developed a Crude oil-Wettability (CO-Wet) database. All IFT measurements were recorded with the Pendant-drop method. The experiments utilized the OCA20 apparatus, by fitting the drop shape to the Young-Laplace equation (**Equation 1-4**). The IFT was estimated by using a model in **Equation 1-5** with a total measurement time of 2000 seconds.

IFT measurements with varying pH and brine salinity were carried out for 41 crude oil samples, to inspect whether crude oil properties are predictive of IFT, and vice versa. This is meant to facilitate core analysts in the task of relating capillary pressure measurements to different fluid pairs, or to design core floods with model fluids. This database is highly relevant to this thesis, due to the comprehensive set of variables and crude oils utilized, thus exploiting the full potential of multivariate methods. **Table A-8** in Appendix IV reviews the variables included in the dataset. In this thesis, the CO-Wet database has been fitted to a PLS regression model, to inspect whether findings in this experimental work can fit into the correlations found in the CO-Wet database. Variable covariance has also been inspected by extracting a PCA loading plot. Both analysis were performed in the Sirius 9.0 software [61].

5. Results and discussion

5.1. Whole Oil Gas Chromatography

The chromatogram for both crude oils was interpreted by comparing it to the chromatogram obtained for Norwegian Standard Oil[3] (NSO) [82].
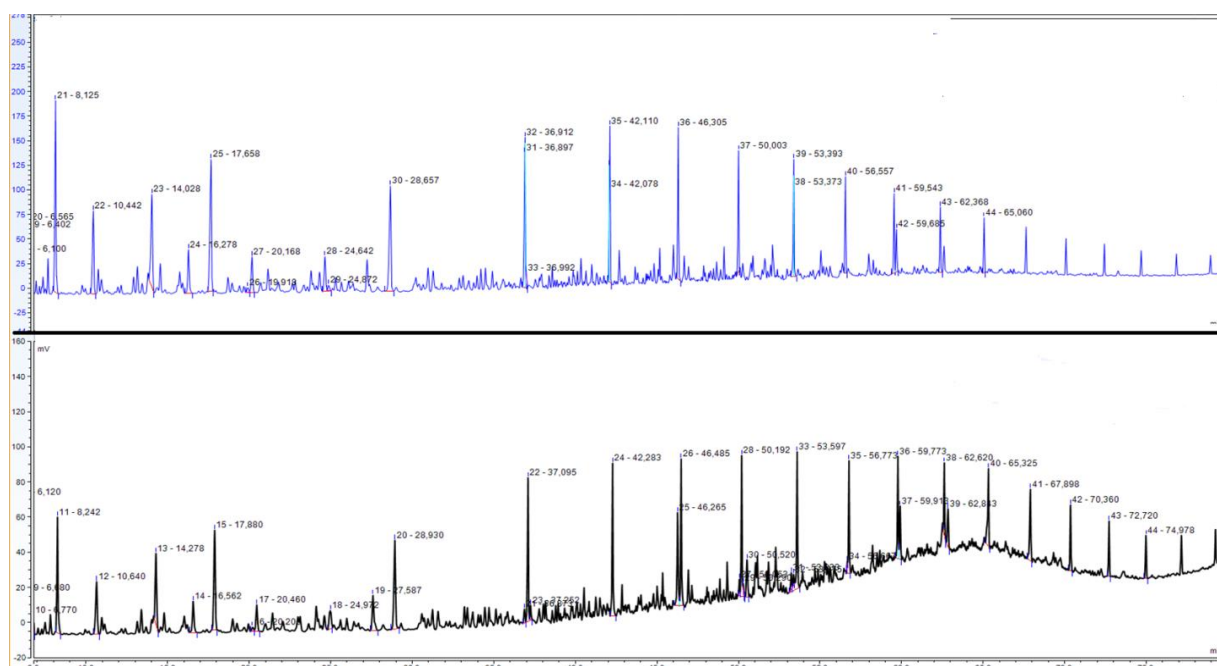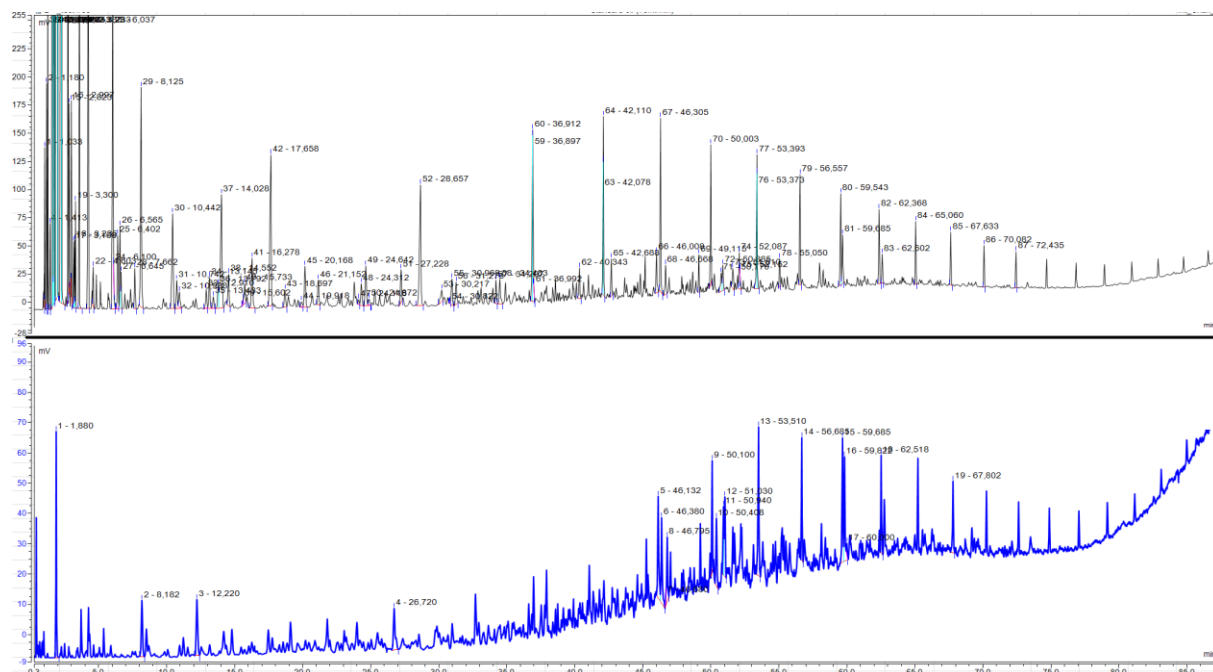

Figure 5-1: A comparison between the WOGC-chromatograms for Norwegian Standard Oil (NSO, top) and crude oil B (bottom). The y-axis is in units of mV, while the x-axis shows time in units of minutes.

It can be seen from **Figure 5-1** that crude oil B is highly comparable to NSO. The presence of short hydrocarbons and small naphthenes can be seen by the peaks early the temperature-program. Larger hydrocarbons (nC_{10+}) in the characteristic normal-distribution start at 37 minutes, until the reference double-peak for pristane occur at 65 minutes. The following peaks are high boiling point waxes (nC_{20+}) that elute slowly at temperatures close to $300^{o}C$.

Crude oil B contains a quite large unresolved complex mixture (UCM) at 60 – 70 minutes. This indicates biodegradation of the oil. However, smaller hydrocarbons are still present, which implies that this process is most likely in the starting phase. To the contrary, the UCM observed in crude oil A (**Figure 5-2**) is accompanied with a very low abundance of small

---

[3] A full chromatogram of NSO from the Norwegian Industry Guide to Organic Analyses (NIGOGA) can be found at http://www.npd.no/engelsk/nigoga/default.htm

hydrocarbon components. This is a clear sign of biodegradation, due to microbial degrading preferring short-chained hydrocarbons while leaving larger molecules [83]. The peak at 1.880 minutes is the nC_6 peak from hexane, which was used for washing the needle. Therefore it is not likely to be a part of the composition in crude oil A. However, the four shorter peaks following the nC_6-peak may be recognized as benzene and cyclohexane, followed by the more separated peaks that may be toluene. Larger hydrocarbons (nC_{13+}) and waxes (nC_{20+}) can be located from 45 minutes into the temperature program.

Figure 5-2: A comparison between the WOGC-chromatograms for Norwegian Standard Oil (NSO, top) and crude oil A (bottom). The y-axis is in units of mV, while the x-axis shows time in units of minutes.

5.2. Infrared Spectroscopy

The results from IR-spectroscopy were analyzed by PLS-regression, where the IFT was chosen as the dependent variable. The IFT value of choice was the mean of the centerpoints from the FCD, which was 24.4 ±0.9 mN·m^{-1} and 27.6 ±0.4 mN·m^{-1} for crude oil A and B, respectively. Four parallells were executed for each crude oil. The scores dendrogram from discrimination analysis (**Figure 5-3**) clearly shows that two separate classes (i.e. crude oil samples) are modeled. The mean of the four parallels were used for the PLS-analysis. Peaks were characterized in accordance with characteristic vibrational frequencies reported by Pavia et al. [49].
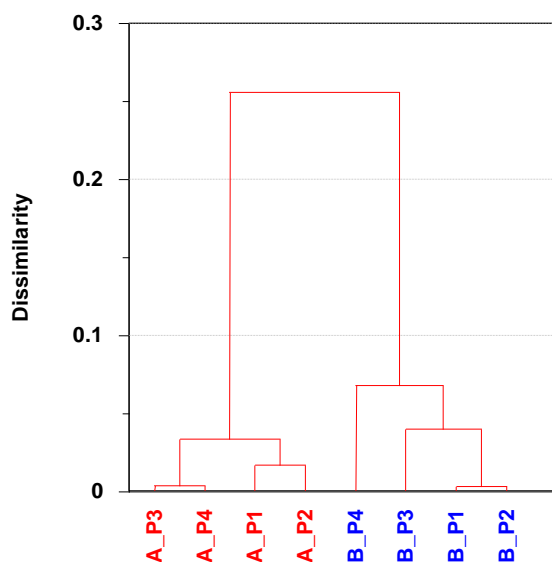
Figure 5-3: Scores dendrogram of parallels for crude oils A and B.

Figure 5-4 compares the spectra of both crude oils and the weighted regression coefficients from the PLS-analysis. Positive regression coefficients correspond to frequencies that have higher adsorbance in crude oil B, while negative coefficients (all wavelengths >730 cm^{-1}) correspond to frequencies that have higher adsorbance in crude oil A. This can also be seen from comparing the two spectra (red = crude oil A and blue = crude oil B).

The PLS regression coefficients (**Figure 5-4**) shows that the highest discrimination power between the two crude oils can be found in the aliphatic C-H stretching region (2835 – 2962 cm^{-1}). The regression peaks pointed out in **Table 5-1** shows that both crude oils have vibration peaks at 2853 cm^{-1} and 2920 cm^{-1}, corresponding to the CH$_2$ stretching region. The minor peak at 2950 cm^{-1} is comparable with the CH$_3$ stretching region (2962 cm^{-1}). The CH$_2$ stretch dominates this region for both oils, which could indicate the presence of naphthenes.

Figure 5-4 also shows that none of the oils appear to contain phenols (3100 – 3700 cm^{-1}), although the baseline for crude oil A indicates higher absorbance in this region. However, the most important peak in the discrimination is that located at 1708 cm^{-1}, which is only adsorbed in crude oil A. This is the typical carboxylic acid C=O stretching-region. A slightly predominant adsorption in the carboxylic acid O-H stretching-region for crude oil A (pointed out in **Figure 5-4**) can also be seen. A close-up of this region is displayed in **Figure A-2**b in Appendix III.
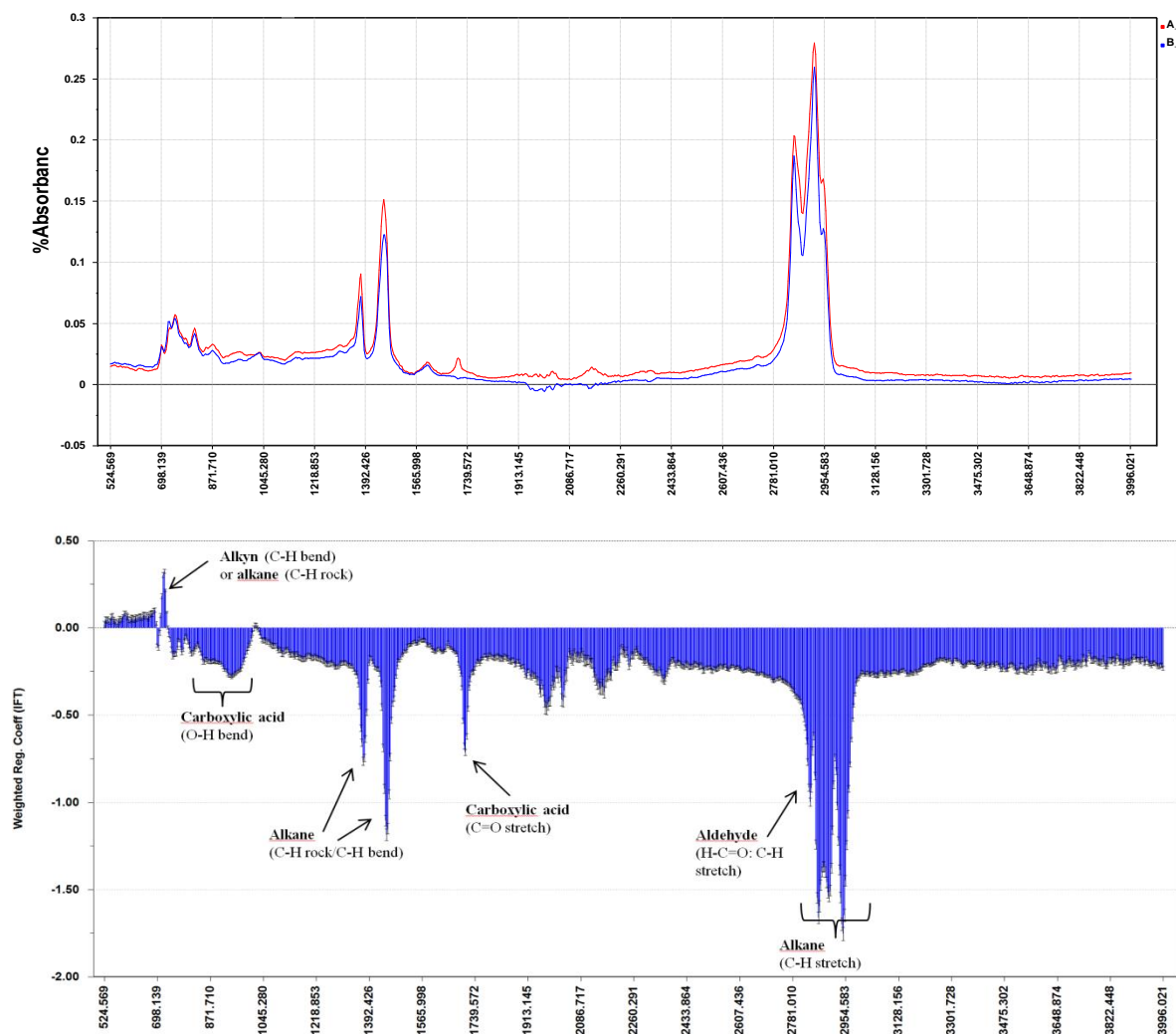
Figure 5-4: Top: the collected spectra for the mean of four variables for crude oil A (red) and B (blue). Bottom: weighted regression coefficients from PLS regression with IFT as the dependent variable.

Table 5-1: Summary of the most important regression coefficients from PLS-regression.

Regions with high regression	Frequency of max. regression	Possible fuctional group	Bond type	Attributed to
860 – 970 cm^{-1}	945 cm^{-1}	Primary and/or tertiary amines	N-H wag	Higher adsorbance in A
		Aromatics	C-H "oop"	
		Carboxylic acids	O-H bend	
1365 – 1380 cm^{-1}	1373 cm^{-1}	Alkane	C-H rock	Higher adsorbance in A
1440 – 1465 cm^{-1}	1450 cm^{-1}	Alkane	C-H bend	Higher adsorbance in A
1701 – 1713 cm^{-1}	1708 cm^{-1}	Carboxylic acids	C=O stretch	Peak only found in A
2820 – 2980 cm^{-1}	2839, 2866, 2900, 2947 cm^{-1}	Aliphatic alkanes	C-H stretch	Higher adsorbance in A

Figure A-2 in Appendix III compares some of the absorbance-bands of interest. The fingerprint-region (Figure a) shows that the overall composition of both crude oils consists of aromatics and saturates, as well as some nitrogen-containing compounds. No notable differences can be found in this region, despite the previously discussed observation that crude oil A exhibits a higher absorbance. This is with the exception of the region from 500 – 700 cm^{-1}, which is the only region where crude oil B has higher absorbance. This may be due to aliphatic amines or C-O stretching in esters or ethers. These may be associated with asphaltenes, which are found to be significantly more abundant in crude oil B than in crude oil A (**Table 5-3**).

The spectra of all parallels for the two crude oils in **Figure A-1** (Appendix III) shows large deviations between parallels in the region 1800 – 2040 cm^{-1}. Thus, these regression coefficients should not be interpreted in terms of crude oil characteristics.

In summary, chromatographic and spectroscopic data indicate that crude oil A may be higher in naphthenes, and presumably significantly higher in naphthenic acids than crude oil B. The composition in crude oil B is more concentrated in short-chain saturates than crude oil A, and is generally more "average" in its composition. This can be suggested based on the similarity between the chromatogram of Norwegian Standard Oil.

5.3. Density and asphaltene quantification

The results from the density measurements in **Table 5-2** show that crude oil densities are not significantly different. Thus, the oils cannot be discriminated based on dissimilarities in concentrations of heavy crude oil components. However, it means that both crude oils are characterized as medium density oils (**Table 2-1**). Many comparative studies concerning the CO/W interfacial system compare heavy and light oils [10, 28]. Therefore, it is of interest to compare two medium oils, thus discriminating their interfacial activity as a result of other factors than differences in the concentration of heavy species.

Table 5-2: Results from density measurements and API gravities calculated from **Equation 2-3**.

Crude oil	Fluid density [g·cm^{-3}]	API gravity	Category
A	0.905 ±0.005	24.4^{o}	Medium
B	0.895 ±0.005	26.1^{o}	Medium

It was found that the asphaltene content in crude oil B is over 8 times as high as in crude oil A. **Table 5-3** gives an overview of the results from the quantification of asphaltenes in the two crude oil samples. The last parallel for crude oil B was removed due to the asphaltene wt% being estimated at 52 %. This value is unrealistically large, and indicates that a random experimental error has occurred during weighting. The uncertainties are calculated from the principle of propagation of error (see Appendix I). The error in mean calculations also includes the standard deviation between parallels.

Table 5-3: Results with uncertainties from asphaltene quantification, with calculated mean wt% asphaltene in crude oil samples.

Parallels	Weight of crude oil sample [m ±0.0001g]	Volume of n-heptane flocculant [V ±0.006 mL]	Weight of asphaltene precipitate [m ±0.0001g]	wt% asphaltene in crude oil [% ±0.02 %]
A-1	1.0080	22.281	0.0034	0.34
A-2	1.0054	22.220	0.0034	0.34
A-3	1.0002	22.100	0.0034	0.34
A-4	1.0090	22.305	0.0031	0.31
			Mean, Crude oil A	**0.33 ±0.02**
B-1	1.0029	22.411	0.0278	2.77
B-2	1.0029	22.411	0.0280	2.79
B-3	1.0023	22.398	0.0276	2.75
			Mean, Crude oil B	**2.77 ±0.02**

5.4. Preliminary studies

Some preliminary experiments were performed prior to and during the screening experiments to inspect the validity of the OCA20 apparatus, the effect of drop volume on pendant-drop measurements and the effect of equilibrating the crude oil and water phase prior to measurement.

5.4.1. Validating the OCA20

n-decane was used as a standard reference for validating the OCA20 apparats. Goebel and Lunkenheimer [84] reported an equilibrium IFT value of 52.3 mN·m^{-1} for *n*-decane in distilled water at 22$^{\text{o}}$C degrees by the pendant-drop method. However, this value was recorded after purifying the *n*-decane phase to remove impurities at the interface. The cited

value was obtained after 5 purification cycles, and did not show any time-dependent IFT decay. Such precautions are outside the scope of this study, and therefore it is satisfactory to reproduce the IFT values reported prior to complete purification. This was in the order of 42 – 51 mN·m^{-1} [84]. **Table 5-4** lists the initial and equilibrium IFT-values, as well as the %-decay for ten IFT-measurement between *n*-decane and distilled water at ambient conditions.

Table 5-4: Recorded IFT values for *n*-decane in distilled water with drop volumes of 45 μL. The bottom row contains mean values with standard deviation.

Initial IFT (T= 0 min) [mN·m^{-1}]	Equilibrium IFT (T= 20 min) [mN·m^{-1}]	Decay [%]
51.1	45.0	11.9
52.0	46.3	11.0
52.1	45.6	12.5
49.9	44.7	10.4
50.8	45.8	9.8
50.4	44.7	11.3
51.6	46.9	9.1
51.5	47.0	8.7
51.5	46.3	10.1
51.9	47.5	8.5
51.3 ± 0.7	**46.0 ± 0.9**	**10 ± 1**

Table 5-4 shows that the IFT between *n*-decane and distilled water has an average decay of 10 ±1%. This implies that some contaminations were present, either in the *n*-decane drop-phase or in the continuous water phase. The supplier of *n*-decane reports impurities of <0.5%, which may cause some interfacial activity if it is present in this batch. Ethanol and distilled water have been utilized for the washing procedure for the sample cell and needle. If the ethanol is not completely washed away before measurement this can be an effective surfactant in the *n*-decane/water system. Precautions were taken when measuring the crude oil samples in terms of washing the measurement cell and needle thoroughly with distilled water before introducing the crude oil.

The obtained equilibrium value for *n*-decane had a standard deviation of ±0.9 mN·m^{-1}, which is satisfactory, but still quite large. If ethanol-contaminations are present, this may be the reason for certain low IFT-measurements biasing the mean value. Thus, parallel measurements were also carried out for crude oil samples to inspect the standard deviation.

5.4.2. The effect of drop volume

The IFT-measurements in the first screening design were measured with varying drop volumes. The drop volume for each water composition was determined as the largest volume

that can be dispensed without the buoyancy force detaching the drop from the needle. The IFT is directly proportional to the drop volume by **Equation 4-6**. The effect of drop volume of pendant drop measurements has been reported to not cause inconsistencies as long as certain experimental conditions are met [41, 77]. For instance, the IFT has been found to vary with drop volume if the drop volume has been below a certain value [41]. The drop volumes found sufficient in the screening design varied between 16.5 – 88.1 µL, and had an average value of 68.3 µL.

To validate the potential volume-dependency the PCA-model was derived with and without drop volume as an independent variable. The loading-plots can be compared from **Figure A-2** in appendix IV. There is no significant difference between the variable correlations, and the model only loses 0.3 % of its explanatory power upon excluding drop-volume as a variable, which is relatively insignificant. Additionally, the reproduced correlation (**Equation 4-2**) between the equilibrium IFT and drop volume is $r^2=0.99$. Thus, they carry the same information, and do not have to be modeled as two separate variables. Therefore, it was concluded that the IFT can be considered to be independent of drop volume in the following experimental work.

5.4.3. The effect of phase-equilibration

The three-dimensional FCD also models the effect of pH. Therefore, all water phases were pre-equilibrated with the crude oil phase, analogously as in the first screening design. This introduced some differences in the equilibrium IFT when comparing the two- and three-dimensional FCD's at neutral pH. Such effects are of crucial importance when considering the validity of laboratory results in the realistic reservoir system.

Table 5-5 compares the equilibrium IFT between equilibrated and non-equilibrated samples when there is no NaOH in the water phase. It can be seen that the equilibrated samples for crude oil A have a consistently higher IFT than the non-equilibrated samples, even though the water composition is unchanged. For crude oil B, the effect of phase-equilibration is insignificant. The differences could possibly be attributed to a higher concentration of polar acids hypothesized to be present in in crude oil A, which could potentially solubilize in the water-phase once they dissociate. The pH-profile in **Figure 5-5** indicate that some mass transfer of acidic species are taking place at neutral pH for crude oil A. Crude oil B does however not appear to transfer any significant acid concentration upon equilibration with the water-phase.

Table 5-5: A comparison of equilibrium IFT obtained for equilibrated and non-equilibrated samples at neutral pH. Uncertainties are based on the standard deviation between centerpoints in the two FCDs.

	Crude oil A			Crude oil B		
	γ_{equil} ± 0.9 [mN·m^{-1}]	$\gamma_{non\text{-}equil}$ ± 0.2 [mN·m^{-1}]	$\gamma_{equil} - \gamma_{non\text{-}equil}$ ± 1.1 [mN·m^{-1}]	γ_{equil} ± 0.6 [mN·m^{-1}]	$\gamma_{non\text{-}equil}$ ± 0.4 [mN·m^{-1}]	$\gamma_{equil} - \gamma_{non\text{-}equil}$ ± 1.0 [mN·m^{-1}]
I=0.03 / X_{Ca2+}=0.00	37.4	30.2	**7.2**	35.3	34.3	**1.0**
I=0.03 / X_{Ca2+}=0.09	34.2	29.2	**5.0**	34.5	34.7	**-0.2**
I=0.65 / X_{Ca2+}=0.00	25.0	21.9	**3.1**	26.8	26.9	**-0.1**
I=0.65 / X_{Ca2+}=0.09	24.5	22.5	**2.0**	26.5	27.7	**-1.2**
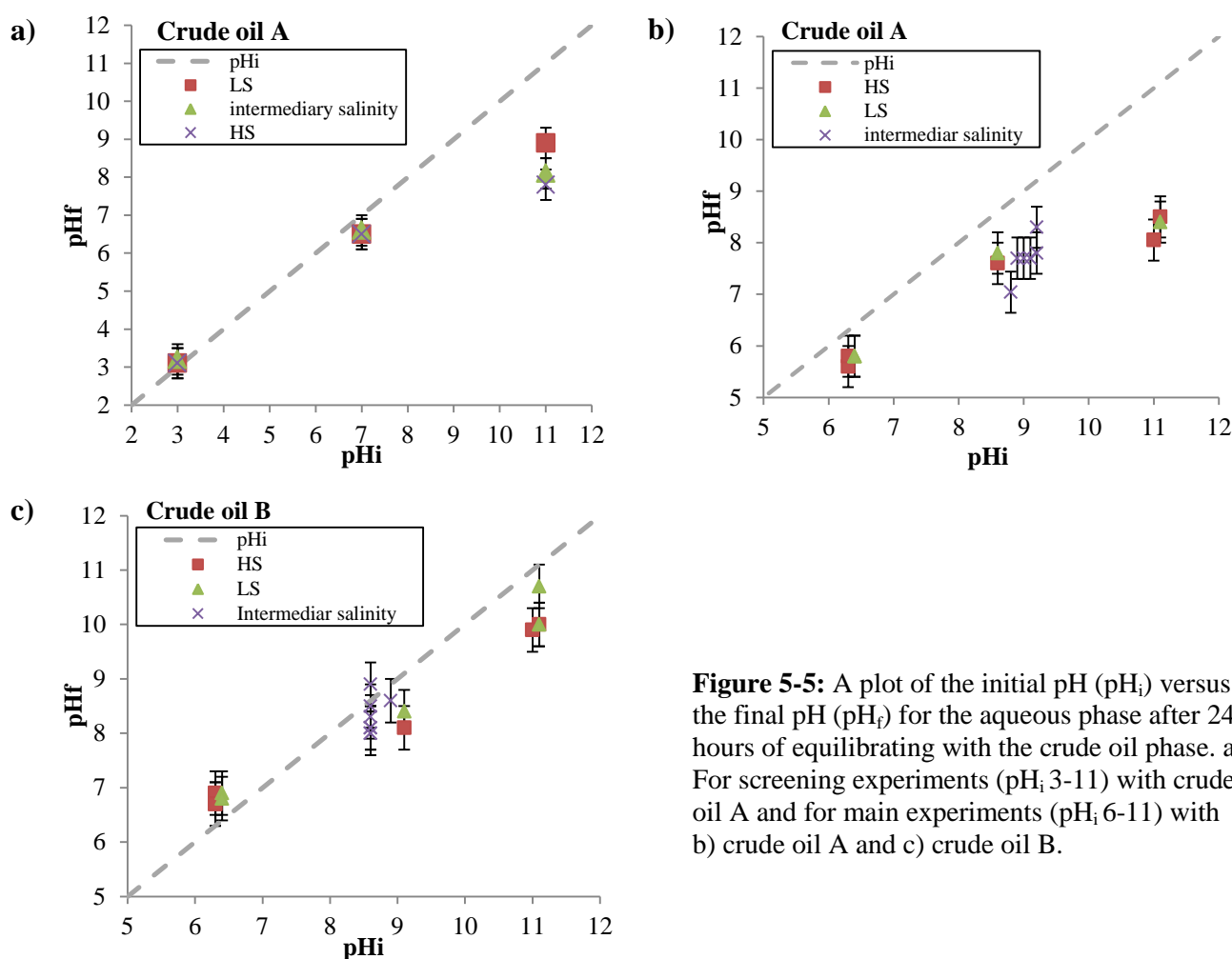
Figure 5-5: A plot of the initial pH (pH$_i$) versus the final pH (pH$_f$) for the aqueous phase after 24 hours of equilibrating with the crude oil phase. a) For screening experiments (pH$_i$ 3-11) with crude oil A and for main experiments (pH$_i$ 6-11) with b) crude oil A and c) crude oil B.

The dynamic processes known to take place in the CO/W system is considered to be initiated by interfacial adsorption of amphiphilic molecules, followed by interfacial reactions. The

following step is thought to be the slow reorganization at the interface, and mass transfer of hydrophilic species produced at the interface by convective diffusion [19, 22, 24, 31]. For the equilibrated samples, these reactions and solubilizing of reaction products may be considered to be more or less completed within the 24 hours equilibration time. For the non-equilibrated samples, however, the interfacial adsorption and reactions will be initiated first when the crude oil drop is dispensed into the water-phase. This may explain why equilibrated samples measure a higher equilibrium IFT for crude oil A.

This explanation could possibly have been validated by increasing the measurement-time of the non-equilibrated samples, to reveal the possible existence of a minimum in the dynamic IFT. This minimum would indicate that the interfacial adsorption and reactions was completed and mass transfer of hydrophilic reaction products start. Thus, interfacially active species desorb from the interface and solubilize in the water bulk, which would increase the IFT. However, the kinetics of these processes is not of main interest to this thesis. It is however interesting to observe that the two crude oils are so differently affected by the equilibration. This may provide important information about the relative concentration of hydrophilic species in the two oils. Thus, it could be hypothesized that crude oil A contains higher concentrations of naphthenic acids with pK_a below neutral pH, which are composed of one to three ring-structures, as was reported by Havre et al. [31].

It may also be hypothesized that surface active dissociated acids have desorbed from the interface to create micelles in the water-phase, which has been reported to be an important part of the acid/base equilibria (**Figure 1-4**) [31]. However, these have been found to occur once the concentration of dissociated acids is sufficiently high, which is very unlikely at neutral pH. At pH 11, however, **Figure 5-5** shows that the acidic concentration of the water-phase has been raised considerably for crude oil A. No non-equilibrated samples were performed at this pH, and the hypothesis can therefore not be validated.

One more observation should be addressed: the increase in IFT for equilibrated samples of crude oil A are significantly more pronounced when the aqueous phase has a low ionic strength. This may indicate that the aqueous solubility of dissociated acids decrease with increasing ionic strength of the system, i.e., there is a salting-out effect. This may also be a result of lower interfacial pH at low ionic strength, which has been suggested by Cratin [59]. If so, this would repress the interfacial dissociations of acids, thus explaining the observed increase in IFT compared to higher ionic strengths.

5.5. Validation of method: equilibrium IFT

The method for deciding equilibrium values for IFT is described in Appendix I. In a less systematic manner, equilibrium conditions can also be found by inspecting the dynamic IFT visually. This can be used to set a threshold for where the time-dependency is insignificant, and furthermore, where the dynamic tracking can be terminated. This method was used in the first screening design with crude oil A. Equilibration times varied from 17 to 171 minutes, and had an average value of 75 ±47 minutes (**Table A-9**, Appendix V).

As can be seen from **Figure 5-6**a, most of the decay takes place <5 minutes. After 25 minutes, there is some alteration of increase and decrease in the IFT, indicating that some time-dependent change is caused by experimental drift. By enlarging the region >5 minutes (**Figure 5-6**b), it can be seen that after 20 minutes, every successive 10 minute increase in drop age produce 5 – 7 measurement points that fall outside a threshold of $|\Delta IFT/_{\Delta DA}| < 0.05$ mN·m^{-1} per minute (indicated by the dotted lines).
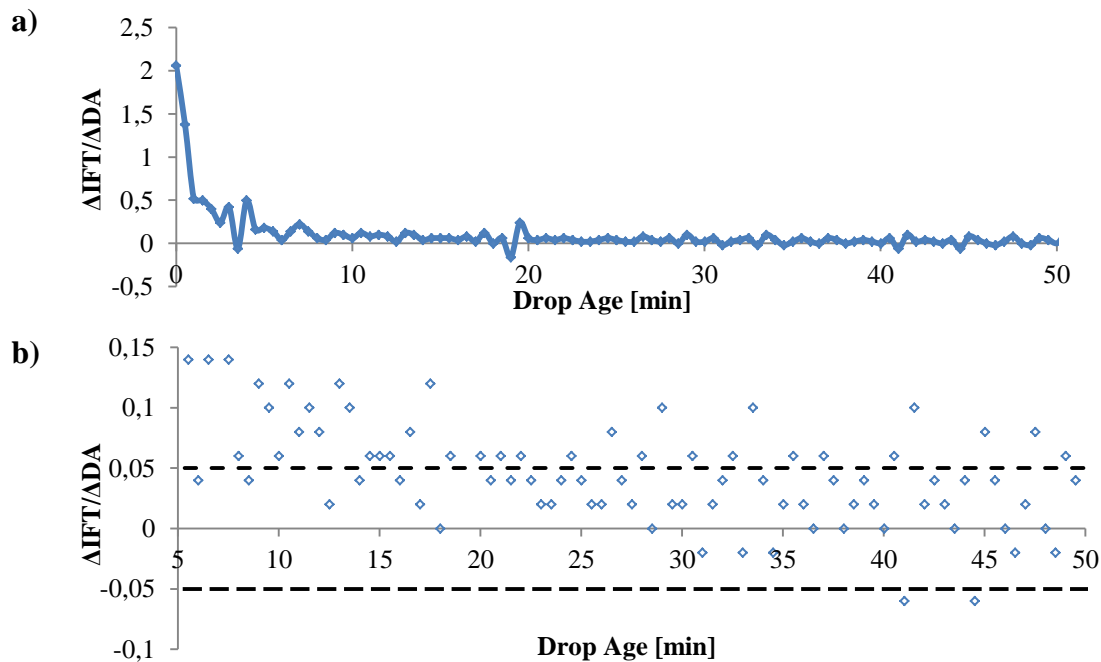
Figure 5-6: a) ΔIFT/ΔDA vs. drop age for a 50 min experimental run. b) A closer look at the dynamic IFT after 5 minutes of measurement.

The advantage of this method is that it demands a shorter measurement time and that the point of equilibrium can be decided based on eying up the dynamic IFT curve directly (no calculations needed). The disadvantages are that it is a less accurate method because the time-dependency of the IFT is not necessarily obvious until a full 60 minute experimental run is

completed. Also, the crude oil –and water composition are known to affect the time-dependency of the IFT [13, 23, 29, 32, 41]. The first screening design showed that the equilibrium drop age varies to a large extent in between compositions, and therefore cause higher variation in equilibrium IFT. Also, there is no intuitive way of calculating the error in the equilibrium IFT.

In comparison, **Figure 5-7** shows the approximation of the point of equilibrium through a regression line that has a minimum at the point of flattening, i.e. where $\partial IFT/\partial DA = 0$. The advantage of this method is that is offers a more consistent method that does not introduce large differences in measurement time (most equilibrium points fall within 60 ±10 minutes), and hence it compares equilibrated IFT-values at more equal terms. The disadvantages are that it demands a longer experimental run and that it introduces inaccuracy by approximating a regression line. The extent to which this inaccuracy affects the results can be quantified by the coefficient of determination (R^2), which poses an advantage with respect to error-calculations.

$$IFT = 0.0016(DA)^2 - 0.139(DA) + 24.143$$
$$R^2 = 0.9045$$
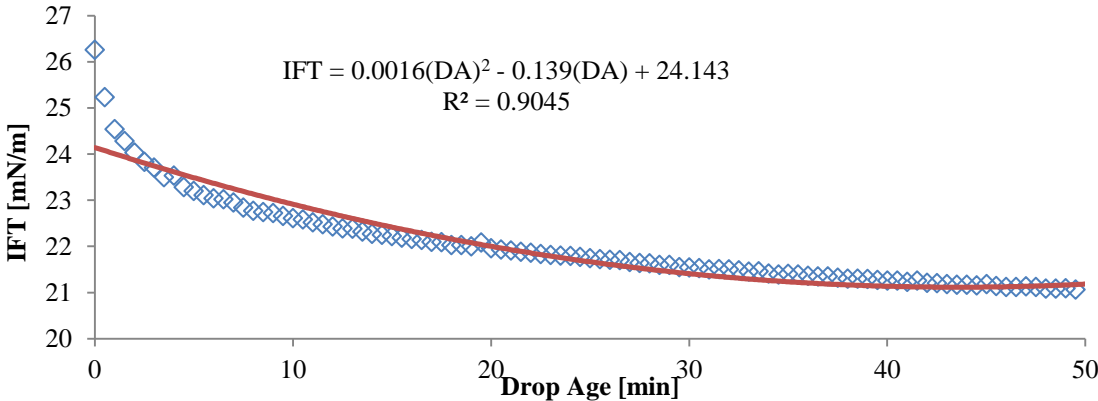
Figure 5-7: A display of the fit for the 2nd degree polynomial regression line calculated by excel analysis tools.
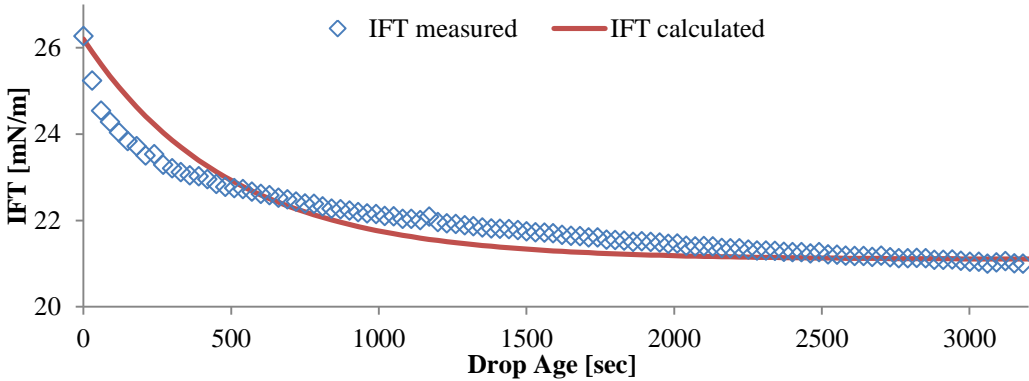
Figure 5-8: A display of the fit for the exponential decay function (**Equation 1-5**) for the best fit for the relaxation time (τ).

A third method for comparison is the monoexponential decay-model (**Equation 1-5**) as displayed in **Figure 5-8**. By comparing **Figure 5-8** and **Figure 5-7** it can be seen that the curve-fit supplied by the 2nd degree polynomial has a better overall fit with the slowly decaying dynamic behavior that occurs after reorganization. However, this curve does not account for the reorganization phase that has been suggested for the initial decay [13, 23, 29, 32, 41, 43]. The decay-function approximates the time-scales for reorganization by fitting the coefficient for interfacial reorganization (τ) to the expression in **Equation 1-5**.

For the curve modeled in **Figure 5-8** the interfacial reorganization obtains the best fit for $\tau=488$ seconds, or approximately 8 minutes. This value is considerable higher than the time-scales found by Buckley and Fan [23, 41, 43] for the 41 crude oil studied in the CO-Wet database, where the average reorganization phase was found to be 230 ±146 seconds. These times are based on a measurement time of 2000 seconds (33 minutes) with the pendant-drop method. In comparison, Kelesoglu et al. [29] utilized the monoexponential decay-model for measurement times of 300 minutes. The average time-constants for crude oil in water were found to be in the order of 4626 ±1020 seconds. For the pendant-drop measurements of 60 minutes utilized in this thesis, time constants were found to be 966 ±236 seconds for crude oil A and 947 ±322 seconds for crude oil B (**Table A-12**, Appendix V). In terms of per cent variation, it can be calculated that the low measurement times used by Buckley et al. produced variations of 63.5%, while increasing the measurement times to 300 minutes (Kelesoglue et al.) and 60 minutes (in this thesis) only had deviations of 22.0% and 24.4%/34.0%, respectively. Thus, the monoexponential model appears to be highly dependent on measurement-time.

The advantage of using the monoexponential model is that it provides a quantification of the relative kinetics of dynamic processes that occurs at the interface. These values can be compared across various water –and crude oil compositions. The disadvantage is that there are three coefficients that needs to be fitted (γ_{eq}, γ_o and τ), which means that some initial investigation of the equilibrium value needs to be performed. A comparison of the equilibrium IFT fitted by the monoexponential –and polynomial model can be found in **Table A-7** in appendix V. A display of the fit between the monoexponential function and the measured dynamic IFT for all experiments performed for the three-dimensional FCD is available in appendix V. The model cannot be fitted to the cases where a minimum is observed, which was the case for some of the measurements performed with crude oil B at caustic conditions.

5.6. Screening experiments

The first screening experiments (**Table 4-1**) were standardized by means of **Equation 4-3** and decomposed into two principal components (PC), which recovered 77.8 % of the total variation. The plot for RSD vs. Leverage (**Figure A-3**, Appendix IV) shows that all objects are within acceptable range. Graphical representations of the PCA are showed in **Figure 5-9**.
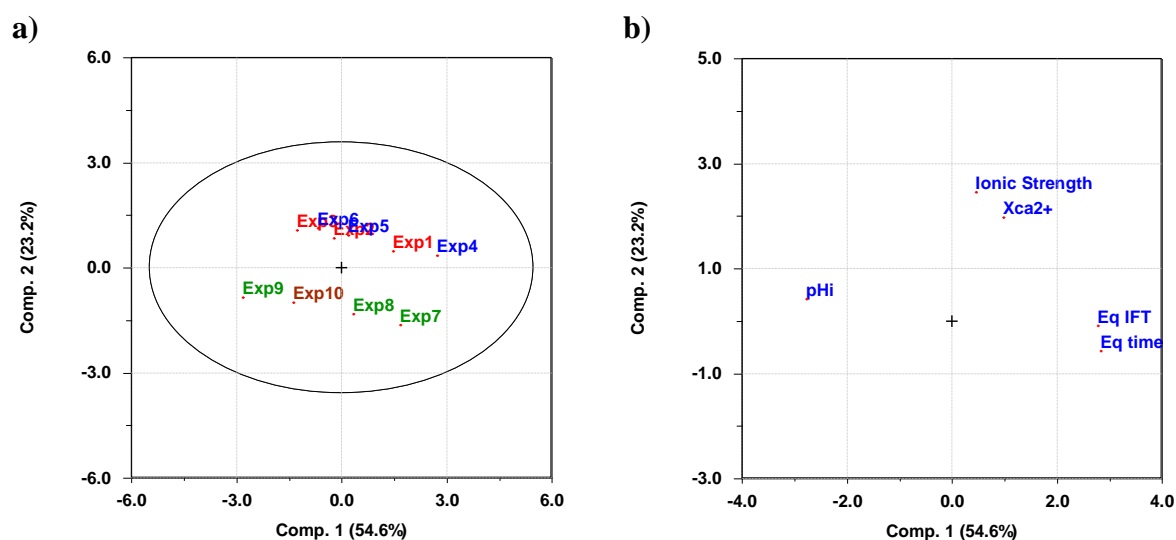

Figure 5-9: a) Scores and b) loadings for the first screening with crude oil A.

The score plot (**Figure 5-9**a) shows groupings for an ionic strength of 0.09 (green objects) and ionic strength of 0.40 and 0.23 (red and blue objects). This may indicate that there exists an optimum ionic strength between 0.09 and 0.23, whereas increasing the ionic strength further past 0.23 does not promote large variations.

The loadings (**Figure 5-9**b) shows that the equilibrium IFT is strongly negatively correlated to the pH ($r^2 = -0.98$), but very weakly correlated to the ionic strength and Ca^{2+} content ($r^2 = 0.07$). These two relationships can be isolated, as displayed in **Figure 5-10**.

The most notable effect on the equilibrium IFT was obtained at caustic conditions, low ionic strength and no Ca^{2+}, which produced an equilibrium IFT of 7.0 mN·m^{-1}. Additionally, this experiment reached equilibrium conditions in only 17 minutes, while all other experiments required an average measurement time of 84 ±46 minutes. Exp10 (the brown object in **Figure 5-9**a) was included to inspect the effect of adding a small amount of Ca^{2+} (136 ppm) to this experiment. This increased the equilibrium IFT to 21.1 mN·m^{-1} and the measurement time required was 54 minutes. This observation indicates that metal-complexes (**Equation 2-2** and **Equation 2-3**) may have formed, thus removing the interfacially acive dissociated acids

from the interface and presumably dissolving them in the water phase or stabilizing the CO/W emulsion film. This mechanism has been reported by several researchers [5, 10, 19, 20, 24, 31].
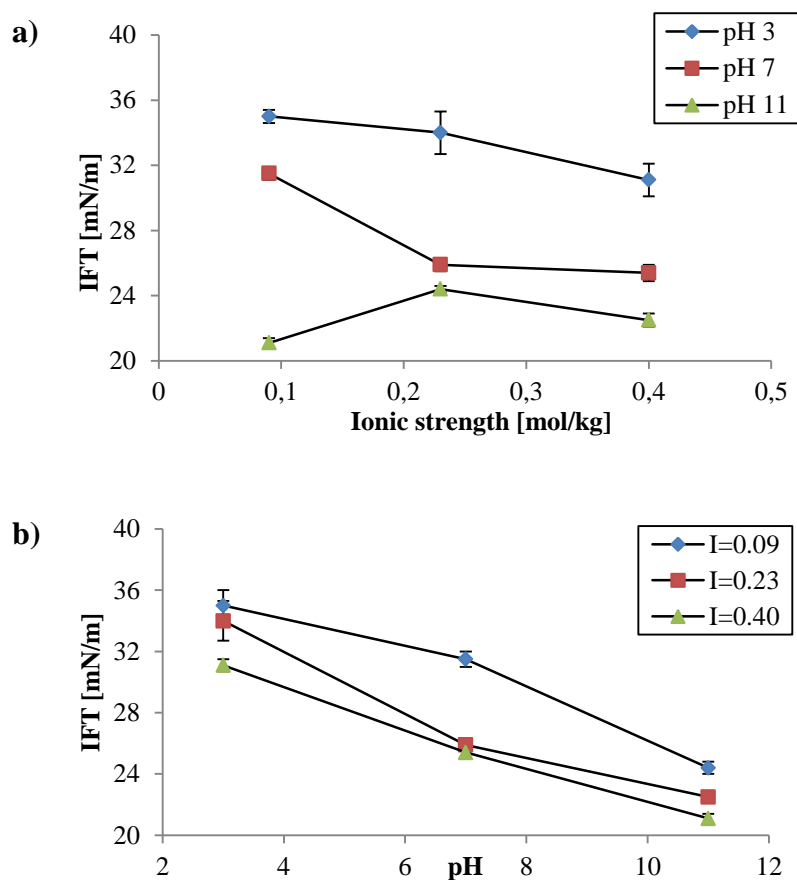
Figure 5-10: An isolation of the relationship between a) IFT and ionic strength and b) IFT and pH. Experiment 9 has been replaced with the object containing a low amount of Ca^{2+}.

Figure 5-10 shows an almost linear relationship between the IFT and pH. This is not consistent with other reports on the pH-dependence of the IFT, which suggests that the IFT is at an optimum at neutral pH, but decrease at low and high pH [13, 18, 29, 32, 41, 43]. This has been attributed to the protonation of basic species at low pH and dissociation of acids at high pH. Thus, this increase in IFT at low pH may indicate that crude oil A does not contain significant amounts of basic species that become interfacially active at low pH, but rather promotes a decrease in the concentration of dissociated acids.

The second screening only considers two variables: ionic strength and molar fraction of Ca^{2+}. It is therefore unnecessary to decompose the dataset into PCs. **Figure 5-11** shows the variation in IFT as a function of variation in ionic strength (Figure a) and molar fraction of Ca^{2+} (Figure b), both at neutral pH conditions. The lines are polynomial trend-lines fitted by excel analysis tools. These indicate that IFT decrease with increasing ionic strength for both

crude oils, while no trend can be spotted when modeling the IFT as a function of Ca^{2+} content. However, **Figure 5-11**a does not show indications of the optimum hypothesized to exist between I=0.10 mol·kg^{-1} and I=0.23 mol·kg^{-1} for crude oil A. Instead, it appears as if the ionic strength causes a continuous decrease in the IFT, or that it has an optimum around I=0.35 mol·kg^{-1}.
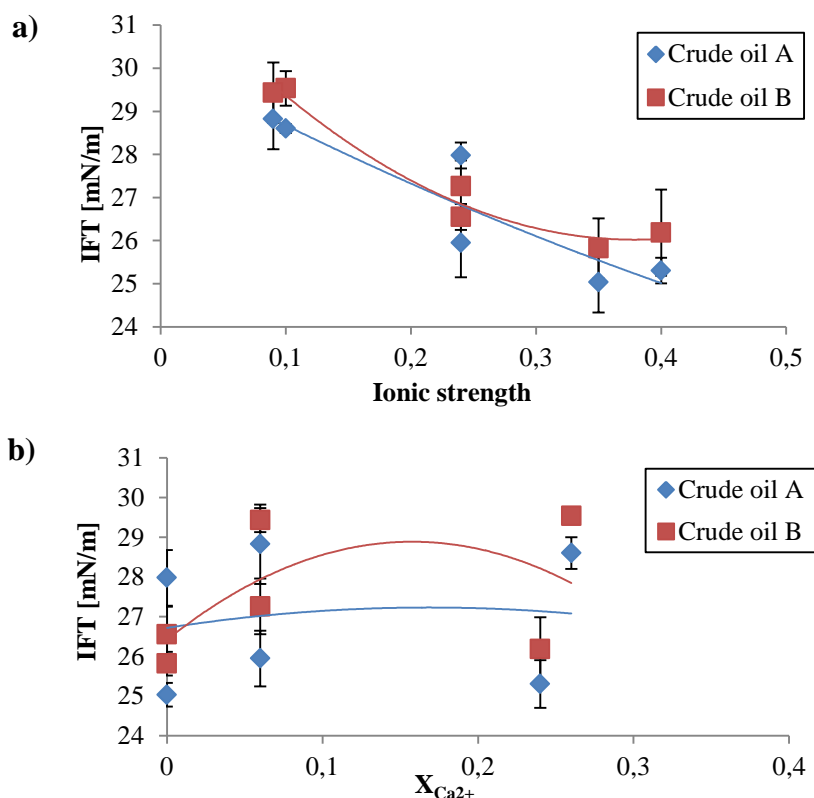
Figure 5-11: Plots of a) IFT vs. ionic strength, and b) IFT vs. the molar fraction of Ca^{2+}.

In summary, the first screening experiments indicate that there may be an optimum ionic strength for crude oil A around I=0.1-0.2 mol·kg^{-1}, while the second screening may be interpreted to contain an optimum closer to I=0.4 mol·kg^{-1}. Several reports [1, 2, 24, 38] have indicated that the ionic strength has an optimum effect on the IFT, as a result of reaching a saturation level in terms of ionic screening of charged species adsorbed at the CO/W interface. More levels for the ionic strength should be further inspected, to see if a trend can be elucidated once more measurement points are included.

pH is the most important variable for obtaining a reduction in the IFT for crude oil A. The plot of IFT as a function of pH for crude oil A implies that the relationship is seemingly linear. Further investigation of this relationship should include a pH value in between neutral pH and pH 11, to inspect the possible curvature of the response-surface.

The concentration of Ca^{2+} does not appear to be significant at neutral pH conditions for either crude oils. However, the most drastic effect on the IFT for crude oil A is found to be at caustic conditions and low ionic strength with no Ca^{2+} present. This drastic reduction in the IFT is almost eliminated by adding trace-amounts of Ca^{2+}. Therefore, the effect of Ca^{2+} should not be excluded from further experiments, but it may be more meaningful to inspect the effect of $X_{Ca2+} = 0.0$ compared to $X_{Ca2+} \in (0.0, 0.1)$, instead of higher concentrations.

It is not yet known if higher concentrations of monovalent ions can eliminate the drastic reduction at caustic conditions and in the absence of Ca^{2+}. However, Na^+ has been proposed to not form strong complexes, but rather act as an efficient ionic specie in screening of the EDL formed in the vicinity of the CO/W interface [18, 30, 38]. Thus, it would be reasonable to assume that higher concentrations of Na^+ will promote further reduction in the IFT, which has been reported by Jennings [20] and Sharma et al. [19]. This hypothesis may be tested by including measurements at high ionic strength, caustic conditions and in no Ca^{2+}. Additionally, it is still unknown if the effect of caustic conditions and no Ca^{2+} is as drastic for crude oil B. At the time being, it can be hypothesized that the effect will not be as drastic, as a consequence of assuming that the acid concentration in crude oil B is lower than in crude oil A. It has not been reported that asphaltenes associate with Ca^{2+} in the same way as acids.

5.7. Face centered designs

The FCD was carried out twice for each crude oil: once for variables X_{Ca2+} and ionic strength (two-dimensional, **Figure 4-1**a), and once where the pH was included (three-dimensional, **Figure 4-1**b). The aim of the two-dimensional FCD is to inspect the importance of ionic strength and type of metal cation at pH neutral conditions, which is closest to the pH conditions in the reservoir. The aim of the three-dimensional FCD is to investigate the effect of introducing caustic conditions to the CO/W system, which is the approach in alkaline waterflooding. All calculated regression coefficients calculated from yate's algorithm are tabulated in Appendix IV.

5.7.1. Two-dimensional FCD

Figure 5-12 shows the biplot of the scores and loadings extracted by PCA for the two-dimensional standardized subset. The red markers are the face centered points (axial points)

and the green markers are the centerpoints. The standardized PCA-models recover 93.6 % of the variance of crude oil A, and 95.7 % of the variance for crude oil B.

Crude oil A **Crude oil B**
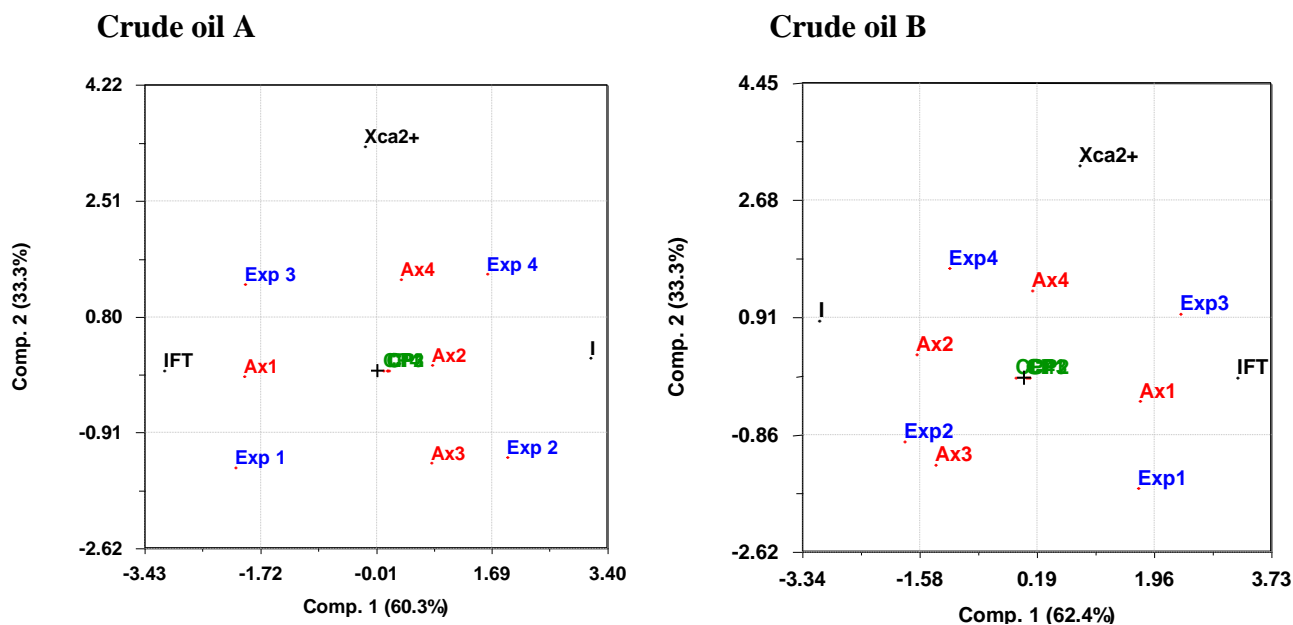
Figure 5-12: Biplot of scores and loadings for objects and variables by means of PCA.

A comparison of the biplots of the experiments (**Figure 5-12**) to the general structure of the design (**Figure 4-1**a) shows that the response is not purely linear. The two variables are located along each axis (comparable to the x –and y-axis) and experiments and axial points are slightly displaced compared to their levels' position in the coordinate-system.

The molar fraction of Ca^{2+} is non-correlated to the IFT whereas the ionic strength is strongly negatively correlated to the IFT for both crude oils. Thus, as it has been hypothesized from the screening designs, the IFT mainly depends on the ionic strength at pH neutral conditions. This may be explained by the presumed low concentration of dissociated acids, and therefore low accumulation of interfacially active charged species that have affinity towards Ca^{2+}-complexation. However, as can be seen from **Table 5-6**, the variation in IFT among the experimental points is very low in general.

Table 5-6 compares the mean IFT for the total experiments (including axial points) and the mean IFT from four centerpoints. The standard deviation in the centerpoints is very low, which reflects good reproducibility. This can also be seen from the overlapping CP-objects in the biplot.

Table 5-6: A comparison of the mean IFT for the full experiment and for the centerpoints.

	Mean IFT (γ_{mean}) ±st.dev. (σ) [mN·m⁻¹]	
	Crude oil A	**Crude oil B**
Experiments	25.6 ±3.9	29.8 ±3.8
Variance* [%]	7.7	6.5
Centerpoints	24.8 ±0.2	29.8 ±0.4

*calculated as (σ/γ_{mean})×100%, i.e. the coefficient of variation.

According to the comparison between the experiments and the centerpoints, the response in crude oil A produce a slightly curved surface, while crude oil B does not. This could also be seen in the regression model. Regression coefficients are listed in **Table A-6** in Appendix IV.

The regression coefficents found to be of most significane differed between the two crude oils; both **I** and **I**^{2} were significint factors for crude oil A (which reflect that there might be some curvature in the model) while **I** was sufficient for obtaining a good model in crude oil B. **Figure A-5** in Appendix IV compares the original model to thoes dervide with only significant factors. Thus, the IFT for the crude oils appear to respond differently to changes in the ionic strength: the IFT between crude oil B and saline water decrease with increasing ionic strength, while crude oil A may decrease towards an optimum within the levels inspected. However, more measurement-points are needed in order to draw any conclusions. Also, these measurements are non-equilibrated, which has been found to introduce some differences in the IFT with respect to the ionic strength of the water phase (see discussion in Chapter 5.4.3). The effect of ionic strength will be discussed more closely in Chapter 5.8, where only equilibrated measurements are considered.

5.7.2. Three-dimensional FCD

The curvature of the response surface may be inspected analogously as for the two-dimensional FCD, by comparing the mean response from centerpoint to the mean response of the experiments and axial points. These are shown in **Table 5-7**. It can be seen that the variance among the measurement points is considerably higher than for the two-dimensional FCD. The centerpoints of crude oil A produce a lower IFT than the mean of the design, which implies that the response surface is curved. However, the mean of the centerpoints for crude oil B are not significantly different from the mean of the design. This difference may also be seen from the regression coefficients for the model (listed in **Table A-7** in Appendix IV). The response in IFT for crude oil A appears to be governed by more complex interactions between the water phase composition, where all the main factors (X_{Ca2+}, I and pH) and the interaction

between pH and ionic strength contribute to significantly to changes in the IFT (see normal distribution of regression coefficients in **Figure A-6**a in Appendix IV). The variation in IFT for crude oil B is however more equally contributed to be all factors, with pH being slightly predominant to the variation (see normal distribution of regression coefficients in **Figure A-6**b in Appendix IV).

Table 5-7: A comparison of the mean IFT for the full experiment and for the centerpoints.

	Mean IFT (γ_{mean}) ±st.dev. (σ) [mN·m^{-1}]	
	Crude oil A	**Crude oil B**
Experiments	25.2 ±8.7	27.6 ±6.1
Variance* [%]	34.7	22.3
Centerpoints	24.6 ±0.8	27.3 ±0.3

*calculated as $(\sigma/\gamma_{mean})\times100\%$, i.e. the coefficient of variation.

The aim of the following discussion will be to propose possible mechanisms that may correlate the predominant variations in the IFT to the known variations in the two crude oil's composition. The three-dimensional structure of this FCD produces less intuitive PCA-graphics. Instead, **Figure 5-13** provides a visualization of the three-dimensional variable-space only consisting of the experimental points and mean response for the centerpoints.
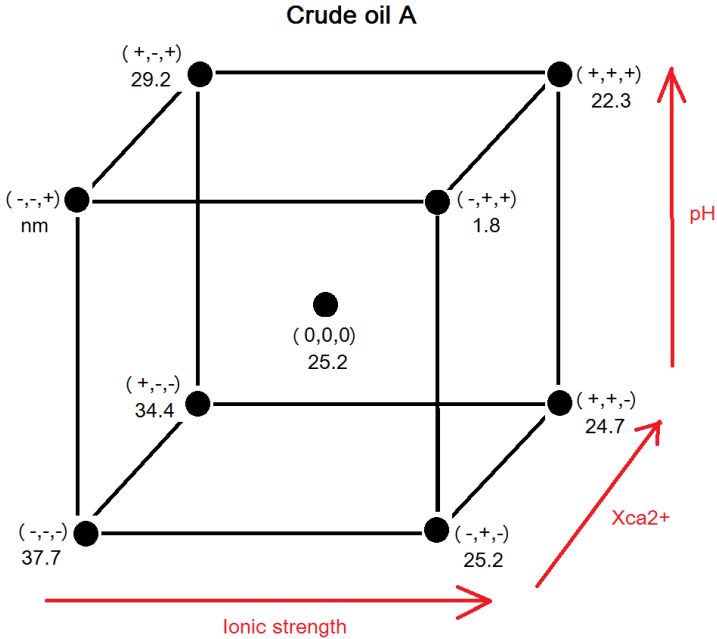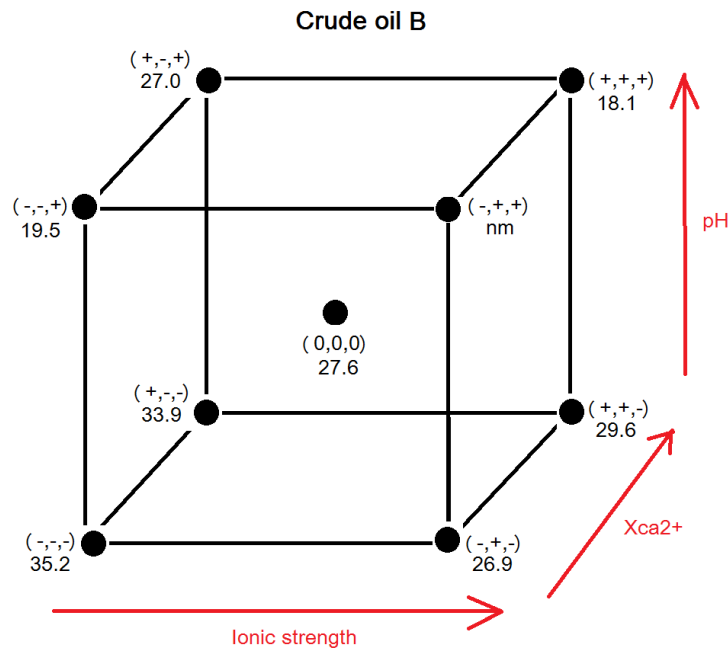
Figure 5-13: Representation of the measurement-points in the three-dimensional variable-space for the FCD. Axial points have been omitted for clarity. nm = not measureable.

Both oil's IFT is clearly most affected by changes in the pH, which can be seen from comparing the top (high pH) and bottom (neutral pH) two-dimensional variable space in **Figure 5-13**. The largest reduction in the IFT was observed in the caustic system with only monovalent ions for both crude oils. The IFT of crude oil A was unmeasurable at low ionic strength, whereas increasing the ionic strength produced a measurable, but very low IFT of 1.8 mN·m^{-1}. This low IFT is most likely caused by the high concentration of dissociated acids that accumulate at the interface to lower the IFT. The increase in IFT upon introducing Ca^{2+} to the system, which was observed in the screening experiments for crude oil A, is also observed here. The effect appears to be highly important for both crude oils, but more so for crude oil A. Reports suggest that this is caused by the formation of metal-complexes with dissociated acids, which dissolve in the aqueous phase or bridge acids at the interface [10, 18, 19]. This effect has been reported by several researchers, and is considered to be a challenging aspect of alkaline waterflooding in the case of acidic oils like crude oil A.

It may be hypothesized that the reason why the high ionic strength solution was measurable was that the increased salinity promoted a salting-out effect. This would presumably reduce the solubility of the hydrophilic acids in the water phase and result in a higher partitioning coefficient and a slight increase in the CO/W interfacial film stability. This could be directly observed, as stable CO/W emulsions were obtained for crude oil A at caustic conditions with no Ca^{2+} (**Figure 5-14**). The high ionic strength solution destabilized enough to be measured

after 24 hours, but the low ionic strength solution did not. Also, the stable emulsion had a considerably larger mass transfer of crude oil species, and changed the color and consistency of the crude oil phase from black and viscous to brownish gray and less viscous. **Figure 5-14**a and b compares the stable emulsions at caustic conditions and at pH neutral conditions, while **Figure 5-14**c compares the stable and unstable emulsions at caustic conditions as a consequence of whether or not Ca^{2+} is present in the water phase. These pictures are taken immediately after mixing the two phases.

a)

b)

c)

d)
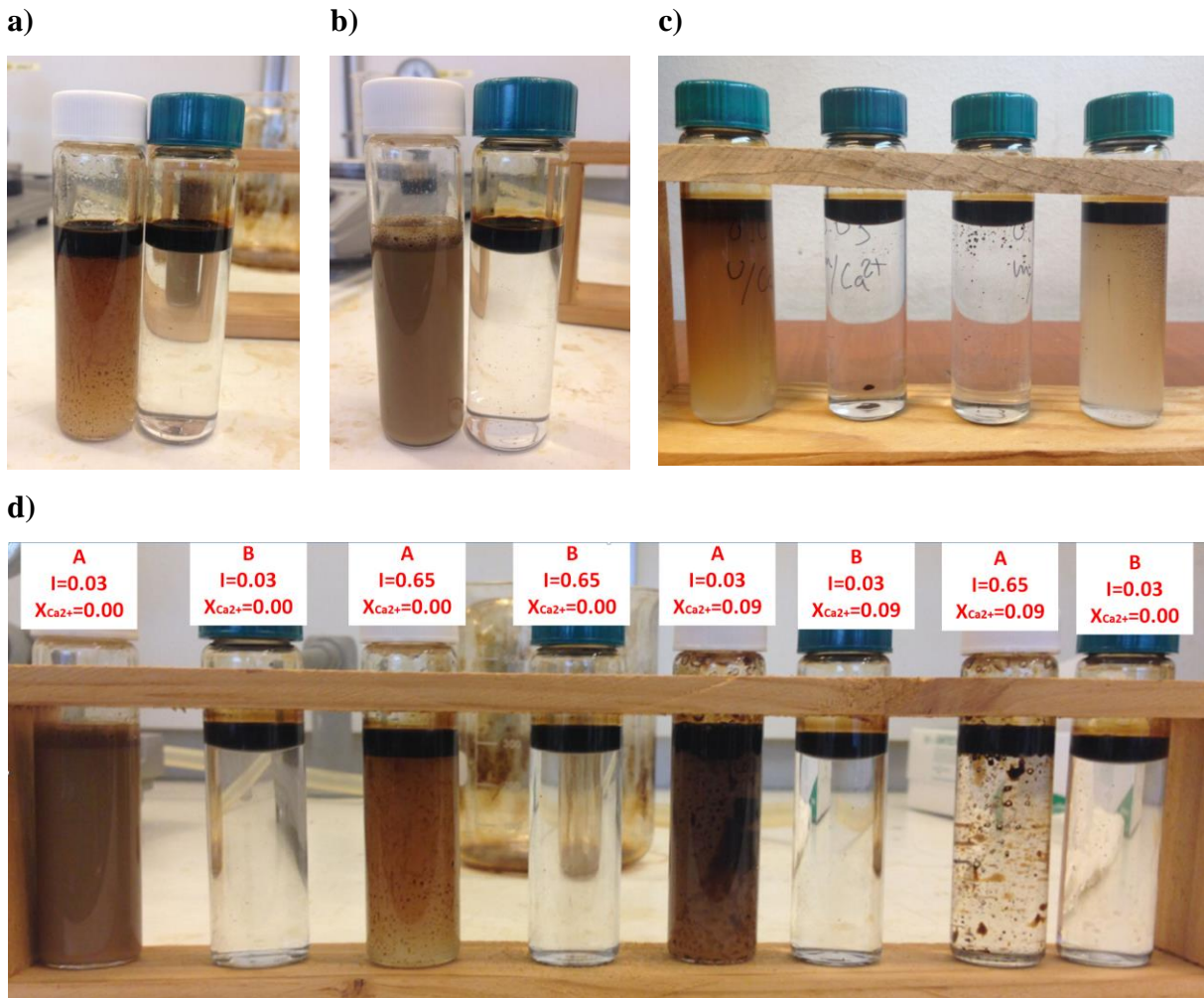
Figure 5-14: A comparison between crude oil A at basic pH (left) and neutral pH (right) at a) high ionic strength, and b) low ionic strength. c) A comparison between crude oil A at basic conditions with and without Ca^{2+} present. The middle two emulsions contain Ca^{2+}, while the outer two do not. d) A comparison of the CO/W emulsions for the two crude oils at caustic conditions. The water composition and type of crude oil is specified in the labels

Figure 6-14d compares the CO/W emulsions of the two crude oils at caustic conditions. It can be seen that crude oil B does not form stable emulsions, and does not appear to transfer any notable concentrations of hydrophilic species from the oil phase to the water phase. It can also be seen from the pH-profile in **Figure 5-5** in Chapter 5.4.3 that crude oil B does not alter the

water phase pH upon equilibration to any significant extent. This provides further support to the proposition that the composition in crude oil B is low in hydrophilic acids compared to crude oil A.

However, crude oil B was also unmeasurable at caustic conditions and in the absence of Ca^{2+}, but only at high ionic strength. The reason for this was completely different from that of crude oil A, i.e., it was not caused by a heavy mass transfer. Instead, a drastic change in the crude oil's consistency was observed. This can be seen from **Figure 5-15**, which shows how the oil phase failed to form a pendant-drop due to the consistency changing to a lumpy and thick mass.
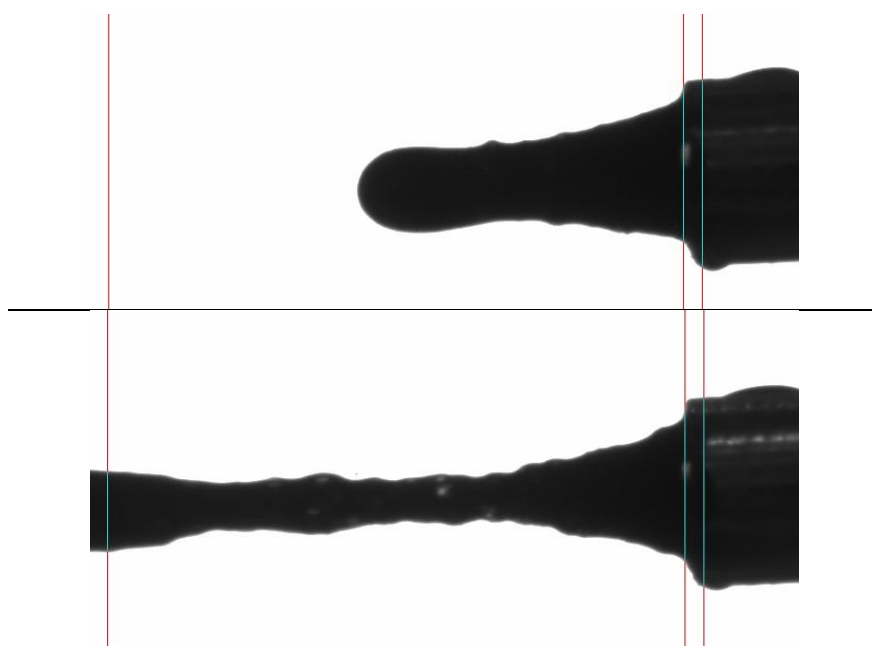
Figure 5-15: A display of the crude oil being continuously dispensed out of the needle for crude oil B at high pH and ionic strength, and in the absence of Ca^{2+}.

The reason for this behavior may be attributed to the high concentration of asphaltenes in crude oil B, compared to that found in crude oil A (**Table 5-3**). There have been some disagreements among researchers on the point of asphaltenes' interfacial properties [13, 14, 23, 32, 41, 43]. However, several reports indicate that asphaltenes' interfacial activity is dependent on, or at least enhanced by, co-adsorption with naphthenic acids. Thus, it may be hypothesized that the acid concentration is not high enough in crude oil B for this synergistic effect to obtain spontaneous emulsification.

It has also been hypothesized that asphaltenes form aggregates that bulk together irreversibly at the interface over time, to form a dense, elastic, skin-like interface [13, 14, 29, 32]. This

hypothesis may be supported by comparing the oil phase in **Figure 5-15** to the pendant-drops in the report by Jeribi et al. [32, p271]. These drops clearly show the elasticity of the oil phase when aggregates form skin-like interfaces when given a sufficient time to aggregate. Langevin et al. [14] postulated that the surface rheology provides a better description of the interfacial behavior than the IFT once these aggregates dominate the interface.

However, this behavior was only observable at high ionic strength, while the corresponding measurement at low ionic strength measured a relatively high IFT of 19.5 $mN \cdot m^{-1}$. By comparison, crude oil A was unmeasurable at these conditions. The drastic increase in IFT for crude oil B at caustic conditions and with low ionic strength of only monovalent cations may be attributed to the lack of asphaltene-aggregates forming, or that they dissolve in one of the bulk phases rather than adsorbing at the interface. The crude oil consistency did not appear to have changed at these conditions, which indicate that no substantial interfacial adsorption of aggregates occurred. Also, there was no visible mass transfer to the water phase (**Figure 5-14**) which indicate that, if aggregates have formed, they are rather dissolved in the oil phase. It is also not likely that asphaltene-aggregates dissolve in the water phase in a similar way as micelles of naphthenic acids are considered to do [31].

However, the observation may be attributed to EDL-effects. It may be hypothesized that increasing the ionic strength, thus reducing the EDL-thickness, will reduce the electrostatic repulsion between charged species adsorbed at the interface. This effect was found to be relatively low at neutral conditions (as discussed in the previous chapter). At caustic conditions, however, this is a potential explanation for the observed drastic lowering in the IFT for both crude oil systems, due to the presumed increase in charged surfactant species. Thus, it can be postulated that high ionic strength promotes interfacial adsorption of asphaltene aggregates in crude oil B, where the aggregates' hydrophobic part are solubilized in the oil phase. At low ionic strength, however, the EDL is expanded and the electrostatic repulsion between charged interfacially adsorbed species is higher. This may lead to the majority of the aggregates to rather be dissolved in the oil bulk phase, which deprive their interfacial activity and allow for a pendant-drop to be formed.

The observations for crude oil A at caustic conditions with only monovalent ions may also be attributed to EDL-effects. However, at low ionic strength it is likely that the salting-out effect is too low to oppose mass transfer of hydrophilic species, whereas the high ionic strength repress mass transfer enough for the system to be sufficiently stable for obtaining measurable results with the pendant-drop. Thus, the electrostatic effects that govern the stability of the

two CO/W emulsions may be suggested to be similar with respect to EDL-effects allowing for efficient interfacial adsorption and the resulting drastic decrease in IFT. On the other hand, the salting-out effect may be the important mechanism for the stability of the CO/W system for crude oil A, presumably due to the high concentration of hydrophilic acids. The salting-out effect is however not presumed to have any significant effects on the CO/W system for crude oil B, due to asphaltenes not following the same process of convective diffusion as naphthenic acids [13, 54, 55].

Apart from the drastic variations at caustic conditions, **Figure 5-13** also shows that both crude oils have the highest IFT at low ionic strength, no Ca^{2+} and neutral pH. Thus, neutral pH conditions at low ionic strength appear to be unable to promote any substantial interfacial reactions. This may be discussed as a consequence of the theoretical modeling of interfacial pH of the system. Cratin's model for interfacial pH [59] suggests that the acids' interfacial pK_a must necessarily be higher than the bulk pK_a, which has to be compensated for by a higher water-bulk pH. This may be seen at caustic conditions, in the presence of Ca^{2+}; **Figure 5-13** shows that increasing the ionic strength decreases the IFT from 29.2 to 22.3 mN·m^{-1} for crude oil A and from 27.0 to 18.1 mN·m^{-1} for crude oil B. This may be attributed to the increase in counter ions available to screen the interfacial charge and equalizing the distribution of H$^+$ [18, 24, 31]. Also, a salting-out effect will take place to some extent. Both of these processes may lead to higher concentrations of ionized species accumulating at the interface, which will lower the IFT of the CO/W system.

It should also be noted that **Figure 5-13** does not take axial points into consideration. These are important to the inspection of the response surface for the system. After the first screening design, it was suggested that the IFT decrease almost linearly with increasing pH. The inclusion of axial points at pH 9 can be combined with neutral pH and high pH as displayed in **Figure 5-15**.


61

b)
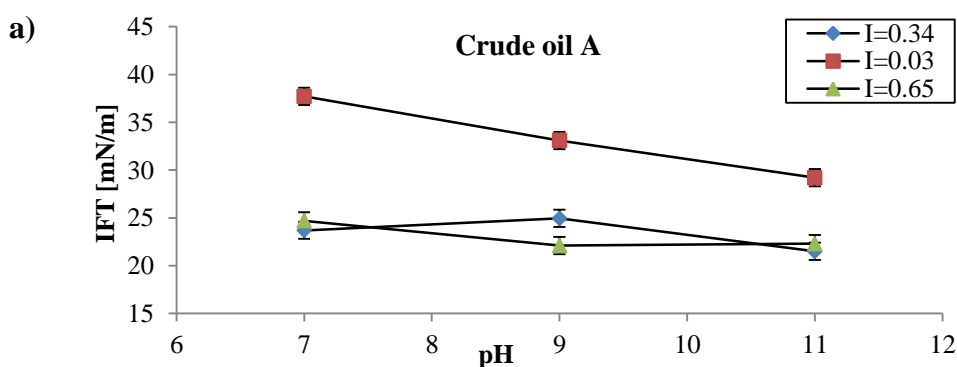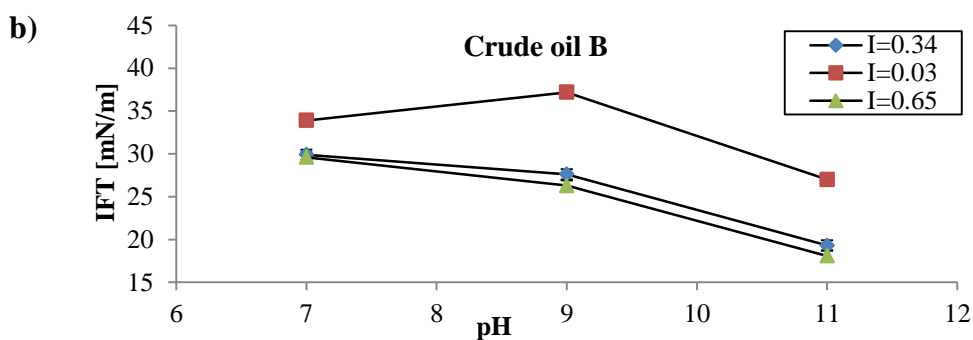
Figure 5-16: The IFT as a function of pH for various ionic strengths, in the presence of Ca^{2+}. a) Crude oil A and b) crude oil B.

Figure 5-16a show that the relationship between the IFT and pH for crude oil A is close to constant at higher ionic strengths, but seemingly linear at low ionic strength. This difference may also be attributed to EDL-effects and the model for the interfacial pH. It has previously been hypothesized that crude oil A might contain concentrations of naphthenic acids that have a pK_a close to 5, which is a value reported by several researchers [18, 28, 29, 31, 56]. If this is the case, then increasing the pH above this value would not be expected to further drastic increases in the concentration of interfacially active dissociated acids. This would also require that the interfacial pH is equal to or above the pK_a of the acids. $I \geq 0.34$ mol·kg^{-1} appears to be sufficient for screening the interfacial charge, and thus equalizing the interfacial –and bulk pH according to Cratin's model [59]. However, at $I=0.03$ mol·kg^{-1}, the interfacial pH may be more concentrated in H^+ ions due to a lack of counterions available in the water bulk phase. Thus, by gradually increasing the water bulk phase pH, the interfacial pH is correspondingly increased. This would promote a gradual increase in interfacial saponification of acids that can lower the IFT of the system. This mechanism was also suggested by Havre et al. [31] and Farooq et al. [18].

The IFT for crude oil B is more sensitive to increasing the pH above 9. This may be a critical pH for the dissociation of acids present in crude oil B. Several reports [29, 31, 56] show that the IFT tend to pass through two distinct optimums when modeled as a function of pH; one at the pK_a of the acids, and one at a second pK_a or at the point in which the interfacial pH is increased to that of the bulk pH. Thus, crude oil B may have one of these optimums between pH 9 and pH 11. Thus, it may be hypothesized that the pK_a of the acids that potentially dissociate at increasing pH have a pK_a closer to 9 or higher. Also, the relationship between the IFT and pH does not appear to be as affected by the ionic strength of the water phase. This would imply that other mechanisms than interfacial saponification of acids is involved in the IFT lowering at increasing pH.

5.8. The effect of ionic strength

The effect of the ionic strength on IFT is less clear when modeled in a multivariate framework, due to its small effect compared to varying the pH and the covariance between pH and Ca^{2+}-content. By combining the experiments from different designs, a total of 8 experimental ionic strengths have been performed for crude oil A and 5 have been performed for crude oil B. These include results from the first screening and the three-dimensional FCD. It has been found that pre-equilibration of samples have a significant effect on the experimental pH, and thus on the experimental IFT measurement. Thus, results from the non-pre-equilibrated second screening and the two-dimensional FCD have been excluded.
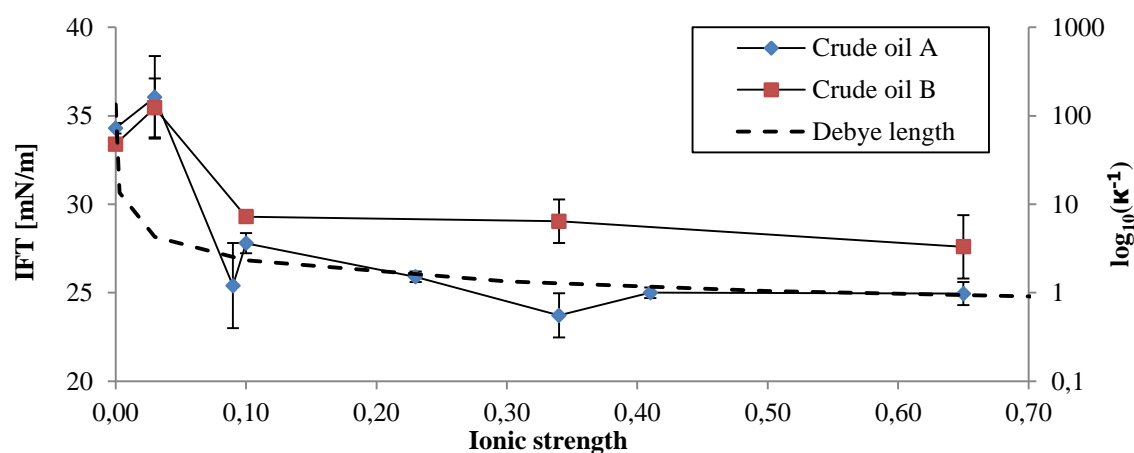
Figure 5-17: The IFT versus ionic strength with standard deviation from various, pre-equilibrated experimental designs at neutral pH. The dotted line is the decay in the Debye length.

The ionic strength appears to have a maximum effect at $I \approx 0.1$ mol·kg^{-1} for both crude oils. Further increase in the ionic strength does not appear to promote any subsequent drastic reductions in the IFT. This may be connected to the effect of ionic strength on the EDL-thickness, quantified by the Debye length. This is emphasized in **Figure 5-17**, where it can be seen that the measurement points appear to follow the decay in the Debye length. Thus, EDL-effects may account for the relationship between the IFT and ionic strength of the water-phase.

At higher pH, it is believed that the interfacial accumulation of charged species increase drastically, which may acquire higher concentrations of aqueous salts to screen this increased interfacial charge. **Figure 5-18** displays the IFT as a function of ionic strength at high pH, in the presence of Ca^{2+}. Only measurements from the three-dimensional FCD are modeled,

which is too few measurement-points to obtain a good view of the possible optimums. However, it appears as if an optimum may be present at an ionic strength <0.34 mol·kg^{-1}.
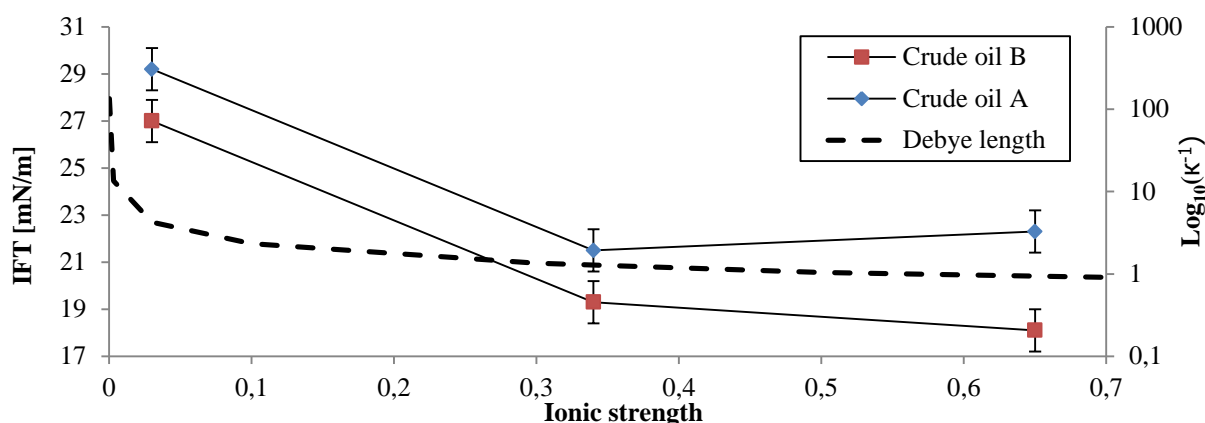
**Figure 5-18:** The IFT as a function of ionic strength at pH 11 in the presence of Ca^{2+}.

5.9. The CO-Wet database

Experimental results for crude oil A and B were included in the PLS-model for distilled water and 0.1 M NaCl at neutral pH (**Table 5-8**). It was not possible to obtain any satisfactory predictions by PLS-analysis of the IFT for the crude oils utilized in this thesis. This was due to the limited information about crude oil characteristics that has been possible to measure. Also, crude oil A was categorized as an outlier by RSD vs Leverage plots in both model, due to high RSD (**Figure A-9** in Appendix IV). However, this may be a result of TAN numbers (or other measures of acidity) are not included in the model, and thus cannot account for the low IFT observed for this oil. Crude oil B did not stand out in the dataset. This oil was found to be highly comparable to composition in Norwegian Standard Oil (**Figure 5-1**). Thus, crude oil B may be considered to be rather average in its composition, and therefore more easily integrated in the dataset.

Table 5-8: Experimental input-variables for the crude oils in the PLS regression model.

Crude oil	nC$_7$-asph [wt%]	API gravity [^{o}]	pH$_f$	Distilled water			0.1 M NaCl		
				γ_o [mN·m^{-1}]	γ_{eq} [mN·m^{-1}]	τ [s]	γ_o [mN·m^{-1}]	γ_{eq} [mN·m^{-1}]	τ [s]
A	0.33	24.4	6.4	25.0	22.1	480	20.8	18.0	668
B	2.77	26.1	6.5	27.0	23.7	444	24.8	21.1	632
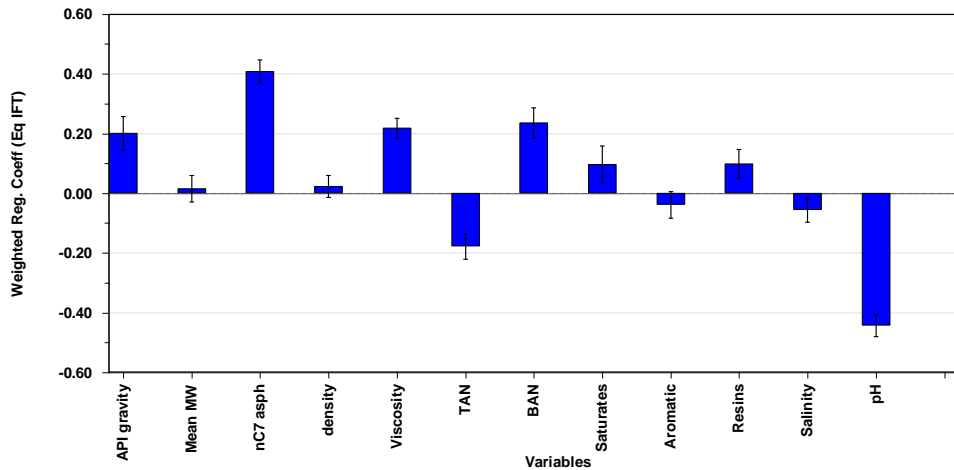
Figure 5-19: A comparison of the most significant crude oil properties for predicting the IFT for all water compositions. Regression coefficients and error bars are derived by PLS-analysis.

Figure 5-19 shows that the IFT is strongly negatively correlated to the pH, while it is highly positively correlated to the wt% of asphaltenes flocculated with *n*-heptane. This latter correlation would indicate that asphaltenes did not act as a surfactant, which is one of the conclusions that was proposed by Buckley et al. [23, 41]. This is not contradictory to the results obtained in this thesis, as crude oil B has measured a consistently higher IFT than crude oil A at pH neutral conditions (**Table 5-5**). Several studies report that the interfacial activity of asphaltenes depends on the total crude oil composition. That is, asphaltenes may show high interfacial activity in the form of interfacial co-adsorption with naphthenic acids [13, 54, 55] or be solubilized in the oil bulk phase by resin-molecules [8, 14, 27]. Thus, there may be certain patterns of covariance that cannot be extracted by the PLS approach. However, a loading plot derived by PCA may provide a better view of covariance between the variables.
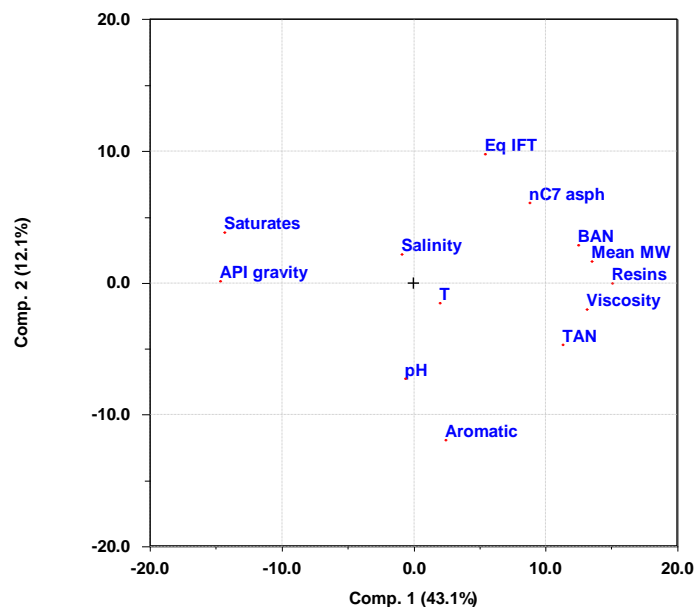
Figure 5-20: Loading plot for variables included in the CO-Wet database.

65

The loading plot shows that the IFT is also highly negatively correlated to the wt% of aromatics, by r^2=-0.93, which is the same magnitude of positive correlation between the IFT and wt% asphaltenes. These two crude oil properties have a negative correlation of r^2=-0.73, i.e., crude oils high in asphaltenes tend to be low in aromatics, and vice versa. Thus, even though the PLS-analysis implies that the wt% of aromatics is insignificant to predicting the IFT (**Figure 5-19**), there may be an underlying relationship between these properties that guard the interfacial activity. No literature has been found explicitly on this subject, but it may be hypothesize that the covariance is related to concentrations of acids and bases in the oils. The loading plot shows that the wt% of asphaltenes is more positively correlated to BAN, while the wt% of aromatics is more positively correlated to TAN. Thus, inter-dependence between water phase pH, aromatic acids (i.e., naphthenic acids) and asphaltenes with basic functional groups may be the underlying pattern that governs the variance in IFT.

This is only one of several possible interpretations of the variance displayed in **Figure 5-20**. However, the main point is that **Figure 5-19** and **Figure 5-20** emphasize the complexity and ambiguity that governs the correlation and covariance between CO/W interfacial activity and crude oil composition. Thus, while the difference in naphthenic acids and asphaltene content have been hypothesized to be the main sources of interfacial activity between the two crude oils inspected in this thesis, there is most likely a more complex underlying pattern.

6. Conclusion

The aim of this thesis has been to investigate the correlation between interfacial properties and phase composition in two separate CO/W systems. This has been carried out through four different experimental designs where the CO/W IFT has been measured for two different oils and varying pH, ionic strength and type of metal salt in the water phase. The crude oils were found to differ in acidic content, which is hypothesized to be significantly higher in crude oil A, and in asphaltene content, which has been found to be significantly higher in crude oil B. Crude oil A also appears to be biodegraded.

At simulated reservoir conditions, i.e., high ionic strength in the presence of Ca^{2+} and pH close to neutral, the IFT was relatively high. The ionic strength appeared to have an optimum reducing effect on the IFT at 0.1 $mol \cdot kg^{-1}$ which may be attributed to EDL-effects.

The water composition that caused the most drastic reductions in the IFT was found to be sufficiently effective to reduce the IFT below measurement level for the pendant-drop method. This occurred at caustic conditions with only monovalent metal cations, but differed in terms of ionic strength for the two crude oils. Crude oil A was unmeasurable at low ionic strength (I=0.03 $mol \cdot kg^{-1}$), while crude oil B was unmeasurable at high ionic strength (I=0.65 $mol \cdot kg^{-1}$). For crude oil A, this may be attributed to the presumed high concentration of naphthenic acids that can dissociate at high pH and adsorb at the CO/W interface to effectively lower the IFT. This was found to cause spontaneous emulsification and an observable mass transfer of crude oil species to the water phase. It was found that very low additions of Ca^{2+} were sufficient to stabilize the emulsions and increase the IFT considerably, to ultimately eliminate the effect of caustic conditions.

Spontaneous emulsification or observable mass transfer was not obtained for crude oil B, but a change in the crude oil consistency was observed. This may be attributed to the high concentration of asphaltenes, which are hypothesized to form irreversible aggregates at caustic conditions. The addition of Ca^{2+} increased the IFT, but not as significantly as for crude oil A.

In summary, the experimental results reported in this thesis strongly imply that interfacial activity in the CO/W system depends on both the composition of the water phase and the crude oil phase. However, differences were less clear at neutral pH compared to high pH.

7. Suggestions for further work

The variation in interfacial activity observed in this thesis has been attributed to the difference in asphaltene –and acidic content in the two crude oils. However, through investigating a more extensive dataset (Chapter 5.9), it is clear that there are several potential interactions between the chemical and physical properties of crude oil that govern the IFT of the CO/W system. Therefore, an elaboration on the characterization of these physical and chemical properties will be the relevant extension of the work performed in this thesis. The specific suggestions for further work can be summarized by the following points:

More quantitative measures of the crude oil chemical composition

Quantitative measures can be based on Buckley et al.'s CO-Wet database, as listed in **Table A-8** in Appendix IV. Especially SARA-fractions and TAN and BAN numbers may be more applicable to discovering correlations with physical properties, such as IFT, zeta-potentials or CO/W partitioning of crude oil species. Quantitative measures can also be related to qualitative findings from FT-IR and WOGC.

Expand the selection of crude oils

More variation in sources of interfacially active crude oil components may be discovered if more crude oils are modeled simultaneously. This may provide more conclusive evidence in terms of the important crude oil components at varying water phase composition. A larger selection of crude oils (and crude oil characteristics) will also lead to a better exploitation of multivariate methods' potential in modeling underlying patterns of covariance.

Characterization of crude oil acid structures

Mass spectroscopy of crude oil acids has provided important information about interfacial properties in previous studies [54-56]. This can give information about the pK_a of the acids, which allows for the calculation of the partition coefficients for varying water phase composition. This may provide some quantitative evidence for the hypothesis that crude oil A contains high concentrations of hydrophilic naphthenic acids with a pK_a close to 5, which has been suggested in this thesis.

Characterization of crude oil asphaltenes

The many contradictory reports on asphaltenes' interfacial activity may be related to the vast diversity of asphaltene structures and the different functional groups they possess. The possible synergistic interfacial effects between asphaltenes and naphthenic acids may be validated by inspecting the potential existence of basic functional groups or basic heteroatoms in the asphaltene fraction. This may also be related to the IFTs dependence on the water phase pH.

More quantitative measures of crude oil physical properties

The regression coefficients for Buckley et al.'s CO-Wet database (**Figure 5-19**) also imply that the viscosity of the crude oil is a significant parameter for predicting the IFT. Zeta-potential measurements at varying ionic strength and pH can additionally be investigated. This may be used to determine the critical concentrations of ionic species that provide efficient screening of the interfacial charge and at what pH the interfacial charge start to accumulate. This may also be related to observations in CO/W emulsion stability.

Relating the CO/W system to the CO/W/reservoir rock system

Rock minerology has been reported to play a major role in the efficiency of EOR waterflooding [1, 2, 7]. By including this in the experimental domain, results may have a higher relevance to the realistic interactions taking place in the reservoir. For instance, contact angle measurements may be correlated to the variation found in the IFT in this thesis. This will allow for direct calculations of potential alterations of the capillary pressure in the simulated reservoir system (**Equation 1-2**).

Literature

1. Alotaibi, M.B., R. Nasralla, and H. Nasr-El-Din, *Wettability Studies Using Low-Salinity Water in Sandstone Reservoirs.* SPE Reserv. Eval. Eng., 2011. **14**(6): p. 713-725.

2. Alotaibi, M.B. and H.A. Nasr-El-Din, *Effect of Brine Salinity on Reservoir Fluids Interfacial Tension*, in *SPE EUROPEC/EAGE Annual Conference and Exchibition* 2009, Texas A&M Univerity, SPE: Amsterdam, Netherlands. p. 1-14.

3. Terry, R.E., *Enhanced Oil Recovery*, in *Encyclopedia of Physical Science and Technology*, R.A. Meyers, Editor 2001, Academic Press: Birmingham Young University. p. 503-5018.

4. Nasralla, R.A. and H.A. Nasr-El-Din, *Impact of cation type and concentration in injected brine on oil recovery in sandstone reservoirs.* Journal of Petroleum Science and Engineering, 2014. **122**: p. 384.

5. Cooke, C.E., R.E. Williams, and P.A. Kolodzie, *Oil Recovery by Alkaline Waterflooding.* Journal of Petroleum Technology, 1974. **26**(12): p. 1365-1374.

6. Shiran, B.S. and A. Skauge, *Enhanced Oil Recovery (EOR) by Combined Low Salinity Water/Polymer Flooding.* Energy Fuels, 2013. **27**(3): p. 1223-1235.

7. Buckley, J.S. and Y. Liu, *Some mechanisms of crude oil/brine/solid interactions.* Journal of Petroleum Science and Engineering, 1998. **20**(3): p. 155-160.

8. Speight, J.G., *Part 1: History and Terminology*, in *The Chemistry and Technology of Petroleum*, B. Raton, Editor. 2014, CRC press. p. 3-174.

9. Nutting, P.G., *Chemical Problems in the Water Driving of Petroleum from Oil Sands.* Industrial & Engineering Chemistry, 1925. **17**(10): p. 1035-1036.

10. Trujillo, E.M., *The Static and Dynamic Interfacial Tensions Between Crude Oils and Caustic Solutions.* Society of Petroleum Engineers Journal, 1983. **23**(04): p. 645-656.

11. Satter, A., G.M. Iqbal, and J.L. Buchwalter, *Practical enhanced reservoir engineering: assisted with simulation software*. 2008: Pennwell Books.

12. Berg, J.C., *An introduction to interfaces & colloids : the bridge to nanoscience*. 2010, Hackensack, N.J: World Scientific.

13. Poteau, S., et al., *Influence of pH on stability and dynamic properties of asphaltenes and other amphiphilic molecules at the oil-water interface.* Energy Fuels, 2005. **19**(4): p. 1337-1341.

14. Langevin, D., et al., *Crude Oil Emulsion Properties and Their Application to Heavy Oil Transportation.* Oil & Gas Science and Technology, 2004. **59**(5): p. 511-521.

15. *Enhanced Oil Recovery*. [cited 2015 27. sept.]; Available from: http://energy.gov/fe/science-innovation/oil-gas-research/enhanced-oil-recovery.

16. *Saline water*. Water Science Glossary of Terms 2015.

17. Buckley, J.S., *Evaluation of Reservoir Wettability and its Effect on Oil Recovery*, 1996, US Department of Energy: US.

18. Farooq, U., et al., *Interfacial Tension Measurements Between Oil Fractions of a Crude Oil and Aqueous Solutions with Different Ionic Composition and pH.* Journal of Dispersion Science and Technology, 2013. **34**(5): p. 701-708.

19. Sharma, M.M., L.K. Jang, and T.F. Yen, *Transient interfacial tension behavior of crude-oil/caustic interfaces.* SPE Reserv. Eng., 1989. **4**(2).

20. Jennings Jr, H.Y., *A study of caustic solution-crude oil interfacial tensions*, 1974, Chevron Research Co.

21.   Trabelsi, S., et al., *Effect of Added Surfactants on the Dynamic Interfacial Tension Behaviour of Alkaline/Diluted Heavy Crude Oil System Effet de l'ajout de tensioactifs sur le comportement dynamique de la tension interfaciale du système solution alcaline/brut dilué.* Oil & Gas Science and Technology, 2013. **67**(6): p. 963.

22.   Touhami, Y., V. Hornof, and G.H. Neale, *Dynamic interfacial tension behavior of acidified oil/surfactant-enhanced alkaline systems 2. Theoretical studies.* Colloids and Surfaces A: Physicochemical and Engineering Aspects, 1998. **133**(3): p. 211-231.

23.   Buckley, J.S. and T. Fan, *Crude Oil/Brine Interfacial Tension.* PRRC, New Mexico Tech, 2005: p. 1-12.

24.   Standal, S.H., et al., *Partition Coefficients and Interfacial Activity for Polar Components in Oil/Water Model Systems.* Journal of Colloid And Interface Science, 1999. **212**(1): p. 33-41.

25.   ASTM, *ASTM D4175: Standard Terminology Relating to Petroleum, Petroleum Products, and Lubricants*, in *Annual Book of Standards*, A.S.f.T.a. Materials, Editor 2005, American Society for Testing and Materials: Philadelphia, PA.

26.   Killops, S.D. and V.J. Killops, *Introduction to organic geochemistry.* 2013: John Wiley & Sons.

27.   Midttun, Ø., *A physical-chemical and chemometric study of interfacially active components in crude oils*, 1999, Department of Chemistry, University of Bergen: Bergen.

28.   Hutin, A., J.-F. Argillier, and D. Langevin, *Mass Transfer between Crude Oil and Water. Part 1: Effect of Oil Components.* Energy & Fuels, 2014. **28**(12): p. 7331-7336.

29.   Keleşoğlu, S., P. Meakin, and J. Sjöblom, *Effect of Aqueous Phase pH on the Dynamic Interfacial Tension of Acidic Crude Oils and Myristic Acid in Dodecane.* Journal of Dispersion Science and Technology, 2011. **32**(11): p. 1682-1691.

30.   Farooq, U., et al., *Electrophoretic Measurements of Crude Oil Fractions Dispersed in Aqueous Solutions of Different Ionic Compositions—Evaluation of the Interfacial Charging Mechanisms.* Journal of Dispersion Science and Technology, 2013. **34**(10): p. 1376-1381.

31.   Havre, T.E., J. Sjöblom, and J.E. Vindstad, *Oil/Water-Partitioning and Interfacial Behavior of Naphthenic Acids.* Journal of Dispersion Science and Technology, 2003. **24**(6): p. 789-801.

32.   Jeribi, M., et al., *Adsorption kinetics of asphaltenes at liquid interfaces.* J. Colloid Interface Sci., 2002. **256**(2): p. 268-272.

33.   Brandt, H.C.A., et al., *Thermodynamic Modeling of Asphaltene Stacking.* The Journal of Physical Chemistry, 1995. **99**(26): p. 10430-10432.

34.   Ese, M.H., X. Yang, and J. Sjöblom, *Film forming properties of asphaltenes and resins. A comparative Langmuir– Blodgett study of crude oils from North Sea, European continent and Venezuela.* Kolloid-Zeitschrift und Zeitschrift für Polymere., 1998. **276**(9): p. 800-809.

35.   Mullins, O.C., *The Asphaltenes*, in *Annu. Rev. Anal. Chem.* 2011. p. 393-418.

36.   Erstad, K., et al., *Changes in Crude Oil Composition during Laboratory Biodegradation: Acids and Oil–Water, Oil–Hydrate Interfacial Properties.* Energy & Fuels, 2009. **23**(8): p. 4068-4076.

37.   Watson, J., et al., *Formation of carboxylic acids during aerobic biodegradation of crude oil and evidence of microbial oxidation of hopanes.* Organic Geochemistry, 2002. **33**(10): p. 1153-1169.

38.   Lashkarbolooki, M., S. Ayatollahi, and M. Riazi, *The Impacts of Aqueous Ions on Interfacial Tension and Wettability of an Asphaltenic–Acidic Crude Oil Reservoir*

during Smart Water Injection. Journal of Chemical & Engineering Data, 2014. **59**(11): p. 3624-3634.

39. Standal, S., et al., *Effect of polar organic components on wettability as studied by adsorption and contact angles.* Journal of Petroleum Science and Engineering, 1999. **24**(2): p. 131-144.

40. Laplace, P.S., *Traité de mécanique céleste/par PS Laplace...; tome premier [-quatrieme].* Vol. 4. 1805: de l'Imprimerie de Crapelet.

41. Buckley, J. and T. Fan, *Crude oil/brine interfacial tensions.* Petrophysics, 2007. **48**(3): p. 175-185.

42. Buckley, J.S. and J. Wang, *Crude oil and asphaltene characterization for prediction of wetting alteration.* Journal of Petroleum Science and Engineering, 2002. **33**(1): p. 195-202.

43. Fan, T. and J.S. Buckley, *Crude Oil IFT Measurements by the Pendant Drop Method*, in *Semi Annual Report*, U. DOE, Editor 2004, United States Department of Energy. p. 4-19.

44. Fan, T. and J. Buckley, *Rapid and accurate SARA analysis of medium gravity crude oils.* Energy Fuels, 2002. **16**(6): p. 1571-1575.

45. Agilent Technologies, I., *What Gas Chromatography Is*, in *Agilent Gas Chromatographs: Fundamentals of Gas Chromatography*, I. Agilent Technologies, Editor 2002, Agilent Technologies, Inc. : Wilmington, Delaware 19808-1610 USA.

46. Miller, J.M., *Chromatography : concepts and contrasts*. 2nd ed. ed. 2005, Hoboken, N.J: Wiley.

47. Ventura, G.T., et al., *Analysis of unresolved complex mixtures of hydrocarbons extracted from Late Archean sediments by comprehensive two-dimensional gas chromatography (GC×GC).* Organic Geochemistry, 2008. **39**(7): p. 846-867.

48. Williamson, K. and K. Masters, *Macroscale and microscale organic experiments*. 2010: Cengage Learning.

49. Pavia, D.L., *Introduction to spectroscopy*. 4th ed. ed. 2009, Belmont, Calif: Brooks/Cole.

50. DiGrado, B.D. and G.A. Thorp, *American Petroleum Institute Standards.* The Aboveground Steel Storage Tank Handbook: p. 139-177.

51. GmbH, A.P. *Density Meter*. 2015 [cited 2015 07.09.2015].

52. Carson, C.C., *Handbook of Chemistry and Physics.* American Journal of Public Health, 1935. **25**(4): p. 509-510.

53. Wang, J. and J. Buckley, *Procedure for Measuring the Onset of Asphaltene Flocculation.* PRRC Report, 2001: p. 01-18.

54. Varadaraj, R. and C. Brons, *Molecular origins of heavy crude oil interfacial activity part 2: Fundamental interfacial properties of model naphthenic acids and naphthenic acids separated from heavy crude oils.* Energy Fuels, 2007. **21**(1): p. 199-204.

55. Varadaraj, R. and C. Brons, *Molecular origins of heavy oil interfacial activity part 1: Fundamental interfacial properties of asphaltenes derived from heavy crude oils and their correlation to chemical composition.* Energy Fuels, 2007. **21**(1): p. 195-198.

56. Hoeiland, S., et al., *The effect of crude oil acid fractions on wettability as studied by interfacial tension and contact angles.* J. Pet. Sci. Eng., 2001. **30**(2): p. 91-103.

57. Skauge, A., et al., *Effects of Organic Acids and Bases, and Oil Composition on Wetability*, in *1999 SPE Annual Technical Conference and Exhibition, 3-6 Oct.*, S.P. 56673, Editor 1999, Society of Petroleum Engineers: Houston, Texas.

58. Hoeiland, S., et al., *The effect of crude oil acid fractions on wettability as studied by interfacial tension and contact angles.* Journal of Petroleum Science and Engineering, 2001. **30**(2): p. 91-103.

59.   Cratin, P.D., *Mathematical modeling of some pH-dependent surface and interfacial properties of stearic acid.* Journal of dispersion science and technology, 1993. **14**(5): p. 559-602.

60.   Kpalma, K. and J. Ronsin *An Overview of Advances of Pattern Recognition Systems in Computer Vision* 2009. 169-190.

61.   Kvalheim, O.M., *Sirius 8.0*, in *Sirius*, O.M. Kvalheim, Editor 2009, Pattern Recognition Systems AS: Universistetet i Bergen.

62.   Brakstad, F., et al., *Kjemometri i brukernes perspektiv*, in *Anvendelse av kjemometri innen forskning og industri*, R. Nortvedt, Editor. 1996, Tidsskriftforlaget Kjemi: Oslo. p. 553-565.

63.   Thelin, B., et al., *Försöksålanering och optimering för experimentalisten*, in *Anvendelse av kjemometri innen forskning og industri*, R. Nortvedt, Editor. 1996, Tidsskriftforlaget Kjemi: Oslo. p. 81-106.

64.   Box, G.E.P., J.S. Hunter, and W.G. Hunter, *Chp. 11: Modeling, Gepmetry and Experimental Design*, in *Statistics for Experimenters, 2nd ed.*, J.D. Balding and P. Bloomfield, Editors. 2005, John Wiley & Sons, Inc.: Hoboken, New Jersey, U.S. p. 437-483.

65.   Tobias, P. and L. Trutna, *5.3.3.6.1. Central Composite Designs (CCD)*, in *NIST/SEMATECH e-Handbook of Statistical Methods*, W. Gauthrie, Editor, NIST/SEMATECH: National Institute of Technology (NIST), U.S.

66.   NIST/SEMATECH. *e-Handbook of Statistical Methods*. 10.04.2015].

67.   NIST/SEMATECH e-Handbook of Statistical Methods, h.w.i.n.g.d.h.i.h., *5.7. A Glossary of DOE Terminology*, in *NIST/SEMATECH e-Handbook of Statistical Methods*, National Institute of Science and Technology (NIST), U.S.

68.   Gauthrie, W. and M. Natrella, *1.3.5.18. Yates Algorithm*, in *NIST/SEMATECH e-Handbook of Statistical Methods*, W. Gauthrie, Editor, NIST/SEMATECH: National Institute of Science and Technology (NIST), U.S.

69.   Isaksson, T. and T. Næs, *1.8 Prinsipal Komponent Analyse*, in *Anvendelse av Kjemometri innen Forskning og Industri*, R. Nortvedt, Editor. 1996, Tidsskriftforlaget Kjemi AS: Bergen, Norway. p. 145-151.

70.   Ugland, K.I. and B.G.J. Massrt, *1.9 Klassifisering*, in *Anvendelse av Kjemometri innen Forskning og Industri*, R. Nortvedt, Editor. 1996, Tidsskriftforlaget Kjemi AS: Bergen, Norway. p. 153-167.

71.   Grung, B., *1.6 Det matematiske grunnlaget for latent variabel-metoder*, in *Anvendelse av kjemometri innen forskning og industri*, R. Nordtvedt, Editor. 1996, Tidsskriftforlaget Kjemi AS: Bergen, Norway. p. 121-128.

72.   Karstang, T.V., *1.7 Forbehandling av data*, in *Anvendelse av Kjemometri innen Forskning og Industri*, R. Nortvedt, Editor. 1996, Tidsskriftforlaget Kjemi AS: Bergen, Norway. p. 129-144.

73.   *Chromeleon 7.2 Chromatography Data System*, T.F.S. Inc., Editor 2015, Thermo Fisher Scientific Inc.: http://www.dionex.com/en-us/products/chromatography-software/chromeleon72/lp-73027.html.

74.   Fonnes, S.H., *Analytisk karakterisering av asfaltener felt ut ved forskjellige betingelsar frå Athabasca bitumen*, 2014, The University of Bergen.

75.   Dataphysics Instruments, G., *OCA20 User Manual*, G. Dataphysics Instruments, Editor: Filderstradt, Germany.

76.   Arashiro Emerson, Y. and R. Demarquette Nicole, *Use of the pendant drop method to measure interfacial tension between molten polymers.* Materials Research, 1999. **2**(1): p. 23.

77.   Morita, A., D. Carastan, and N. Demarquette, *Influence of drop volume on surface tension evaluated using the pendant drop method.* Kolloid-Zeitschrift und Zeitschrift für Polymere., 2002. **280**(9): p. 857-864.

78.   Bashforth, F. and J.C. Adams, *An attempt to test the theories of capillary action: by comparing the theoretical and measured forms of drops of fluid.* 1883: University Press.

79.   Harkins, W.D. and F. Brown, *The determination of surface tension (free surface energy), and the weight of falling drops: The surface tension of water and benzene by the capillary height method.* Journal of the American Chemical Society, 1919. **41**(4): p. 499-524.

80.   Buckley, J.S. and T. Fan, *Crude Oil/Brine Interfacial Tensions1.* 2007.

81.   Buckley, J.S. *Chemistry of the Crude oil/Brine Interface.* in *3rd International Symposium on Evaluation of Reservoir Wettability and its Effect on Oil Recovery* 1996. University of Wyoming, Laramie.

82.   Wilhelmsen, H.M.W.A., et al. *NIGOGA - The Norwegian Industry Guide to Organic Geochemical Analyses.* 2000. 102.

83.   Tomren, A.L. and T. Barth, *Comparison of partial least squares calibration models of viscosity, acid number and asphaltene content in petroleum, based on GC and IR data.* Fuel, 2014. **120**: p. 8-21.

84.   Goebel, A. and K. Lunkenheimer, *Interfacial tension of the water/n-alkane interface.* Langmuir, 1997. **13**(2): p. 369-372.

Appendix I: Calculations

A.1. Determining the equilibrium IFT

Step 1   Plot IFT versus Drop Age to obtain a curve displaying the dynamic IFT.
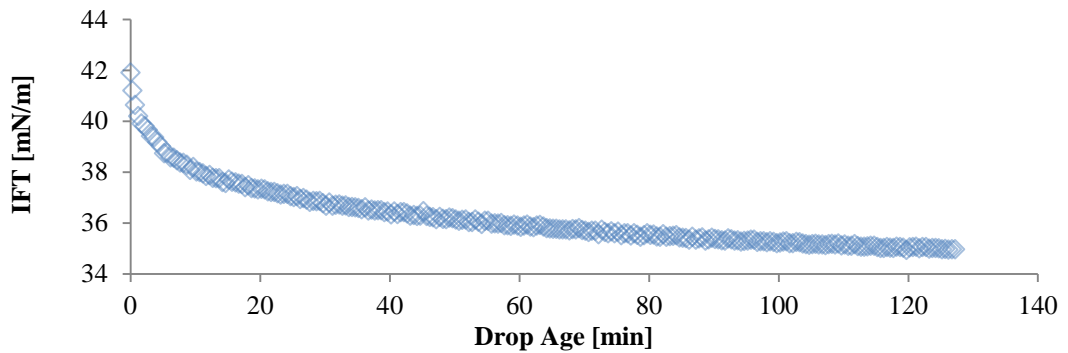
Step 2   Fit the dynamic IFT to a 2nd degree polynomial by applying Excel Analyze Application. DA = Drop Age [min].

$$IFT = 0,0004DA^2 - 0,0765DA + 39,069$$
$$R^2 = 0,92$$
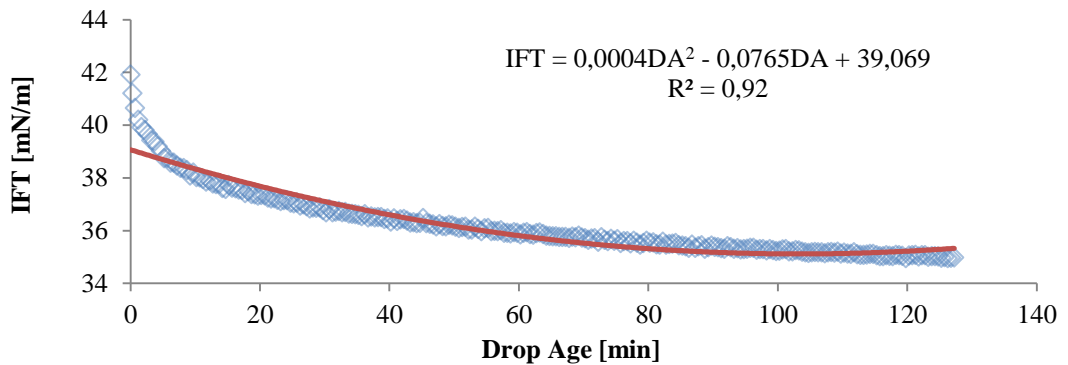
Step 3   Remove the region of rapid decay in the momentary dynamic IFT. This is set at a threshold of $\frac{\Delta IFT}{\Delta DA} > 0.2$ for a minimum of three consequtive measuring points.

$$IFT = 0,0003DA^2 - 0,0581DA + 38,472$$
$$R^2 = 0,9817$$
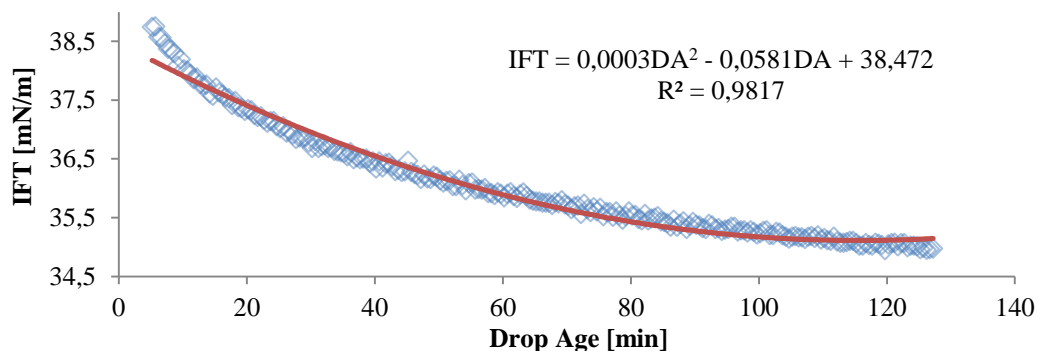
Step 4   Find the global minimum of the fitted line by differetiation. This corresponds to the point on the parabola where $\frac{\partial(\text{IFT})}{\partial(\text{DA})} = 0$, i.e. the drop age (DA) where there is

no further decay in the dynamic IFT.

$$\text{IFT(DA)} = 0.0003\text{DA}^2 - 0.0581\text{DA} + 38.472$$

$$\frac{\partial}{\partial(\text{DA})}(0.0003\text{DA}^2 - 0.0581\text{DA} + 38.472) = 0.0006\text{DA} - 0.0581$$
$$\rightarrow 0.0006\text{DA}_{\text{Eq.}} - 0.0581 = 0$$
$$\rightarrow \text{DA}_{\text{Eq.}} \cong 96.833$$

Step 5   Calculated the equilibrated IFT by finding the IFT at the equilibrated drop age ($\text{DA}_{\text{Eq.}}$).

$$\text{IFT}_{\text{Eq}}(\text{DA}_{\text{Eq}}) = \text{IFT}_{\text{Eq}}\ (96.833)$$
$$= 0.0003 \times (96.833)^2 - 0.0581 \times 96.833 + 38.472$$
$$\rightarrow \mathbf{IFT_{Eq}} \cong \mathbf{35.659}$$

Step 6   Determine the last significant digit from uncertainty calculations.

Conclusion   The equilibrium IFT is obtain at a drop age of 96.8 minutes, and is 35.7 ±0.7 mN·m^{-1}.

A.2. Uncertainty-determination

The uncertainty in IFT measurements have been calculated as the standard deviation (**Equation A-1**) between 2 – 4 parallel measurements or as the standard deviation between centerpoints of the experimental design. The uncertainty in asphaltene-quantification was determined based on the principle of propagation of error (**Equation A-2**).

$$s = \sqrt{\frac{1}{n-1}\sum_{i=1}^{n}(x_i - \bar{x})^2} \qquad \textbf{Equation A-1}$$

$$e_{\text{tot}} = \sqrt{e_1^2 + e_2^2 + e_3^2} \qquad \textbf{Equation A-2}$$

Where s is the standard deviation, n is the number of parallels, x_i is the measured value and $\bar{x}$ is the average measured value. e_{tot} is the total error in propagation of error, where e_1, e_2 and e_3 represent the errors associated with the three weightings, each with an error of ±0.0001 g.

Appendix II: Water compositions

Table A-1 Experimental water compositions in the first set of screening experiments.

Exp #	Molality [mol·kg^{-1}]			X_{Ca2+}	Ionic Strength [mol·kg^{-1}]	Salinity [ppm]
	Na$^+$	Ca^{2+}	Cl$^-$			
1	0.0859	0.0000	0.0859	0.00	0.09	5021.4
2	0.0346	0.0661	0.1667	0.25	0.23	9354.8
3	0.2799	0.0418	0.3635	0.06	0.41	20995.3
4*	0.0791	0.0034	0.0859	0.02	0.09	4999.3

*Only used for inspecting the behavior of Exp 1 if Ca^{2+} is present at pH 11.

Table A-2: Water composition pH measured before (pH$_i$) and after (pH$_f$) equilibration with the crude oil phase. For the first screening design.

Exp #	Acidic pH [±0.3]		Neutral pH [±0.3]		Basic pH [±0.3]	
	pH$_i$	pH$_f$	pH$_i$	pH$_f$	pH$_i$	pH$_f$
1	3.0	3.1	7.0	6.5	11.0	8.9
2	3.0	3.2	6.9	6.7	11.0	8.1
3	3.0	3.1	6.8	6.5	10.9	7.8
4*	-	-	-	-	11.0	7.6

*Only used for inspecting the behavior of Exp 1 if Ca^{2+} is present at pH 11.

Table A-3: Experimental water compositions in the second set of screening experiments.

Exp #	Molality [mol·kg^{-1}]			X_{Ca2+}	Ionic Strength [mol·kg^{-1}]	Salinity [ppm]	pH [±0.3]
	Na$^+$	Ca^{2+}	Cl$^-$				
1	0.0619	0.0082	0.0783	0.06	0.09	4527.6	6.9
2	0.0664	0.1153	0.2970	0.24	0.41	16673.8	6.6
3	0.3563	0.0000	0.3563	0.00	0.36	20823.9	6.4
4	0.012	0.0308	0.0736	0.26	0.10	4119.1	7.0
5	0.2430	0.0000	0.2430	0.00	0.24	14198.1	6.9
6	0.1734	0.0234	0.2203	0.06	0.24	12737.4	6.9

Table A-4: Experimental water compositions in the two- and three-dimensional FCDs.

	Molality [mol·kg⁻¹]			$X_{Ca^{2+}}$	Ionic Strength [mol·kg⁻¹]	Salinity [ppm]
	Na^+	Ca^{2+}	Cl^-			
Exp1, 5	0.0186	0.0047	0.0279	0.091	0.033	1603.1
Exp2, 6	0.0326	0.0000	0.0326	0.00	0.033	1902.7
Exp3, 7	0.3721	0.0930	0.5580	0.091	0.651	32062.2
Exp4, 8	0.6512	0.0000	0.6512	0.00	0.651	38053.3
CP, Ax1, 2	0.2588	0.0277	0.3143	0.046	0.342	18223.2
Ax1	0.3421	0.0000	0.3421	0.00	0.342	19990.9
Ax2	0.1949	0.0489	0.2927	0.091	0.342	16816.9
Ax3	0.0247	0.0026	0.0300	0.046	0.033	1735.6
Ax4	0.4949	0.0522	0.5992	0.046	0.651	34711.4

Table A-5: Water composition pH measured before (pH_i) and after (pH_f) equilibration with the crude oil phase. For the three-dimensional FCD. Nm= not measurable.

		Neutral pH [±0.3]		Basic pH [±0.3]	
		pH_i	pH_f	pH_i	pH_f
Crude oil A	Exp1, 5	6.3	5.6	11.1	8.5
	Exp2, 6	6.3	5.8	11.0	8.1
	Exp3, 7	6.4	5.8	11.1	8.4
	Exp4, 8	6.4	5.8	11.1	Nm
	CP	-	-	7.6	6.7
	Ax1	-	-	7.8	7.0
	Ax2	-	-	7.7	6.7
	Ax3	-	-	7.6	6.8
	Ax4	-	-	7.6	6.8
	Ax5	6.8	6.6	-	-
	Ax6	-	-	11.0	8.1
		Neutral pH [±0.3]		Basic pH [±0.3]	
		pH_i	pH_f	pH_i	pH_f
Crude oil B	Exp1, 5	6.3	6.9	11.1	10.2
	Exp2, 6	6.3	6.7	11.0	10.9
	Exp3, 7	6.4	6.7	11.1	10.9
	Exp4, 8	6.4	6.9	11.1	10.0
	CP	-	-	7.6	7.0
	Ax1	-	-	7.8	7.3
	Ax2	-	-	7.7	7.0
	Ax3	-	-	7.6	7.1
	Ax4	-	-	7.6	7.1
	Ax5	6.9	6.6	-	-
	Ax6	-	-	11.0	10.6

Appendix III: IR-spectra
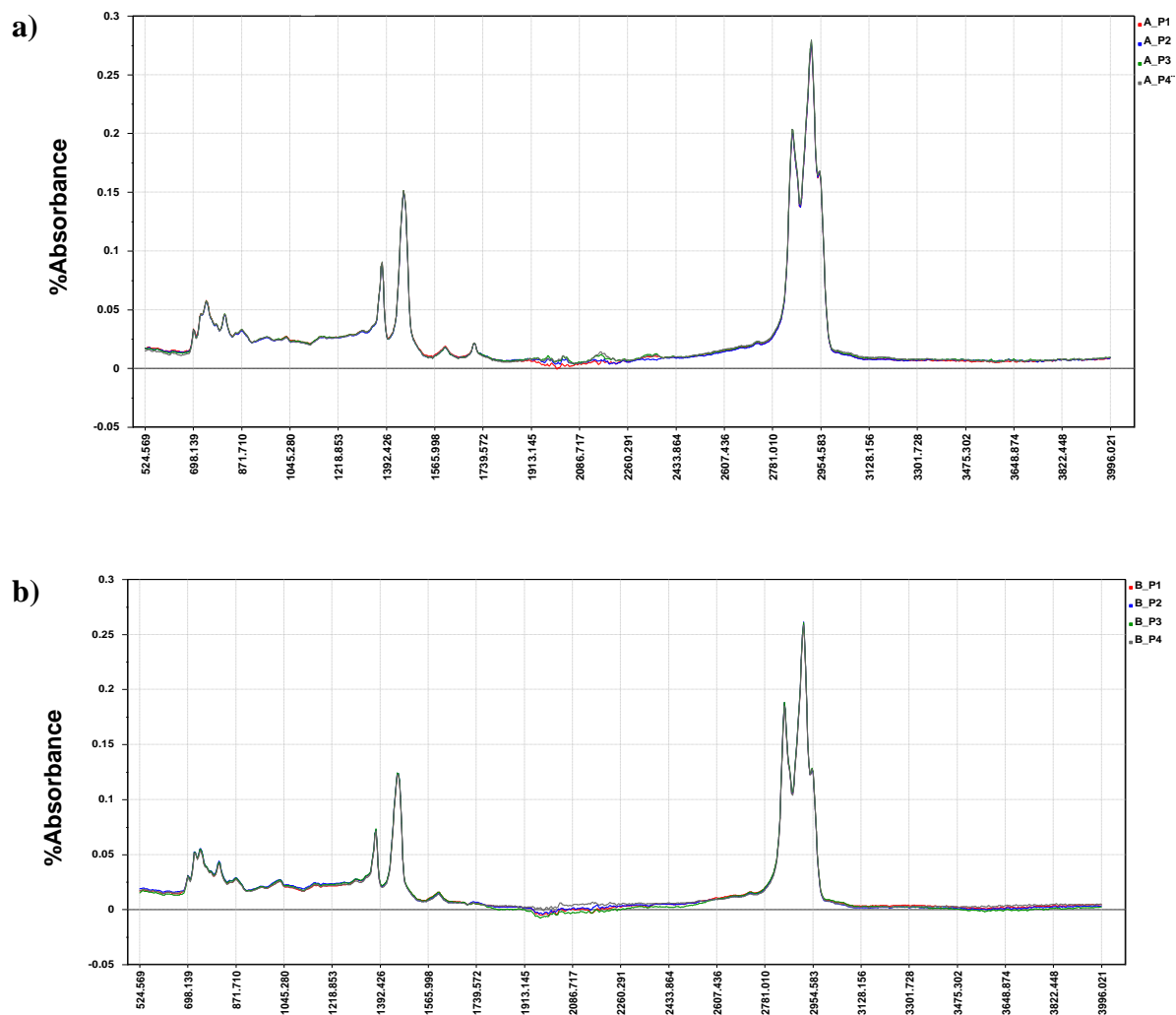
Figure A-1: Collected IR-spectra of all four parallels for a) crude oil A and b) crude oil B.
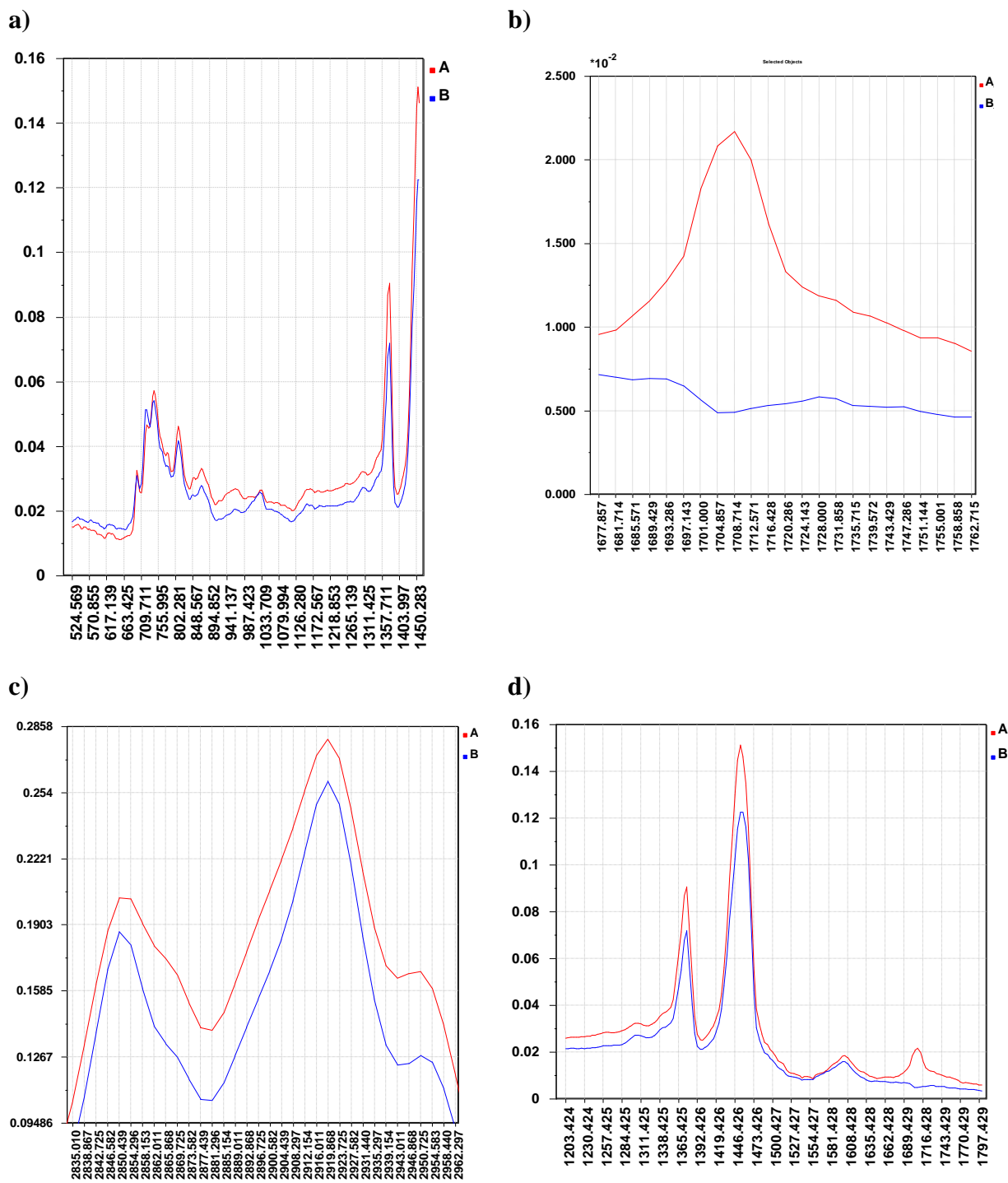
Figure A-2: Comparison of a) the fingerprint-region and b) the carbonyl-region (C=O stretching region). c) A comparison of crude oil A (red) and B (blue) in the infrared 2750 – 3020 cm^{-1} region. d) A comparison of crude oil A (red) and B (blue) in the infrared 1200 – 1800 cm^{-1} region. The y-axis is %-absorbance.

Appendix IV: Multivariate plots and data

A.3. Screening and preliminary experiments
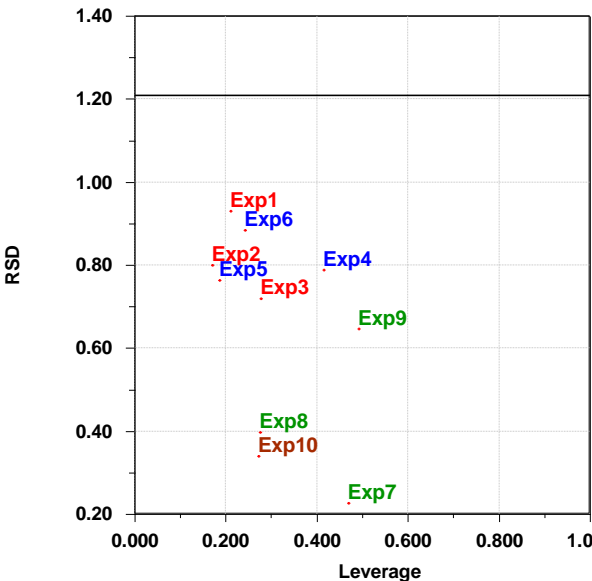
Figure A-3: RSD vs. leverage for objects in the PCA for the first screening design.
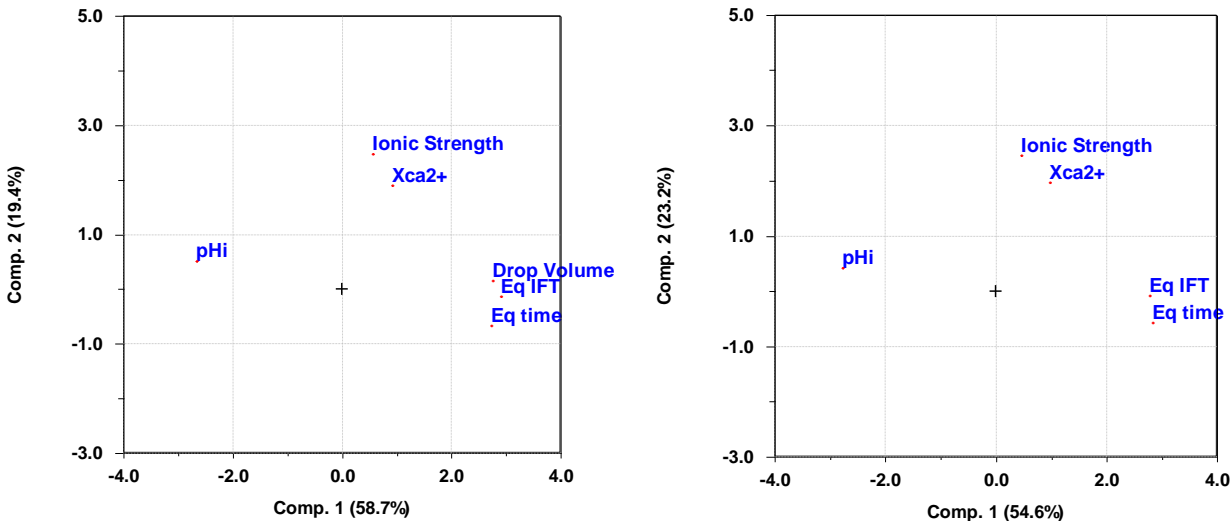
Figure A-4: A comparison of loading-plots modeled with and without drop-volume as an independent variable for the first screening design.

A.4. Two-dimensional face centered designs

Crude oil A

a)
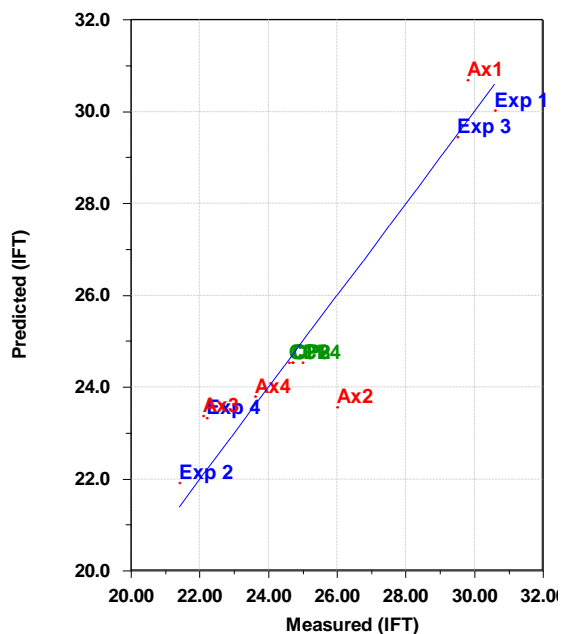
b)
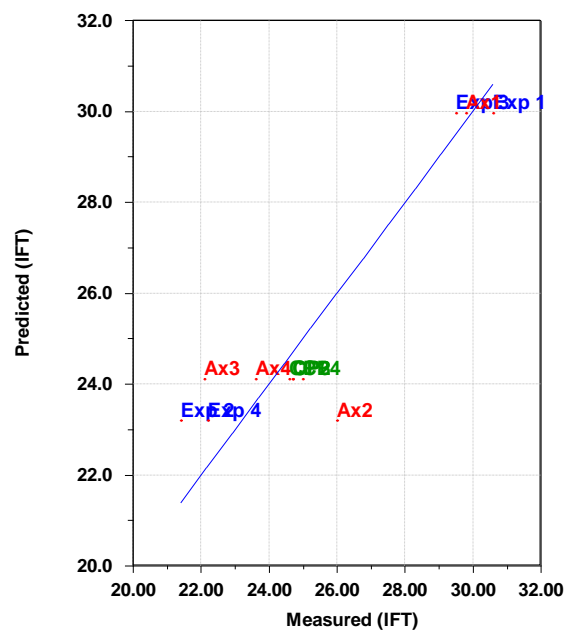
Crude oil B

c)
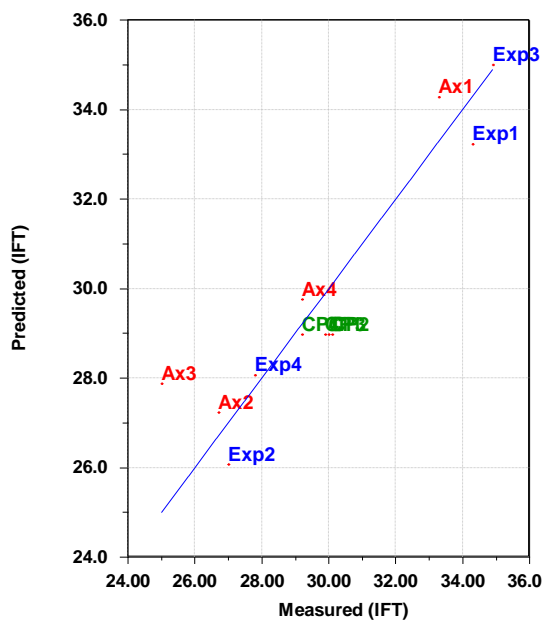
d)
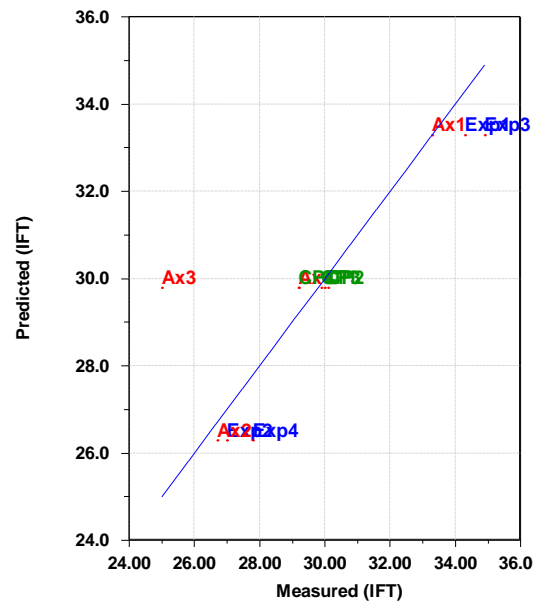
Figure A-5: The regression-model for the two-dimensional FCD when a) all variables contribute to the model for crude oil A, and b) when only the ionic strength (I and I^2) contribute to the model for crude oil A. c) all variables contribute to the model for crude oil B and d) only ionic strength (I) contribute to the model for crude oil B.

Table A-6: Regression coefficients calculated by yate's algorithm for the two-dimensional FCD. The most significant factors are marked in red.

Variable / variable-interaction	Regression coefficient	
	Crude oil A	**Crude oil B**
X_{Ca2+}	0.135	0.940
I	**-4.267**	**-3.524**
$X_{Ca2+}{}^2$	0.025	-0.168
$X_{Ca2+} \times I$	0.305	0.050
I^2	**0.737**	1.779

A.5. Three-dimensional designs

a)

b)
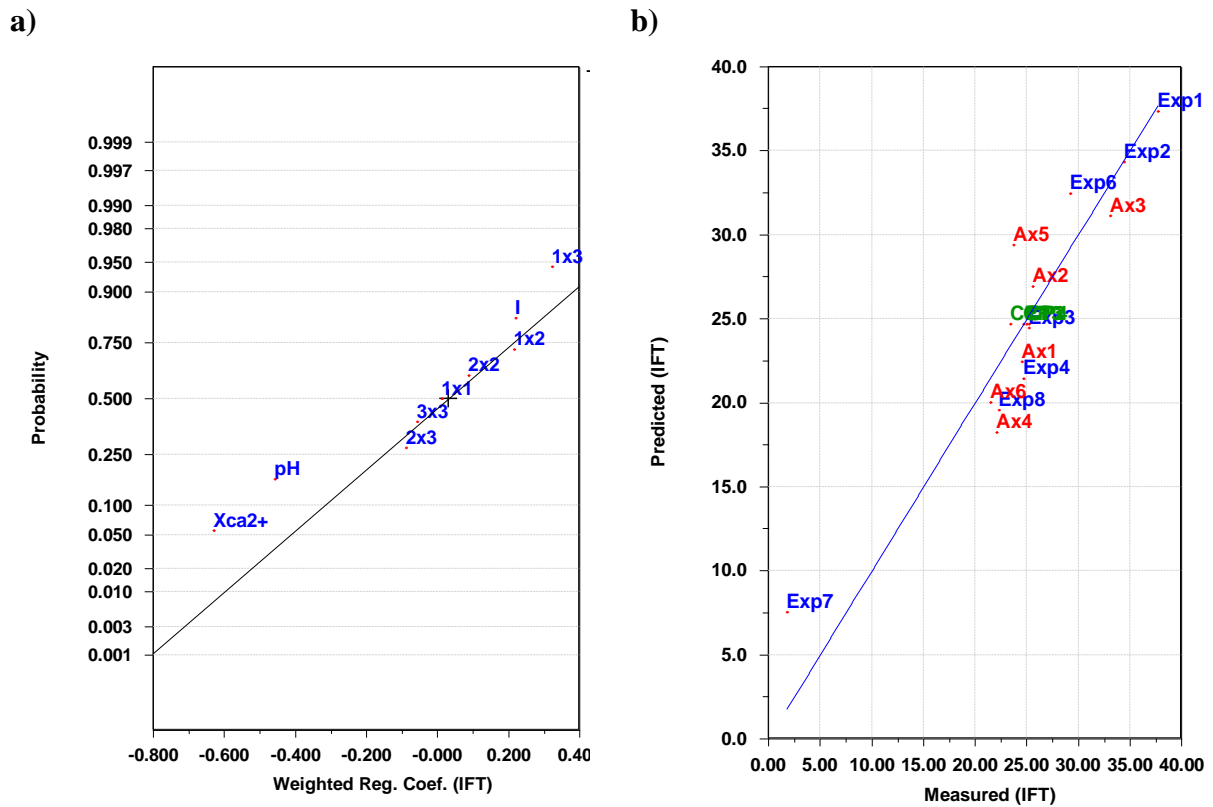
Figure A-6: a) normal plot of the of regression coefficients, and b) predicted versus measured IFT modeled with only significant variables (X_{Ca2+}, pH, I and I×pH).

a)

b)
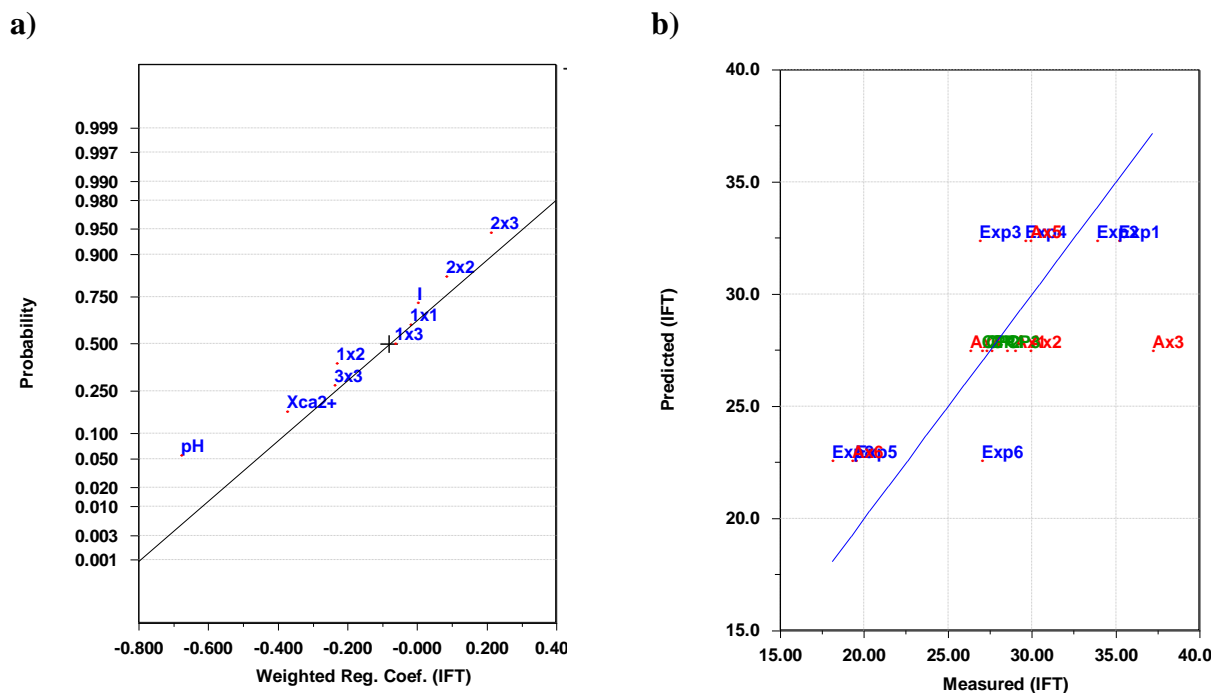
Figure A-7: a) Plot of the normal distribution of regression coefficients, and b) predicted versus measured IFT for the model derived with significant variables (pH).

Table A-7: Regression coefficients calculated from yate's algorithm for the three-dimensional FCD. Significant factors are marked in red.

Variable / variable-interaction	Regression coefficient	
	Crude oil A	Crude oil B
X_{Ca2+}	**4.429**	2.465
I	**-3.609**	-4.586
pH	**-6.681**	**-6.327**
X_{Ca2+}^2	-2.342	-2.642
$X_{Ca2+} \times I$	-0.695	1.613
$X_{Ca2+} \times pH$	6.302	2.673
I^2	-1.260	-1.728
$I \times pH$	**2.014**	-1.745
pH^2	-3.381	-4.571

A.6. CO-Wet database

Table A-8: Overview of variables included in the characterization done by Buckley et al. [23, 41, 43, 44]. The variable names are those used in the PCA plots. The range lists the lowest and highest measured variable value within the dataset.

Variable Name	Unit	Description	Range
API Gravity	o	Standard density measure for crude oils (**Equation 2-3**)	16.5 – 48.0
Mean MW	g/mol	The mean molecular weight of crude oil	141 – 484
nC$_7$-asph	wt%	Amount of asphaltenes precipitated with n-heptane flocculant	0.05 – 8.75
Density	g/ml	The density of the crude oil (**Equation 2-2**)	0.7855 – 0.9524
Viscosity	cP	The viscosity of the crude oil.	1.2 – 661
TAN	mg KOH/g oil	The total acid number of the crude oil	<0.01 – 3.92
BAN	mg KOH/g oil	The total base number of the crude oil	0.11 – 5.19
Saturates	wt%	The amount of saturated components found in the oil (from SARA-analysis)	38.4 – 82.5
Aromatic	wt%	The amount of aromatic components found in the oil (from SARA-analysis)	12.2 – 29.8
Resins	wt%	The amount of resin components found in the oil (from SARA-analysis)	0.7 – 25.8
Salinity	ppm	The salinity of the aqueous phase, regulated with NaCl	0 – 35 000
pH	-	The pH of the water phase, regulated with HCl or NaOH	3 – 11
Init. IFT	mN/m	The initial IFT, measured at zero drop age (T= 0 s). γ_o in **Equation 1-5**	3.4 (nm) – 32.1
Eq. IFT	mN/m	The equilibrium IFT calculated from **Equation 1-5** (γ_{eq})	0.9 (nm) – 28.2
T	seconds	Time/drop age after drop is dispensed	9 – 1000

*nm = not measurable

a) Doubly distilled water
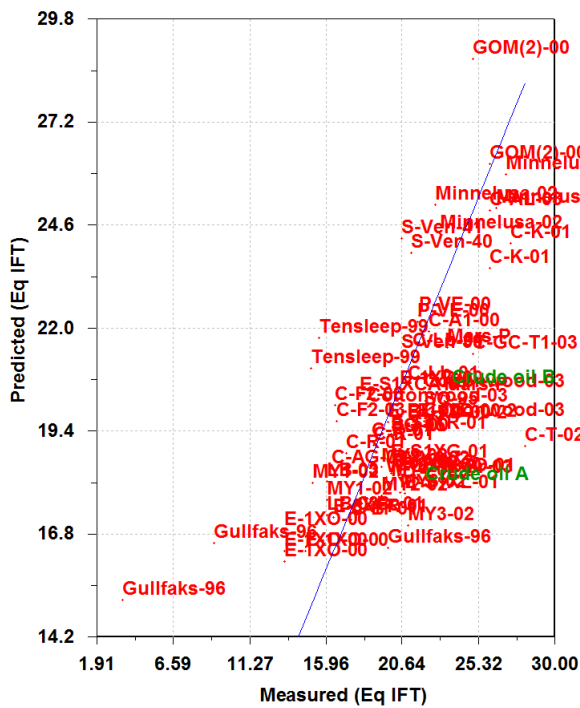
b) 0.1 M NaCl
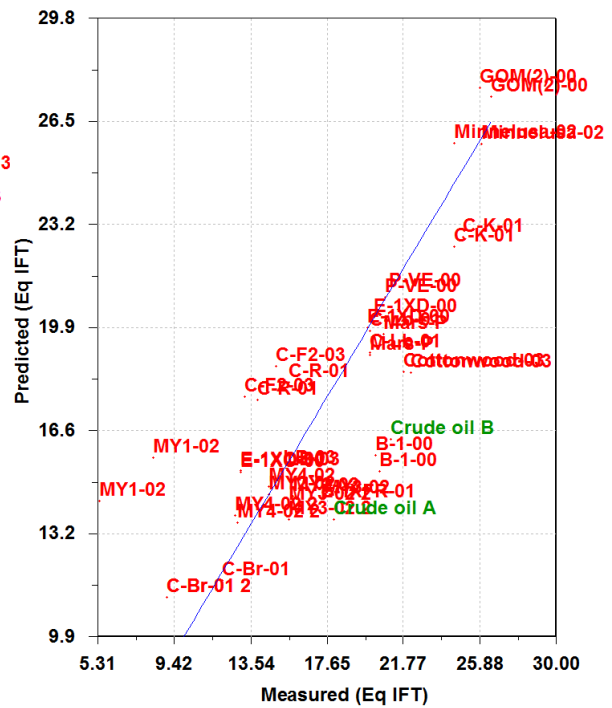
Figure A-8: The PLS regression model, with equilibrium IFT as the dependent variable, for the CO-Wet database [23, 41, 43, 44] and experimental measurement for crude oil A and B included. Crude oils A and B are marked in green.

a)
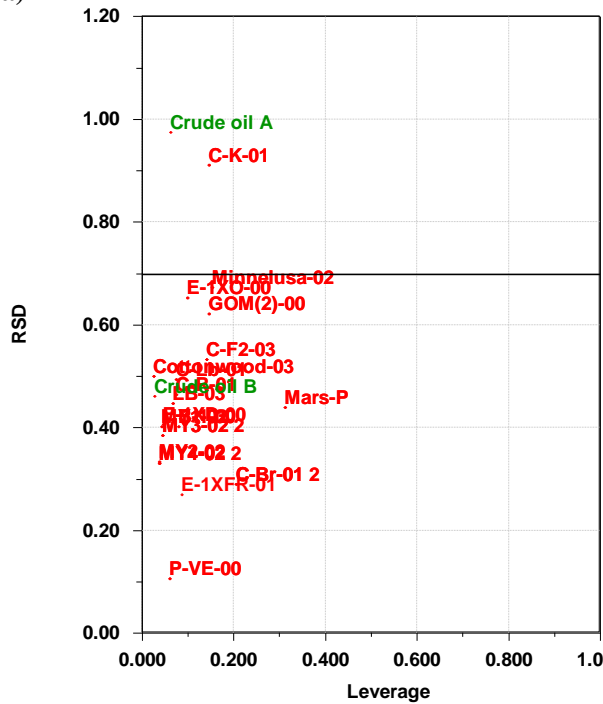
b)
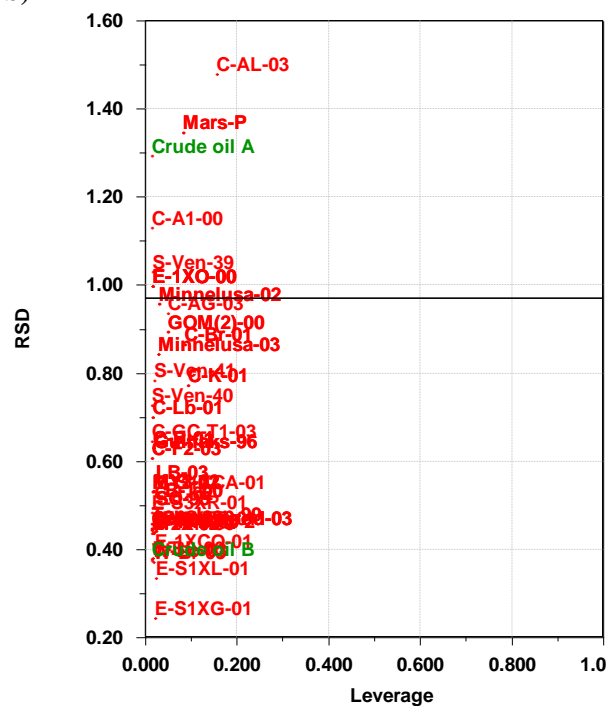
Figure A-9: RSD vs Leverage plots for the latent variables extracted by PLS-regression. The horizontal line symbolizes the critical RSD-value for objects. a) doubly distilled water and b) 0.1 M NaCl.

Appendix V: IFT results

Table A-9: Experimental results from the screening experiments for crude oil A. All values have been obtained by the polynomial model. Standard deviations are calculated from 3 – 5 parallels per measurement.

	Initial IFT [mN/m]	±St. Dev. [mN/m]	Eq. IFT [mN/m]	±St. Dev. [mN/m]	Decay [%]	±St. Dev. [%]	Eq. time [min]	±St. Dev. [min]
Exp1	41.2	0.6	35.0	1.0	15.0	3.6	123	13
Exp2	37.6	0.8	31.5	0.5	16.2	3.0	86	6
Exp3	10.8	1.3	7.0	0.3	35.2	9.4	17	2
Exp4	26.3	1.0	21.1	1.0	19.8	6.6	54	16
Exp5	39.2	1.5	34.0	1.3	13.3	6.4	171	58
Exp6	31.5	1.0	25.9	0.4	17.8	3.8	60	2
Exp7	27.0	0.4	24.4	0.4	9.6	2.8	50	10
Exp8	36.2	0.1	31.1	0.4	14.1	1.3	104	16
Exp9	29.0	0.6	25.4	0.4	12.4	3.1	50	25
Exp10	24.8	0.4	22.5	0.2	9.3	2.2	32	13

Table A-10: Experimental results from the screening experiments for both crude oils. All values have been obtained by the polynomial model. Standard deviations are calculated from 2 – 3 parallels per measurement.

Crude oil A								
	Initial IFT ±0.9 [mN/m]	±St. Dev. [mN/m]	Eq. IFT ±0.9 [mN/m]	±St. Dev. [mN/m]	Decay ±5.0 [%]	±St. Dev. [%]	Eq. time [min]	±St. Dev. [min]
Exp1	33.2	0.3	28.0	0.2	15.7	1.4	68	19
Exp2	33.3	0.3	25.9	0.2	22.2	1.3	72	26
Exp3	31.2	0.7	25.0	0.5	19.9	3.3	62	8
Exp4	30.3	0.8	25.3	0.9	16.5	5.0	62	15
Exp5	35.0	0.7	28.6	0.2	18.3	2.2	61	12
Exp6	35.9	0.1	28.8	0.5	19.8	1.6	77	19
Crude oil B								
	Initial IFT ±0.9 [mN/m]	±St. Dev. [mN/m]	Eq. IFT ±0.9 [mN/m]	±St. Dev. [mN/m]	Decay ±5.0 [%]	±St. Dev. [%]	Eq. time [min]	±St. Dev. [min]
Exp1	29.9	0.1	26.6	0.3	11.0	1.3	61	7
Exp2	31.8	0.5	27.3	1.0	14.2	4.4	69	11
Exp3	30.6	0.6	25.8	0.7	15.7	3.9	68	12
Exp4	31.1	0.2	26.2	0.6	15.8	2.5	65	23
Exp5	33.4	0.3	29.5	0.7	11.7	2.9	67	28
Exp6	31.5	0.3	29.4	0.4	6.7	2.1	71	33

Table A-11: Experimental results from the two-dimensional FCD. All values have been obtained by the polynomial model. Uncertainties are calculated from the standard deviation between parallel centerpoint measurements.

Crude oil A				
	Initial IFT ±0.9 [mN/m]	**Eq. IFT ±0.2 [mN/m]**	**Decay ±3.1 [%]**	**Eq. time ±15 [min]**
Exp1	38.3	30.6	20.1	63
Exp2	26.1	21.4	18.0	89
Exp3	36.1	29.5	18.3	65
Exp4	25.8	22.2	14.0	78
Ax1	34.8	29.8	14.4	72
Ax2	31.0	26.0	16.1	84
Ax3	27.3	22.1	19.0	57
Ax4	29.0	23.5	19.0	68
CP1	30.0	24.6	18.0	67
CP2	28.5	24.7	13.3	97
CP3	29.5	24.7	16.3	67
CP4	30.7	25.0	18.6	88
Crude oil B				
	Initial IFT ±0.4 [mN/m]	**Eq. IFT ±0.4 [mN/m]**	**Decay ±2.3 [%]**	**Eq. time ±5 [min]**
Exp1	37.0	34.3	7.3	71
Exp2	29.5	27.0	8,5	62
Exp3	37.4	34.9	6.7	55
Exp4	30.4	27.8	8.6	68
Ax1	35.6	33.3	6.5	91
Ax2	29.3	26.7	8.9	62
Ax3	26.8	25.0	nfm	nfm
Ax4	33.0	29.2	11.5	53
CP1	33.2	29.9	9.9	68
CP2	32.3	30.1	6.8	68
CP3	32.4	30.0	7.4	62
CP4	32.3	29.2	9.6	74

Nfm= no fit with model

Table A-12: An overview of parameters that have been fitted to the two models used for systematic estimation the equilibrium IFT. Poly = 2nd degree polynomial regression line, and exp = monoexponential model (**Equation 1-5**).

Crude oil A						
	Initial IFT [mN/m]	τ [sec]	Eq. IFT, exp ±0.7 [mN/m]	Decay [%]	Eq. IFT, poly ±0.8 [mN/m]	Eq. time, poly [sec]
Exp1	44.0	861	37.7	14.3	37.7	3489
Exp2	40.5	1172	34.2	15.6	34.4	3878
Exp3	29.4	1300	24.7	16.0	25.2	3498
Exp4	30.2	1025	24.5	18.9	24.7	3930
Exp5	nm	nm	nm	nm	nm	nm
Exp6	32.0	1288	29.5	7.8	29.2	6210
Exp7	3.2	412	1.9	40.6	1.8	2513
Exp8	23.9	1100	22.1	7.5	22.3	2815
CP1	28.0	943	23.7	15.4	23.4	4818
CP2	29.2	883	25.0	14.4	25.0	4105
CP3	29.3	1027	24.7	15.7	24.7	3870
CP4	29.9	899	25.2	15.7	25.2	4001
Ax1	30.1	1020	24.3	19.3	24.5	3732
Ax2	30.0	788	25.6	14.7	25.6	4128
Ax3	38.6	1063	33.1	14.2	33.1	4226
Ax4	29.4	975	24.6	16.3	22.1	3640
Ax5	29.0	1055	24.0	17.2	23.7	4090
Ax6	24.7	548	21.6	12.6	21.5	5010
Mean ±st.dev.		**966 ±236**		**16 ±7**		**3997 ±857**
Crude oil B						
	Initial IFT [mN/m]	τ [sec]	Eq. IFT, exp ±0.6 [mN/m]	Decay [%]	Eq. IFT, poly ±0.3 [mN/m]	Eq. time, poly [sec]
Exp1	40.0	741	35.2	12.0	35.2	3336
Exp2	39.6	1116	34.2	13.6	33.9	5618
Exp3	31.1	1082	26.8	13.8	26.9	3818
Exp4	31.6	787	26.6	15.8	29.6	3336
Exp5	20.1	nfm	nfm	nfm	19.5	nfm
Exp6	33.4	1877	26.6	20.4	27.0	nfm
Exp7	nm	nm	nm	nm	nm	nfm
Exp8	20.0	1201	18.3	8.5	18.1	5160
CP1	34.0	896	27.6	18.8	27.6	3753
CP2	34.4	932	27.3	20.6	27.3	4177
CP3	33.5	864	28.5	14.9	28.5	3788
CP4	34.1	901	26.9	21.1	27.0	4233
Ax1	32.9	512	29.0	11.9	29.0	4020
Ax2	35.2	689	29.8	15.3	29.9	3401
Ax3	45.6	803	37.2	18.4	37.2	3835
Ax4	30.9	810	26.1	15.5	26.3	3229
Ax5	33.3	949	29.9	10.2	29.9	3740
Ax6	20.1	nfm	nfm	nfm	19.3	nfm
Mean ±st.dev.		**947 ±322**		**15 ±4**		**3939 ±708**

nm = not measurable, nfm = no fit with model.
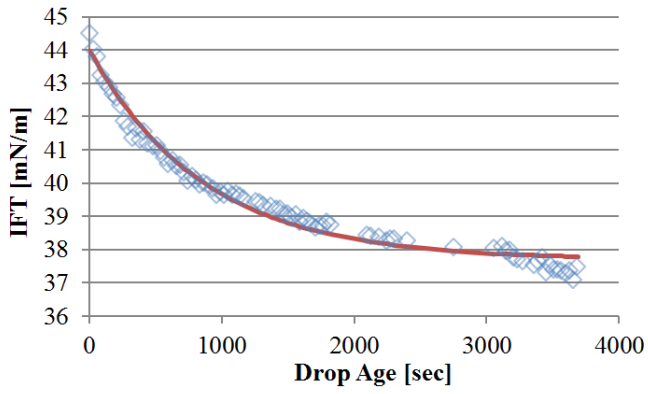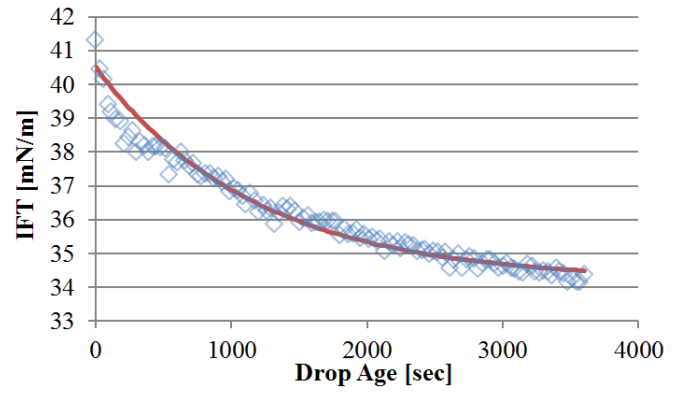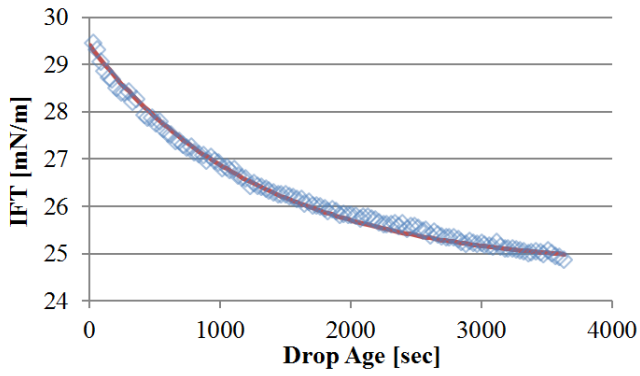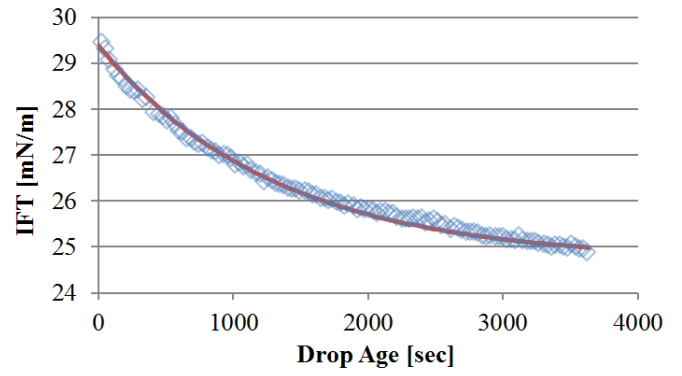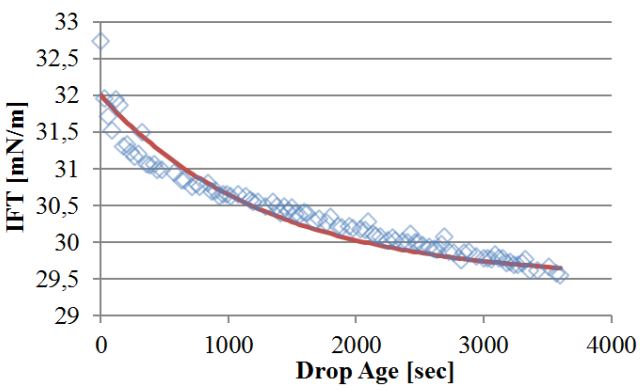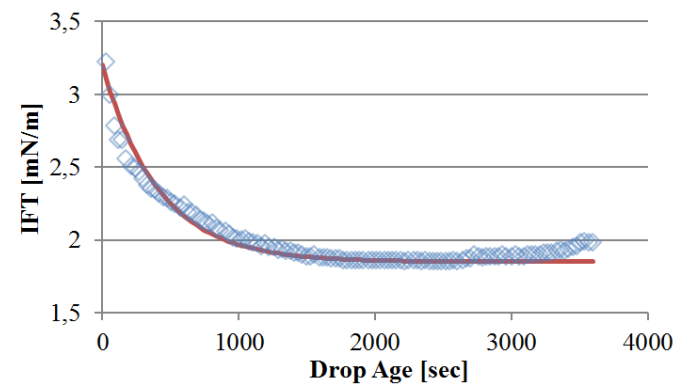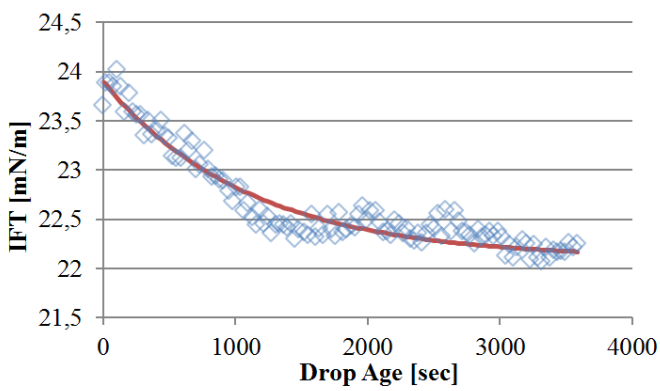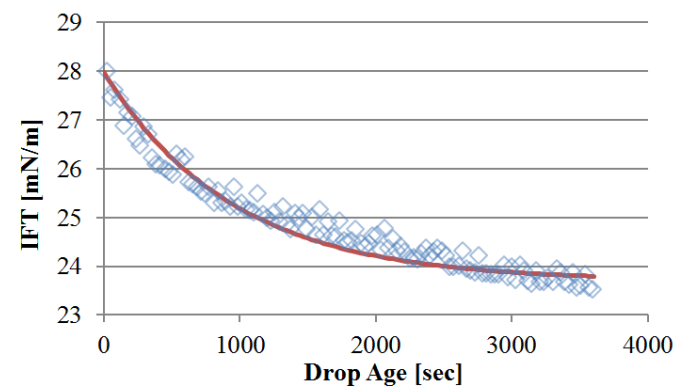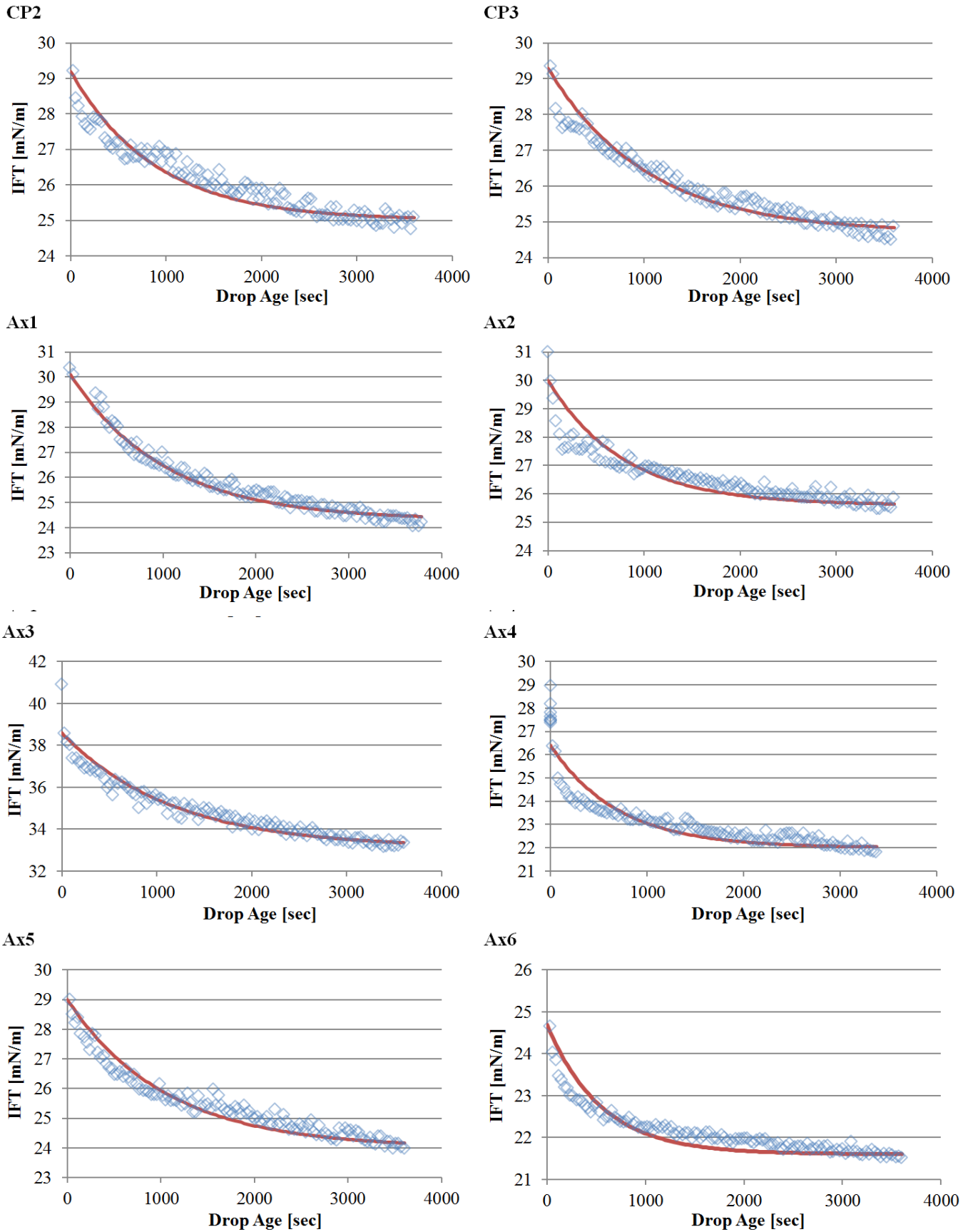
Figure A-10: The experimental dynamic IFT (blue markers) and the fitted mono-exponential decay-function (**Equation 1-5**, red line) for all experiments performed in the three-dimensional FCD for crude oil A.
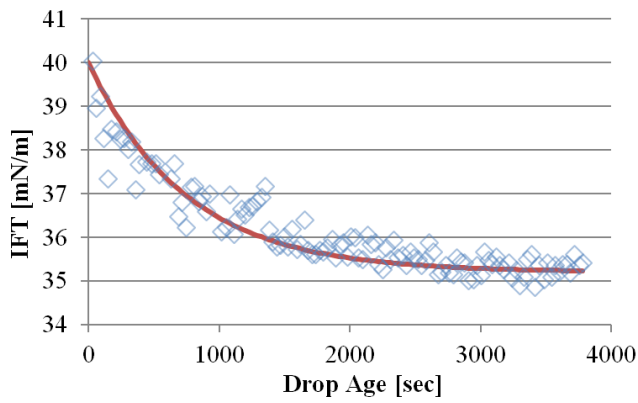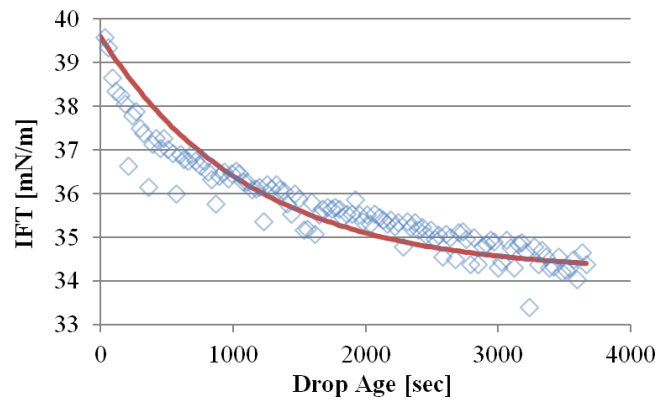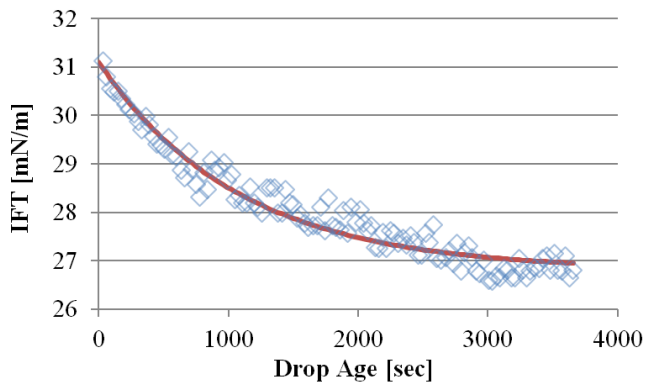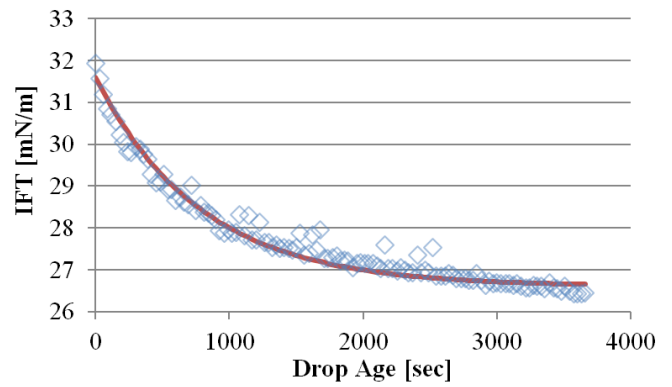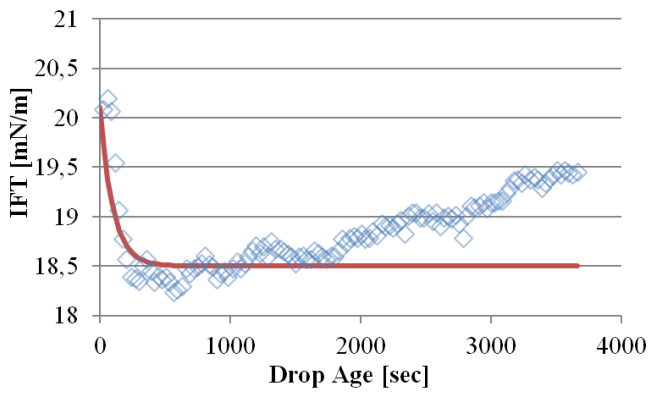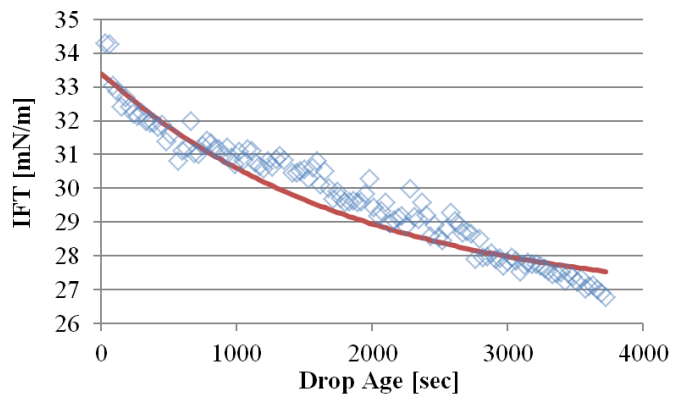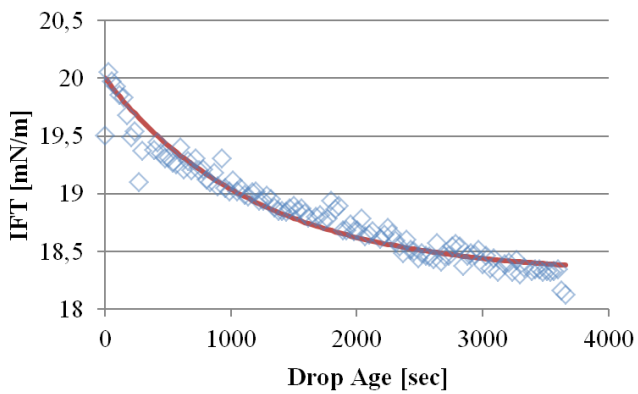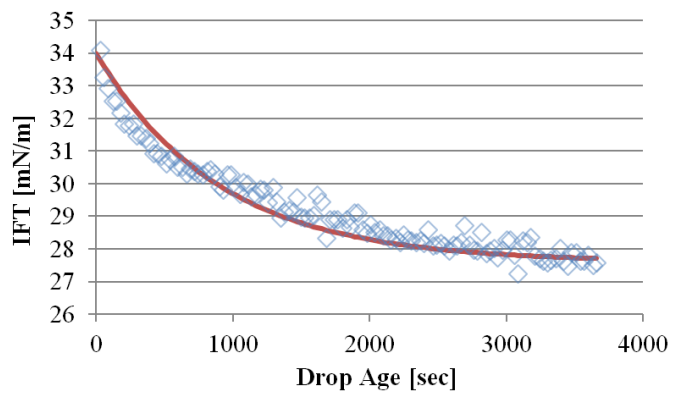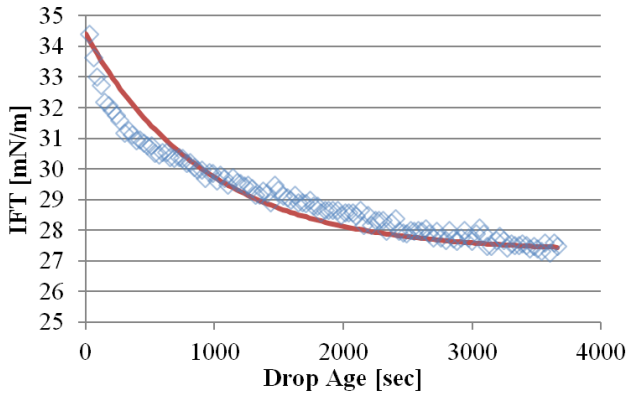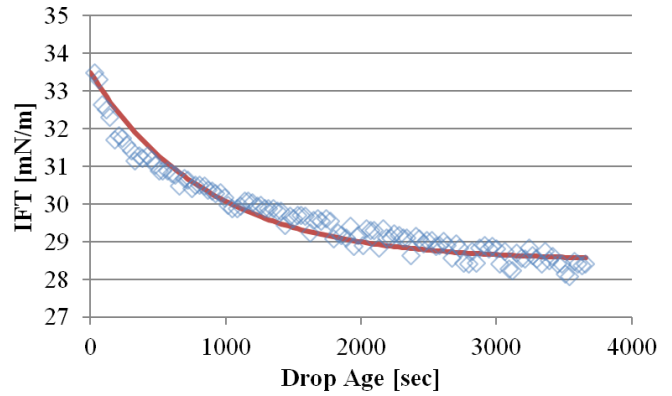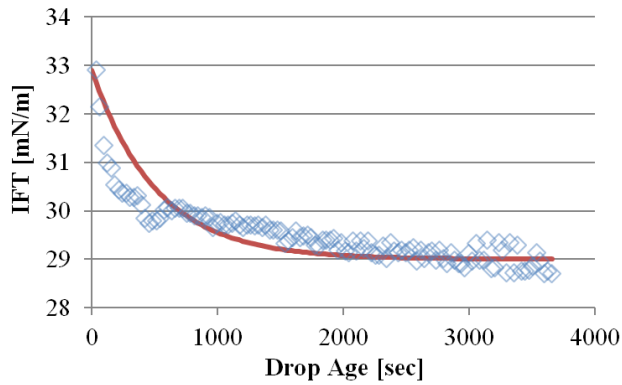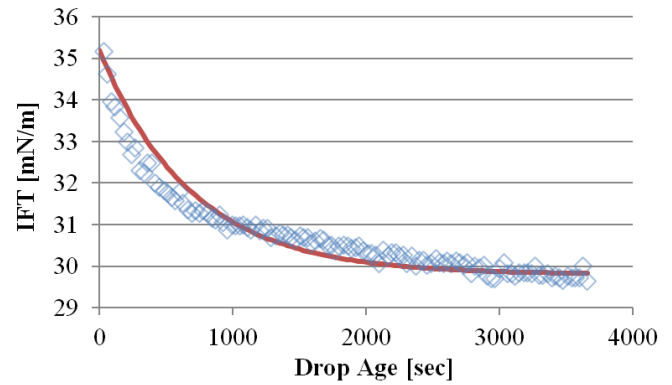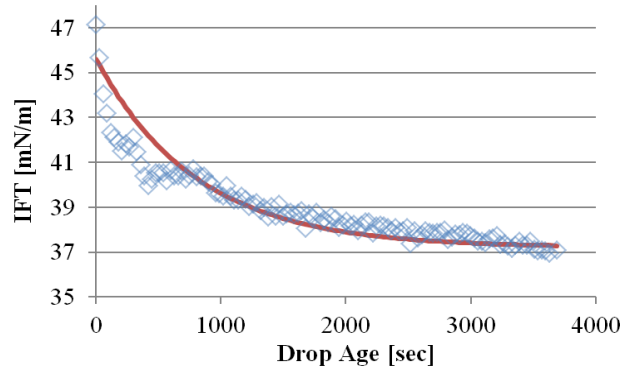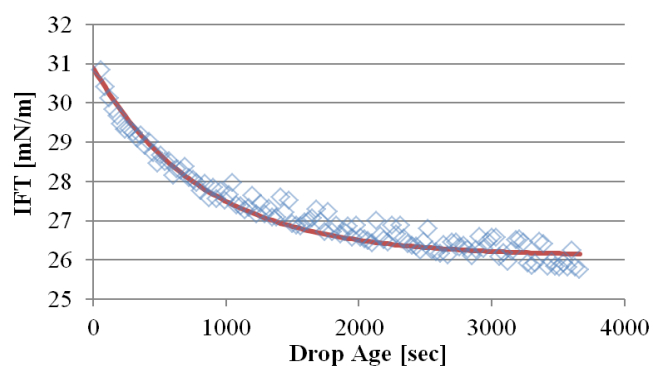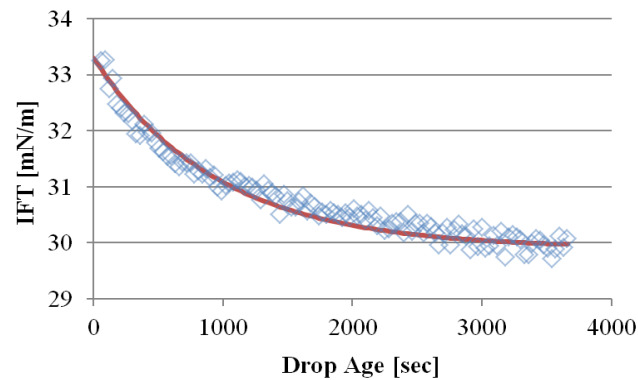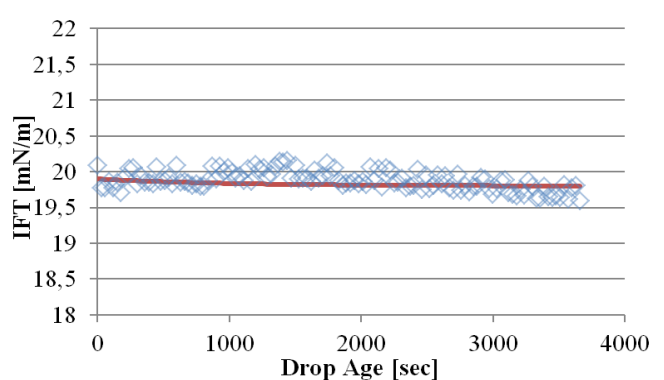
Figure A-11: The experimental dynamic IFT (blue markers) and the fitted mono-exponential decay-function (**Equation 1-5**, red line) for all experiments performed in the three-dimensional FCD for crude oil B.